P. D. Cozzoli, C. O. Kappe et al.

DOI: 10.1002/anie.201101274

Microwave Chemistry

Microwave-Assisted Synthesis of Colloidal Inorganic Nanocrystals

Mostafa Baghbanzadeh, Luigi Carbone, P. Davide Cozzoli, and C. Oliver Kappe**

Keywords:
colloidal nanocrystals · high-temperature chemistry · microwave irradiation · size/shape control · thermal/nonthermal microwave effects

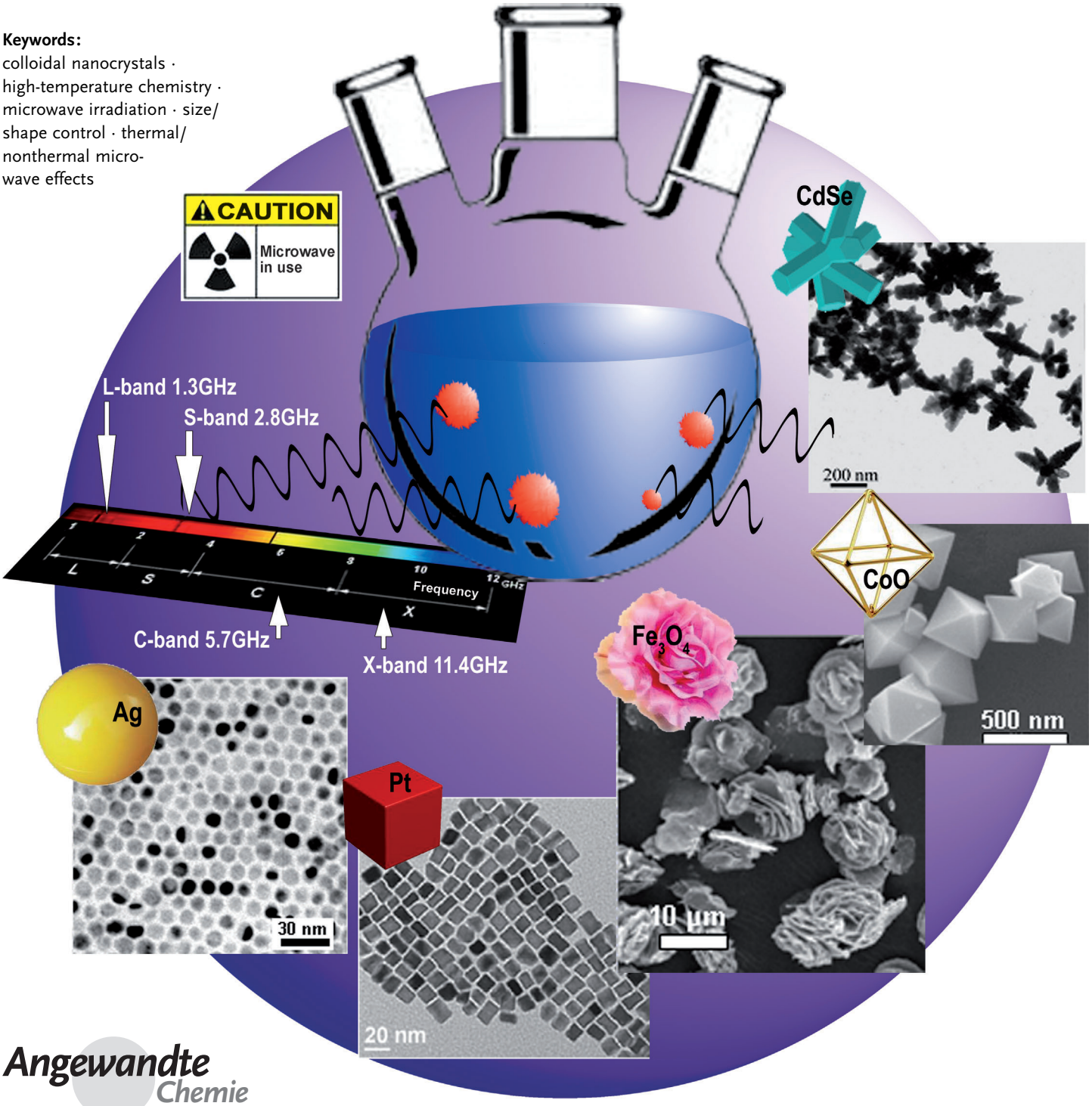

Colloidal inorganic nanocrystals stand out as an important class of advanced nanomaterials owing to the flexibility with which their physical–chemical properties can be controlled through size, shape, and compositional engineering in the synthesis stage and the versatility with which they can be implemented into technological applications in fields as diverse as optoelectronics, energy conversion/production, catalysis, and biomedicine. The use of microwave irradiation as a non-classical energy source has become increasingly popular in the preparation of nanocrystals (which generally involves complex and time-consuming processing of molecular precursors in the presence of solvents, ligands and/or surfactants at elevated temperatures). Similar to its now widespread use in organic chemistry, the efficiency of "microwave flash heating" in dramatically reducing overall processing times is one of the main advantages associated with this technique. This Review illustrates microwave-assisted methods that have been developed to synthesize colloidal inorganic nanocrystals and critically evaluates the specific roles that microwave irradiation may play in the formation of these nanomaterials.

From the Contents

1. Introduction

Since the discovery of the size-dependent behavior of nanoscale matter, colloidal inorganic nanocrystals (NCs), wet-chemically prepared crystalline particles made of a few hundred up to several thousand atoms, have developed more rapidly than other classes of nanomaterials owing to the high degree of control with which their properties can be tailored through geometric and compositional engineering in the synthesis stage and to the versatility with which they can be implemented into a number of technologically valuable applications.[1–20]

Two major reasons account for the exclusivity of NCs: the significant fraction of atoms residing at the surface, relative to the total number of atoms, and the restriction of charge carrier motion to a small space volume. Owing to these contributions, NCs exhibit unique chemical–physical responses that, for a given material composition, systematically correlate with size and shape, a feature prohibited to their bulk counterparts. For instance, owing to the relevant role of the free surface energy term in their formation, NCs exhibit lower melting points and can be easily trapped in metastable crystal phases.[2,3] In semiconductors, quantum confinement sets in once a critical dimensional threshold is crossed, determining a widening of the forbidden band gap and energy level discretization at the band edges, which affords size-tunable optical and electrical responses.[2,4–6] In noble metals, the decrease in NC size below the electron mean free path leads to collective oscillations (plasmons) of the itinerant conduction electrons at the particle surface, which transcribe into intense absorption bands in the visible to near-IR range.[2,4,7] Generally, the size-dependence of the NC electronic structure provides a tool for modulating the redox potentials of the relevant charge carriers,[2,7] while the dominance of high-energy facets and structural irregularities (e.g., edges, corners) at surface in NCs gives rise to improved or unprecedented catalytic activity.[2,8–11] Finally, NCs made of magnetic materials behave as single-domain magnets whose magnetization can be easily influenced by thermal fluctuations in the local environment, depending on the particle geometry and on a variety of surface effects.[11–14]

Colloidal NCs are generated from the reaction of molecular precursors (metal–organic compounds and metal–ligand complexes) in a liquid medium heated to a suitable temperature, often in the presence of some stabilizing organic agents, such as ligands and surfactants, soft templates (e.g., micelles), or coordinating solvents, which can regulate their growth.[11,15–21] As extracted from their growing mixture, NCs are individually recognizable free-standing particles made of a single- or polycrystalline domain with the desired chemical composition and geometry, which mostly dictates their distinctive properties. Depending on the synthetic route by which they are derived, NCs can also bear a monolayer of tightly surface-bound capping molecules that impart solubility and stability to the particles as well as govern their interactions with the environment.[11,17–21] The technological convenience of colloidal NCs over other nanostructures

[*] Dr. M. Baghbanzadeh, Prof. Dr. C. O. Kappe
Christian Doppler Laboratory for Microwave Chemistry and Institute of Chemistry, Karl-Franzens University Graz
Heinrichstrasse 28, 8010 Graz (Austria)
Fax: (+43) 316-380-9840
E-mail: oliver.kappe@uni-graz.at
Homepage: http://www.maos.net
Dr. L. Carbone, Dr. P. D. Cozzoli
National Nanotechnology Laboratory (NNL)—Institute Nanoscience—CNR
Via per Arnesano, 73100 Lecce (Italy)
E-mail: davide.cozzoli@unile.it
Homepage: http://www.nano.cnr.it
Dr. P. D. Cozzoli
Dipartimento di Ingegneria Dell'Innovazione, Università del Salento (Italy)

stands within their robustness and amenability to be richly functionalized and transferred to disparate applications without substantial loss of their native properties, and the ease with which they can be produced on the milligram-to-gram scale with uniform and programmable features meeting specific functional requirements.[1,2,4,5,7–14,18,22–35] As of today, NCs with controlled sized and shapes[11,17,19–21] not only represent model systems for the study of new phenomena in nanostructured solids,[2,4,5,7–10,13,14,22–24] but also serve as building blocks for the bottom-up development of artificial functional materials,[11,25–28] key active elements in miniaturized devices,[29–31] and novel platforms on which innovative concepts in magneto-optoelectronics,[5,11–13,32–34] biomedicine,[11,19,20,35] and catalysis[1,2,7–11,19,20] are being founded.

More recently, in response to the growing demand for multifunctional colloidal objects with enhanced and/or diversified capabilities, nanochemistry research has oriented efforts toward the realization of sophisticate multicomponent heterostructured NCs, broadly termed hybrid nanocrystals (HNCs).[15,16,19,20,36] These are individually addressable composite particles that embody two or more distinct size-/shape-tailored material domains epitaxially interconnected through bonding interfaces in concentric or eccentric core–shell ("onion-like") geometries or phase-segregated oligomer-like architectures. Owing to their structural complexity HNCs act as "smart" encounter platforms where various nonhomologous properties can coexist and exchange-couple, leading to increased functionality, modified or amplified chemical–physical responses, or even emergence of entirely new properties, which are expected to open up further technological opportunities in disparate application fields.[15,16,19,20,36–38]

Wet-chemical approaches have proven to be among the most versatile and effective routes to finely tailor NCs with varying compositional and architectural complexity. Practically, the synthesis of colloids require judicious selection of a few experimental conditions, such as the type of precursors, catalysts, templates, seeds, and organic stabilizers, regulation of their relative concentration ratio by appropriate reactant delivery techniques, and suitable modulation of temperature along the synthesis course.[11,15–17,19–21] A wealth of mechanistic studies, supported by detailed structural investigations, has allowed rationalizing how cautious adjustment of the aforementioned parameters transcribes into control over a number of complex thermodynamic factors and kinetic processes occurring during NC formation, including solution supersaturation, relative polymorph stability, homogenous/heterogeneous nucleation, reactant diffusion, selective surface adhesion of organic species, crystal oriented attachment, and crystallographic-direction-differential lattice development rates. On the basis of such knowledge, useful guiding criteria to realize size, shape and compositional control have been delivered and extensively discussed in several outstanding Reviews.[11,15–17,19–21,36]

However, progress in wet-chemical fabrication is still far from being exhausted and elaborate reaction strategies, on one side, and innovative practical tools, on the other side, have to be sought to reach an increasingly refined level of synthetic ingenuity. To date, most of synthetic development and related mechanistic investigations have mainly considered the impact of chemical parameters and processes on the features of the resulting NCs, while the effects of purely "physical" conditions or perturbations, such as the presence of externally applied electric or magnetic fields,[19,20,39–44] exposure to ultrasound or electromagnetic waves, such as UV/Vis light[11,20] or microwave (MW) irradiation,[45–47] geometry and dimensions of reactors,[48–59] and techniques of reactant delivery and mixing[50–64] have been largely overlooked, and therefore their rational exploitation in NC synthesis remains rather sparse.

Only recently, the ability to realize controllable thermal activation of NC synthesis by means of MW irradiation in place of conventional convective heating has been recognized to be an important prerequisite to better regulating NC formation and enhancing product quality and yield, and has therefore become subject of renewed fundamental and technological interest.[45,46] The use of MW irradiation utilizing modern dedicated MW reactors specifically designed for chemical applications now allows an exquisite control and exact on-line determination of the reaction temperature and pressure inside the reaction vessel, a scenario that, in most instances, is not realized using conventional heating principles. Since the preparation of inorganic NCs often involves complex and time-consuming processing routes at elevated temperatures, the generally very rapid heating of precursor solutions achieved by MW irradiation has proven to be

C. Oliver Kappe is Professor of Organic Chemistry and Director of the Christian Doppler Laboratory for Microwave Chemistry (CDLMC) at the University of Graz, Austria. He received his diploma and his doctoral degree in organic chemistry there (1992). After periods of postdoctoral research at the University of Queensland in Brisbane, Australia and at Emory University in Atlanta, USA, he moved back to the University of Graz in 1996. He obtained his "Habilitation" in 1998 and was appointed Associate Professor in 1999. Since 2011 he holds the position of Professor of "Technology of Organic Synthesis" at the University of Graz.

P. Davide Cozzoli received his MSc degree in chemistry in 1999 and his PhD in 2004 from the University of Bari, Italy. His PhD research was partially carried out at the University of Hamburg, Germany. From 2004 to 2005 he was a postdoctoral fellow at the University of Bari and from 2005 to 2007 a Junior Researcher at the National Nanotechnology Laboratory (NNL) of CNR-INFM, Lecce, Italy. Currently, he is a Senior Staff Researcher at the Faculty of Industrial Engineering of the University of Salento, Lecce, Italy, and leads the Nanochemistry Division of NNL, Institute Nanoscience as a CNR Associate Researcher. He is an Associated Editor for "Science of Advanced Materials" and "Journal of Nanoengineering and Nanomanufacturing".

particularly valuable. Apart from the aforementioned benefits, there have been a number of circumstances reported in the literature under which specific interactions of the electromagnetic field with either precursors, intermediates or the NCs themselves, have been proposed to play a key role in the formation of NCs under MW conditions.

In this Review, wet-chemical strategies that have been developed to synthesize NCs and HNCs will be discussed, keeping a focus on those which have exploited MW irradiation as an alternative means of providing heat. Recent advances in this rapidly growing field will be summarized with an emphasis on discussing the specific advantages that result from the use MW dielectric heating for NCs synthesis. A critical discussion on genuine MW effects underlying NC/HNC formation and quality features will also be given.

2. Microwave-Assisted Synthesis of Nanocrystals: General Concepts

2.1. Microwave Chemistry: Basic Principles

In the past two decades, the use of MW energy to heat chemical reactions has attracted a considerable amount of attention, owing to its successful application in organic/peptide synthesis, polymer chemistry, material sciences, nanotechnology, and biochemical processes.[65,66] In many circumstances, the use of MW dielectric heating as a non-classical energy source has been shown to dramatically reduce processing times, increase product yields, and enhance product purity or material properties compared to conventionally processed experiments.[65,66]

Until recently, heating chemical transformations on a laboratory scale has typically been performed using isomantles, oil baths, or hot plates, in many instances applying a reflux set-up whereby the highest reaction temperature achievable is dictated by the boiling point of the solvent. This traditional form of heating is a rather slow and inefficient method for transferring energy to a reaction mixture, since it depends on convective currents and on the thermal conductivity of the various compounds or materials that have to be penetrated, and often results in the temperature of the reaction vessel being higher than that of the reaction solution. In contrast, MW irradiation realizes efficient internal "in core" volumetric heating (that is, the temperature is raised uniformly throughout the whole liquid volume) by direct coupling of MW energy to the molecules that are present in the reaction mixture.[65,66]

MW irradiation triggers heating by two main mechanisms, namely dipolar polarization and ionic conduction. Whereas the dipoles in the reaction mixture (for example, polar solvent molecules or reagents) are involved in the dipolar polarization effect, the charged particles in a sample (usually ions) contribute to ionic conduction. When irradiated at MW frequencies, the dipoles in the sample align in the direction of the applied electric field. As the electric field oscillates, the molecular dipoles accordingly attempt to re-align themselves along the alternating electric-field streamlines and, in such process, energy is lost in the form of heat through molecular friction and dielectric loss (dielectric heating).[67] The amount of heat generated by this process is directly related to the ability of the dipoles to align itself with the frequency of the applied field. If the dipole does not have enough time to realign (high-frequency irradiation) or reorients too quickly (low-frequency irradiation) with the applied field, no heating will occur. The allocated frequency of 2.45 GHz available in all commercial systems lies in between these two extremes and gives the molecular dipoles enough time to align in the field, but does not permit them to follow the alternating field precisely.

Similarly, in ionic conduction, as the dissolved charged particles in a sample (usually ions) oscillate back and forth under the influence of the MW field, they collide with their neighboring molecules or atoms. These collisions cause agitation or motion, creating heat. These ion conductivity pathways provide a much stronger heat-generating capacity than the dipolar rotation mechanism. These effects are particularly evident when considering the heating behavior of ionic liquids in a MW field.[68,69]

The ability of a specific material or solvent to convert MW energy into heat at a given frequency and temperature is determined by the so-called loss tangent ($\tan\delta$). The loss factor is expressed as the quotient $\tan\delta = \varepsilon''/\varepsilon'$, where ε'' is the dielectric loss, indicative of the efficiency with which the electromagnetic radiation is converted into heat, and ε' is the dielectric constant describing the polarizability of molecules in the electric field.[67,68] In general a reaction medium with a high $\tan\delta$ at the standard operating frequency of a MW reactor (2.45 GHz) is required for good absorption and, consequently, for efficient heating.[66–68] Overall, solvents used in MW chemistry can be classified as high- ($\tan\delta > 0.5$), medium- ($\tan\delta \approx 0.1$–0.5), and low-absorbing ($\tan\delta < 0.1$; Table 1).[69] As for NC synthesis, solvents covering the whole spectrum of MW absorptivity have been used, ranging from strongly (e.g., ionic liquids, ethylene glycol) and moderately absorbing solvents (e.g., water, *N*-methylpyrrolidone, benzyl alcohol) to nearly MW transparent media (e.g., nonpolar alkanes or alkenes). In the latter cases, polar additives, such as ionic liquids or passive heating elements made out of strongly MW-absorbing materials, can be

Table 1: Loss tangent ($\tan\delta$) values for different solvents.[a]

Solvent	$\tan\delta$	Solvent	$\tan\delta$
ethylene glycol	1.350	DMF	0.161
Ethanol	0.941	1,2-dichloroethane	0.127
DMSO	0.825	Water	0.123
2-propanol	0.799	Chlorobenzene	0.101
formic acid	0.722	Acetonitrile	0.062
Methanol	0.659	Acetone	0.054
1,2-dichlorobenzene	0.280	Tetrahydrofuran	0.047
NMP	0.275	Dichloromethane	0.042
[bmim]PF_6[b]	0.185	Toluene	0.040
acetic acid	0.174	Hexane	0.020

[a] Data recorded at 2.45 GHz and 20 °C. [b] [bmim][PF_6] = 1-butyl-3-methylimidazolium hexafluorophosphate. NMP = *N*-methyl-2-pyrrolidone. Data from Ref. [71].

purposely used to increase the absorbance level of otherwise low-absorbing reaction media.[70]

It is important to note that the dielectric properties of most solvents (and other materials in general) vary significantly as a function of the temperature. For example, ethanol is a rather strong MW absorber at room temperature with $\tan\delta = 0.941$. At 100 °C, the $\tan\delta$ of ethanol has already dropped to 0.270, and at 200 °C is 0.080.[71] The reason is that at 2.45 GHz most organic solvents, such as ethanol, are heated primarily by the dipolar polarization mechanism, hence their ability to absorb MW irradiation decreases with increasing temperature as the reduced bulk viscosity leads to reduced molecular friction. In contrast, the ionic liquid 1-butyl-3-methylimidazolium hexafluorophosphate ([bmim][PF_6]) is heated by an ionic conduction mechanism, so its ability to absorb microwaves increases with increasing temperature.[67] The $\tan\delta$ of [bmim][PF_6] rises sharply from 0.185 at 20 °C to 1.804 at 100 °C and 3.592 at 200 °C.[71] Therefore, ionic liquids are extreme MW absorbers at higher temperatures, which makes accurate temperature measurement and reaction control using MW heating difficult.[72]

In addition to the effects of the electric-field component of MW irradiation on materials described above (polarizability or permittivity, ε', and dielectric loss or complex permittivity, ε''), the impact the associated magnetic-field component should be taken into account when magnetic materials are MW-exposed.[73] In this case the corresponding terms are the permeability, μ', and the magnetic loss factor, μ'', where μ'' represents the magnetic loss arising from relaxation and resonance processes under the influence of an alternating magnetic field. Although largely irrelevant for organic/polymer chemistry, the effects of the magnetic-field component may be of importance for MW-assisted NC synthesis, in those circumstances in which NCs of magnetic materials are involved (Section 3).

For inorganic solid-state materials the situation can indeed be rather complex. The mechanisms by which microwaves can couple to a material and the associated energy be subsequently dissipated out of the system can be largely different and difficult to ascertain unambiguously, although they show different dependencies on certain parameters, such as, sample type and microstructure, frequency and temperature. The two main loss mechanisms for non-magnetic materials are based on dipolar and conduction losses.[68,73–75] Dipolar losses dominate in dielectric insulators, while conduction losses prevail in metallic, high-conductivity materials. For example, it is well known that most metals and some metal oxides in a powder form can be heated very efficiently by MW irradiation through coupling to the electric and/or the magnetic component of the MW field.[73] In these strongly conducting or often semiconducting materials MW irradiation induces a flow of electrons (eddy currents) on the surface, which can heat the material through resistance (ohmic) heating mechanisms.[68] For micrometer-sized metal powders suspended in solvents arcing phenomena may occur under certain experimental conditions, these effects being critically dependent on particle size and morphology.[74,75] Magnetic materials also exhibit conduction losses with additional magnetic losses due to hysteresis, domain-wall resonance and electron-spin resonance mechanisms. Although the inherent MW absorption properties of various types of NC powders and solid-state nanocomposite systems are becoming the subject of increasingly detailed investigation,[76] little reliable experimental data have been published regarding the selective MW-driven heating of metal or metal oxide NCs in solution phase (see Sections 3 and 4).

On a typical laboratory scale (less than 20 mL reaction volume), rapid in-core volumetric heating can occur without significant temperature gradients if efficient agitation is ensured,[77] and the temperature is monitored/controlled by fast-responding internal probes.[72,77] The very rapid heating and sometimes extreme temperatures observable in sealed-vessel MW chemistry make it apparent that, on the basis of the Arrhenius law [$k = A\exp(-E_a/RT)$], transformations that require several hours when performed in a solvent at reflux temperature, may reach completion in a few minutes or even seconds using "superheated" solvents in a sealed vessel, autoclave-type, MW reactor.[67,78] These unique features explain the growing popularity of this non-classical heating method in many different fields of chemistry, including the generation of nanomaterials.[65,66]

Since the early days of MW synthesis, the observed reaction rate accelerations and sometimes altered product distributions, compared to those achieved in oil-bath experiments, have led to speculation on the existence of so-called "specific" or "non-thermal" MW effects.[79] Historically, such effects were invoked when the outcome of a synthesis performed under MW conditions was remarkably different from that achieved for the conventionally heated counterpart at the same nominal temperature. On reviewing the current literature it appears that today most scientists agree that in the majority of cases the observed rate enhancements should originate from a purely thermal/kinetic effect, that is, a consequence of the high reaction temperatures that can rapidly be attained when irradiating polar materials in a MW field (see above).[65,66,80,81]

In addition to the aforementioned thermal/kinetic effects, MW effects that are caused by the uniqueness of the MW dielectric heating mechanisms must also be considered. These effects should be termed "specific MW effects", being defined as *rate accelerations that cannot be achieved or duplicated by conventional heating, but are essentially still thermal effects*.[68,80] This category includes, for example: 1) the "superheating" effect of solvents at atmospheric pressure;[80] 2) the selective heating of strongly MW-absorbing heterogeneous catalysts or reagents in a comparatively less polar reaction medium;[80] and 3) the elimination of wall effects caused by inverted temperature gradients.[82] It should be emphasized that rate enhancements falling under this category are essentially still a result of a thermal effect (i.e. a fast and significantincrease in temperature, not otherwise attainable by standard convection heating methods), although it may be difficult to experimentally determine the exact reaction temperature. In contrast, some authors have suggested the possibility of "non-thermal MW effects" (also referred to as athermal effects). These should be classified as *rate accelerations that can be rationalized by neither purely thermal/kinetic nor specific MW effects*.[68,80] Essentially, non-

thermal effects are supposed to result from direct interaction of the MW electric field with specific molecules in the reaction medium, which is not connected to a macroscopic temperature effect. It has been argued, for example, that the presence of an electric field leads to orientation effects of dipolar molecules and, hence, to a change of the pre-exponential factor A or the activation energy (entropy term) in the Arrhenius equation.[79] Furthermore, a similar effect should be observed especially when polar reaction mechanisms are involved, whereby the polarity is increased on going from the ground state to the transition state along the reaction coordinate, resulting in enhancement of reactivity by lowering of the activation energy.[79] As of today, MW effects are still the subject of intense debate and controversy. It remains uncertain as to whether the claimed unique outcome of MW irradiation on chemical reactions derives from misinterpretation of the experimental evidence, mostly related to artifacts connected to temperature measurement, rather than transcribing genuine MW effects.[72,77–79,83] Some of the current theories regarding the involvement of MW effects in NC formation will be discussed in Section 4.

2.2. MW Heating in the Synthesis of Colloidal Nanocrystals

In a typical colloidal preparation, suitable molecular precursors (e.g. organometallic compounds, metal salts, metal-ligand complexes) bearing the atomic elements necessary to build up the NC lattice are induced to react or decompose in a solution that contains specific functional organic species (coordinating solvents, ligands and/or surfactants) or additives (e.g., preformed crystalline seeds, metal nanoparticle catalysts) under controlled atmosphere and selected temperature and pressure conditions. Once the synthesis is initiated, highly reactive intermediate species are generated, commonly referred to as the "monomers", which induce the nucleation of NCs once a critical supersaturation threshold is surpassed, and sustain their subsequent enlargement.

The ability to govern the balance of nucleation and growth processes in liquid media is at the basis of the formation of uniform NCs with predetermined structural, compositional and geometric features and, consequently, precisely size-correlated properties. To achieve this goal key, often indispensible ingredients in the reaction environment are represented by suitable coordinating solvents, ligands and/or surfactants, which are capable to act as both reactivity moderators[11,17,18] and colloidal stabilizing agents.[15,16,19,21] These molecules can play several important roles during the synthesis, for example, by participating in chemical pathways as reactants themselves, complexing with the evolving monomers, forming dynamic soft templates that can pose physical constraints on uncontrollable NC enlargement, or by directly binding to the NC surface to impart kinetic stabilization against uncontrollable flocculation.

NC syntheses can be roughly categorized in two broad classes, depending on the main typology of experimental set-up by which they are accomplished.

The first class of procedures is ambient-pressure syntheses. These are carried in three-neck round-bottom glass flasks, connected through a reflux condenser to a conventional Schlenk line set-up. The flasks are equipped with mechanical or magnetic stirring bars, and heated up under controlled atmosphere to 50–380 °C with convective heating systems, such as electrically supplied isomantles or oil baths, which transfer heat by direct exchange contact. The temperature can be adjusted with an accuracy of ± 5 °C by a feedback system which senses the status of the liquid reaction mixture by an immersion probe that may be directly dipped into the reaction mixture. This set-up is extremely versatile, since it allows for the withdrawing aliquots of the growing NC mixture (e.g., through a syringe inserted through one of the rubber-sealed necks of the flask) for real-time monitoring the synthesis course without the reaction course being significantly disturbed.

Alternatively, the flask may be heated in a domestic MW oven, in which remote temperature control as well as stirring of the solution may be hard to implement. This set-up configuration is most practicable only in those cases in which the reaction initiation does not require harsh and/or precisely determined thermal conditions and can be safely performed under air. As a further limitation, monitoring the reaction course typically requires temporary interruption of MW irradiation to permit extraction of reaction portions. In general, the use of domestic MW ovens or dedicated MW reactors designed for open-vessel usage can be expected to lead to only minor advantages compared to existing classical ambient pressure methods (see above), apart from perhaps the possibility to heat the reaction mixture faster to the desired target (reflux) temperature.

The second category of syntheses involves high-pressure reactions. These are carried in tightly sealed closed vessels, such as stainless steel autoclaves (with inner Teflon liners) that may be heated either in ovens or via inner resistive heating systems. Temperatures as high as 250–300 °C and pressure of the order of 100–350 atm can be reached, however real-time reaction product monitoring clearly remains prohibited.

In light of the technical aspects highlighted above it appears clear that most MW irradiation experiments have been so far limited to syntheses based on simple one-pot, single-step heating-up schemes, whereby all reagents are present in the starting reaction mixture and heated up to a target temperature. It has not been possible to exploit the classical "hot-injection" technique for delivering precursors as a means of separating the nucleation and growth stages, or to perform sequential addition of selected reactants to the growing NCs to improve their size distribution and/or to propel anisotropic development (see Section 2.3). Therefore, any comparison between MW-assisted and conventional convectively heated NC syntheses is far from being straightforward, especially in those cases in which adequate stirring may not be guaranteed, temperature is neither precisely adjustable or known, and/or continuous monitoring of NC growth evolution is prohibited.

Although many of the early pioneering experiments in MW-assisted chemistry, including the generation of NCs, have

been carried out in domestic MW ovens, a recent trend is undoubtedly to use dedicated single-mode sealed-vessel MW reactors specifically designed for synthetic applications.[65] These instruments feature built-in magnetic stirrers, direct temperature control of the reaction mixture with the aid of internal fiber-optic probes or external infrared sensors, and software that enables on-line temperature/pressure control by regulation of MW power output. An example is shown in Figure 1.[68]

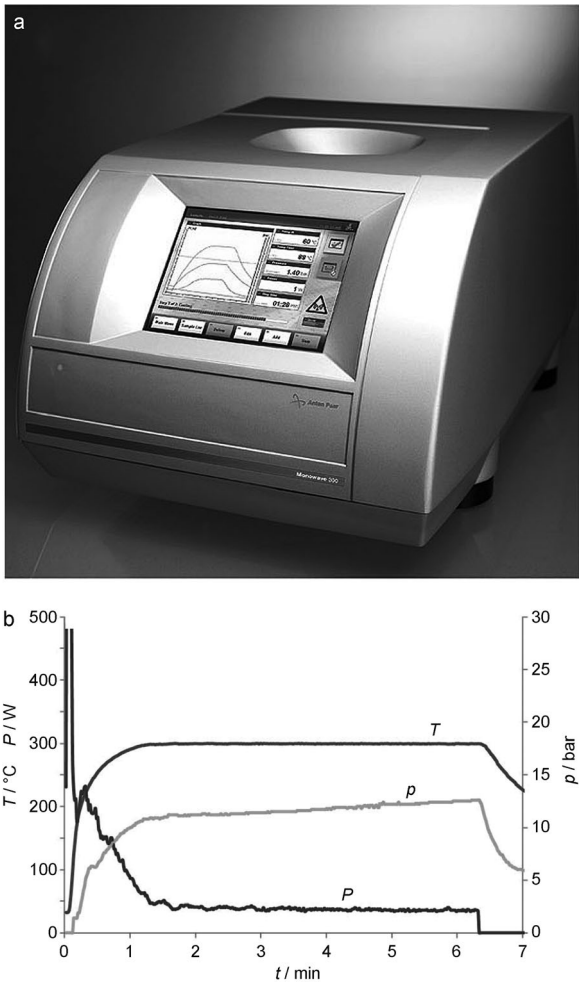

Figure 1. a) Photograph of a single-mode microwave reactor (Monowave 300, Anton Paar GmbH, Austria) capable to operate at up to 850 W magnetron power and equipped with a dual internal/external temperature monitoring system. b) Temperature (*T*), pressure (*p*), and power (*P*) profiles recorded for a 3 mL sample of ethylene glycol MW-heated under sealed-vessel conditions to 300 °C in the Monowave300 reactor. For the sake of clarity only the internal fiber-optic probe temperature profile is shown and the *y*-axis has been cut at 500 W.

While a variety of different MW reactors and processing options are available today, the majority of all currently published MW chemistry protocols involving nanomaterials rely on the use of so-called single-mode MW reactors in combination with sealed vessel processing. Sealed vessel MW processing allows reaction mixtures to be heated very rapidly to temperatures far above the boiling point of the solvent under atmospheric conditions. With modern instrumentation reaction temperatures of 300 °C at 30 atm maximum pressure can be attained on a routine basis (Figure 1b).[72,81] Furthermore, efficient gas-jet cooling at the end of the irradiation/heating cycle can be used to decrease temperatures back to ambient conditions within a few minutes (thermal quenching). As an alternative to batch MW processing, continuous flow/microreactor set-ups heated by MW irradiation have recently also been applied to the synthesis of NCs.[84–87]

2.3. Nanocrystal Formation Mechanisms under MW Irradiation

2.3.1. Size Control

Mechanistic studies and theoretical modeling have shown that satisfactory control over the dimensions and size variance of colloidal NCs can be achieved if a discrete, that is, time-limited, nucleation event quickly relieves the solution supersaturation and subsequent growth of the initially formed embryos takes places under a relatively high and nearly constant diffusion-limited flux of monomers. As long as the solution chemical potential exceeds a certain threshold required to guarantee the thermodynamic stability of the tiniest particles, all NCs will be allowed to evolve to progressively large dimensions, with the overall size distribution of the population narrowing or broadening over time (so-called size "focusing" and "defocusing" regimes, respectively) depending on the time evolution of the residual monomer concentration. Eventually, Ostwald ripening may set in at long reaction times, leading to dissolution of NCs smaller than the "critical size" and, consequently, providing extra monomers to sustain the growth of the larger NCs.[20,21,88] As MW-assisted syntheses are most commonly based on one-pot, single-step schemes, in the absence of coarsening the relative extent of monomer consumption between the nucleation and the growth stages will dictate the final NC size ultimately achievable for a given amount of precursors introduced into the reaction environment.[20,21,88] These dynamics are schematically illustrated in Figure 2. The higher the concentration

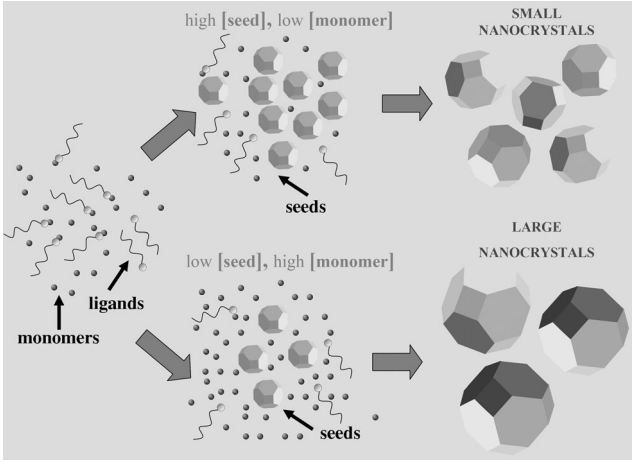

Figure 2. Schematic representation of the most common mechanism of size control realized in MW-assisted colloidal nanocrystal synthesis (in the absence of Ostwald ripening or aggregation phenomena) by one-pot, single-step reaction schemes.

of cluster nuclei that are generated (due, for example, to a fast, intense nucleation burst at high supersaturation levels), the lower the monomer concentration left to feed such seeds, which will therefore only grow to relatively small dimensions. The situation will be reversed if a slow, limited nucleation event produces a low concentration of crystal embryos, which will consequently evolve to proportionally larger NCs.

The different dependence of the nucleation and growth processes on the temperature and monomer concentration, respectively, allows their relative balance to be governed by suitably programming reactant delivery (e.g., by the so-called "hot-injection" technique[19–21,63,88]), by profiting from the particular reactivity of the system (e.g., from a "delayed" nucleation event[88,89]), or by exploiting digestive ripening.[19,21,90]

Because of the inherent constraints imposed by current MW equipment, the "heating-up" method, whereby all the reagents and precursors are co-mixed at ambient temperature and then progressively heated up to a target level, is the almost exclusively applied technique in MW-assisted NC syntheses (note that MW irradiation allows much more rapid heating ramps, compared to those normally achievable by conductive heating systems, see Figure 1 b). This "heating-up" scheme is especially effective in those colloidal environments in which reaching the critical supersaturation threshold is the rate-limiting step.[88,89] This is realized when the monomers are intermediates species that accumulate gradually upon slow reaction or decomposition of relatively stable surfactant (or ligand)-precursor complexes. The combination of a retarded nucleation burst with a fast growth process characterized by a self-catalytic behavior can lead to the desired temporal separation of the nucleation and growth stages, followed by a size-focusing development regime. However, these conditions, which are crucial prerequisites to achieving size monodispersity, may be fulfilled only for relatively few reaction systems.

Increasingly larger NCs with appreciably tight size variances can be synthesized by performing multiple seeded-growth steps in which preformed NCs with selected size, synthesized in a previous independent phase, are combined with calibrated amounts of extra precursors in appropriately composed reaction environments.[20,88] The seeding approach transcribes a simple basic principle of the classical nucleation theory (CNT), according to which the activation energy barrier for the growth of pre-existing NC seeds is much lower than that required to induce homogenous nucleation of new particle embryos from scratch.[20] Alternatively, digestive ripening can be deliberately boosted once the monomer concentration has been depleted to a sufficiently low level, at which selective dissolution of the smallest, most unstable nanoparticles is likely to take place.[19,21,90] Several cases of exploitation of the mechanisms described above can be found in MW-assisted NC synthesis (see Section 3).

2.3.2. *Shape Control*

While crystallization in low-symmetry lattices generally represents a prerequisite to promoting shape deviations in NCs, several circumstances can potentially interrupt isotropic growth evolution, leading to the formation of NCs with anisotropic morphologies as diverse as nanorods, wires, bullets, platelets, ellipsoids, polypods and rings, often under far-from-equilibrium kinetically overdriven growth conditions.[19–21,91] The most common MW-assisted colloidal approaches to shaped NCs, shown in Figure 3, exploit one or more of the following pathways:

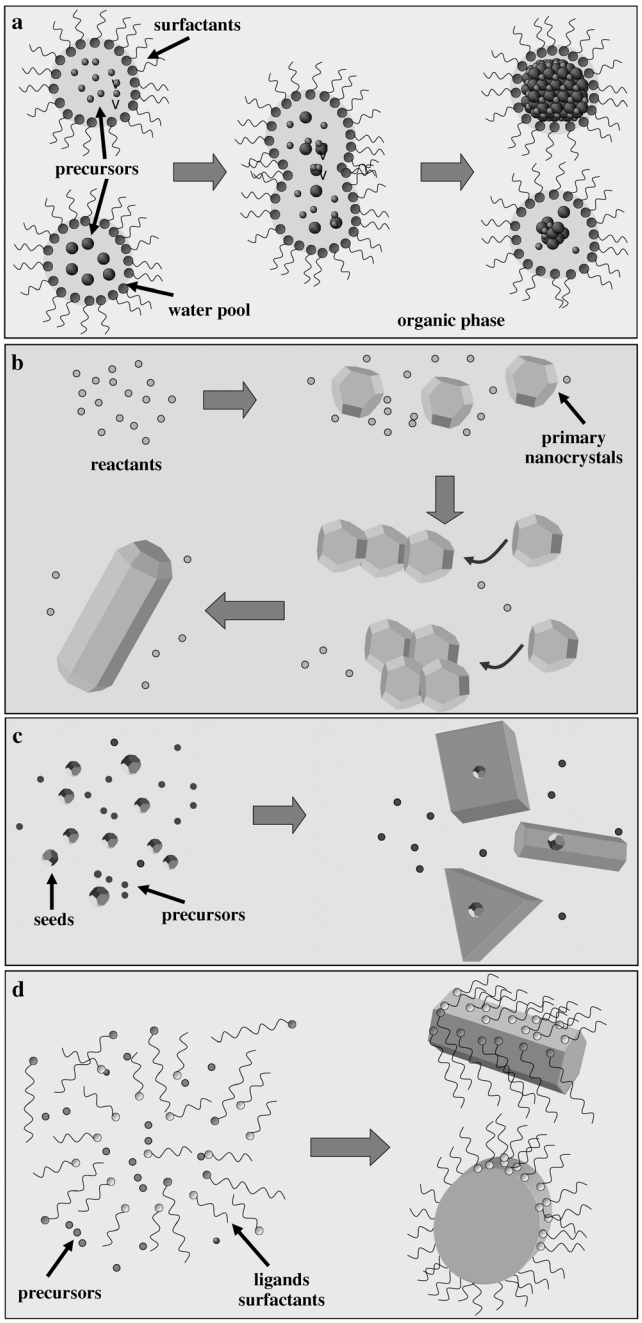

Figure 3. The most common mechanisms underlying the formation of shape-controlled single-material nanocrystals in MW-assisted colloidal synthesis: a) growth confined in micelles; b) crystal-oriented attachment; c) seed-catalyzed growth; d) evolution by facet-preferential ligand/surfactant adhesion.

a) Growth in micelles: A certain degree of size and shape modulation is achievable by performing chemical reactions inside (usually inverse) micelles, as the latter can indeed evolve from spherical into rod-like or cylindrical aggregates, as well as planar bilayers, depending on their formation conditions.[19–21,91,92] Cluster nucleation and growth take place upon fast exchange of the liquid content of the surfactant-stabilized micellar pools, in which precursors have previously been dissolved (Figure 3a). NCs evolving in such confined nanoscale environments can adopt morphologies resembling those of the templates themselves.[20,91]

b) Oriented attachment: This mechanism involves initial generation of nearly isotropic NCs in solution, which then tend to fuse epitaxially along well-defined crystallographic directions as a means to eliminating unstable sets of facets and, hence, lowering the overall surface energy (Figure 3b).[19–21] These pathways proceed effectively when the initial NCs are weakly passivated by organic ligands, so that dipole-induced inter-particle attractive forces and surface chemical reactivity may be enhanced and promote spontaneous one-directional NC attachment under mild conditions[19,20,91]

c) Seed-catalyzed growth: A powerful route to anisotropic growth is represented by seed-mediated reaction schemes.[19–21,91] In these approaches, preformed (usually spherical) NCs of rather tiny dimensions, referred to as the "seeds", are mixed with appropriate coordinating agents and molecular precursors suitable to generate either the same or a dissimilar material. The seeds behave as efficient substrates for catalyzing the formation of the target compound, which is thus initiated selectively at their surface (Figure 3c). This occurs because, according to the CNT, the energetic barrier that has to be overcome for the heterogeneous nucleation and growth of a secondary material onto a pre-existing condensed phase can be much lower than the energy cost required to trigger the generation of separate, free-standing crystal embryos via homogeneous nucleation.[20] As the seeds offer preferential sites for NC nucleation, the otherwise spherical growth symmetry of the NCs evolving out of the catalyst substrates can be easily interrupted. This mechanism can stimulate NC evolution into variable shapes, frequently regardless of the constraints imposed by their inherent crystal structure. Under the action of fast monomer addition and the concurrent operation of facet-selective adhesion of capping agents, such process can lead to development of nanorods, nanowires, platelets and branched nanostructures upon accentuation of crystal growth rate along selected lattice directions.[20,91]

d) Shaping assisted by surface adhesion of stabilizing molecules: For many materials, surfactants, polymers, ligands or coordinating solvents can be identified, which are able to adhere with different binding strengths to the exposed facets of the growing NCs, thereby inducing preferential development of the latter along those crystallographic directions which grow the fastest[19–21,91] (Figure 3d). In general, morphological evolution is a kinetically controlled process that occurs far from thermodynamic equilibrium when the system is propelled by high fluxes of monomers and a steep concentration gradient. Such conditions accentuate the growth rate of the most unstable facets that are usually protected less efficiently by the organic capping agents or are inherently more chemically reactive. In addition, high spatially inhomogeneous diffusion-limited monomer fluxes can induce extra growth instabilities that may propel faster crystal development out of high-energy corners and edges at the surface of the NCs formed in earlier synthesis stages.[19,20] In solvothermal routes a "solvent templating" mechanism has been invoked, according to which solvent-ion precursor complexes locally organize themselves along some preferred crystallographic directions of the initially generated NCs, thereby promoting their anisotropic growth.[11,19–21] On the other hand, at low concentration of monomers and at higher temperatures, thermodynamically controlled growth conditions may be approached, under which NCs may ultimately adopt isotropic shapes characterized by minimal surface energy.[19–21]

The surfactant-adhesion growth mechanism produces pronouncedly faceted NCs of symmetric-phase materials, whereas it leads to strongly anisotropic shapes, such as discs, rods, wires and either single-crystalline or polytypic polypod-/dendrite-like branched habits, when the NCs crystallize in low-symmetry structures.[19–21,91]

2.3.3. *Topology Control: Multimaterial Hybrid Nanocrystals*

The most recent developments of colloidal syntheses involve elegant extension of the techniques described in Section 2.3.1 and 2.3.2 to the fabrication of more elaborate multi-component hybrid nanocrystals (HNCs). The nanoheterostructures are individually composed of clearly distinguishable crystalline sections of different materials, which are arranged in complex core–shell or hetero-oligomer architectures by direct bonding (often epitaxial) junctions.[15,16,19,36] The most widely exploited classes of strategies to synthesize HNCs rely on variously modified seeded-growth schemes, which represent the solution-phase analogue of classical vapor-phase heteropitaxial deposition techniques. These approaches are conceptually similar to those used in seed-catalyzed growth for the preparation of anisotropically shaped single-material NCs, described in Section 2.3.2 In such schemes the domains that will compose the targeted HNCs are formed consecutively along programmed sequences of site-selective heterogeneous nucleation/growth events or induced crystal-oriented coalescence pathways that take place starting from relatively large NC seeds with tailored size and shape parameters. The surface-interface energy balance dictating the ultimate heterostructure topology will depend on the complicate interplay of disparate kinetic processes and thermodynamic circumstances, such as material miscibility, atomic diffusivity, facet-dependent chemical reactivity of the relevant seeds, and insurgence of lattice strain at the heterojunction regions.[36] To date, attempts to exploit MW irradiation in HNC synthesis have exclusively led to sparse examples of bi-component core–shell configurations based on combinations of either metals or non-oxide semiconductors, respectively (see Section 3).

Such core–shell systems are usually built of materials characterized by a close structural similarity, which favors

good epitaxial deposition of the outer shell and consequent healing of structural effects and/or dangling bonds on the pristine core surface. Figure 4 summarizes the two main preparative schemes by which core–shell HNCs have been obtained in MW-assisted synthesis: a) two-step syntheses, whereby the deposition of the secondary material layer takes place onto preformed NC seed "cores", prepared in an independent synthesis in a different environment (Figure 4a); b) one-pot methods, whereby the core and shell sections are formed at distinct times and/or temperatures in the same liquid medium starting from mixtures of the respective precursors and/or stabilizers with largely differing chemical reactivities (Figure 4b).

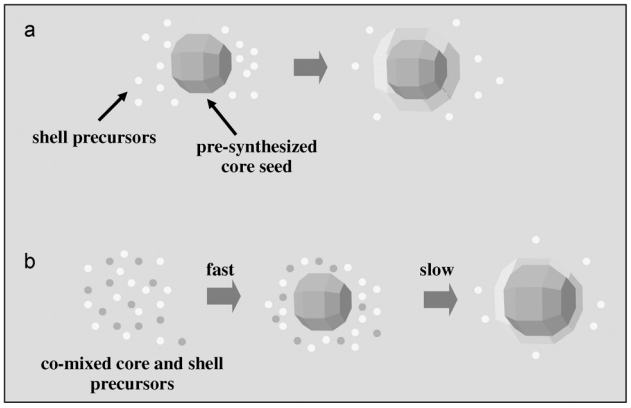

Figure 4. The most common mechanisms underlying the formation of bi-material heterostructured core–shell nanocrystals in MW-assisted colloidal synthesis: a) direct heterogeneous nucleation and growth of the shell material onto preformed nanocrystal seeds; b) temporally separated core and shell formation in one-pot reaction systems.

3. Examples of Microwave-Assisted Nanocrystal Syntheses

3.1. Metals

NCs of coinage and magnetic transition-metals are one of the most fascinating classes of inorganic nanoscale solids, as they exhibit a wide variety of structure-related chemical, optical, electrical and magnetic properties that render them emerging key materials for catalysis, imaging, sensing, and development of advanced spectroscopy techniques.[7,93–95] MW-assisted wet-chemical fabrication of metal NCs features one of the pioneering examples of MW exploitation in NC preparation.[96] As for what concerns reaction selectivity, product yield, and energy saving, the employment of MW irradiation as heat source has been demonstrated or indirectly suspected to provide unique effects and advantages, such as fast heating and attainment of high pressure levels in sealed vessels, "superheating" of solvents above their boiling point or of the growing nanostructures, generation of "hot spots", namely high-reactivity regions at the liquid/solid interfaces of pre-existing particles capped with large dielectric-loss-constant surfactants (see Section 4).[97,98] In the following Sections, the synthesis of the main families of metallic NCs under MW irradiation will be described through illustration of the most significant reports in the field. Relevant reaction parameters, formation mechanisms, and NC product quality features (size, shape, size/shape variances) are summarized in Table 2. Selected transmission electron microscopy (TEM) and high-resolution TEM examples can be found in Figure 5 and Figure 6.

3.1.1. Single-Metal NCs

Especially, MW-assisted syntheses of Ag and Au NCs, both of which form in a face-centered cubic (fcc) crystal structure with very similar lattice constants and exhibit remarkable size- and shape-dependent surface plasmon

Table 2: Synthesis of metal NCs under MW dielectric heating. The Table lists the main experimental conditions, size-morphological features of the resulting nanostructures, mechanistic pathways involved, and growth-governing factors.[a]

Metal	Precursors	Reaction type	Solvent additives	Formation Mechanism	Relevant NC features (morphology size, size variance)	Reaction time, temperature pressure	Ref.
Ag	$CH_3(CH_2)_nCO_2Ag$	alcohol-driven Ag^+ reduction	$CH_3(CH_2)_2OH$ None	1) ligand-controlled nucleation 2) *T*-dependent growth	spheres 4.9–7.4 nm $\sigma = 9$–12%	2–5 min 140–155 °C 1 atm	[107]
Ag Au Pt	$AgNO_3$ $H[AuCl_4]$ $H_2[PtCl_6]$	alcohol-driven $Ag^+/Ag^+/Au^{3+}/Pt^{4+}$ reduction	*t*BuOH, *i*PrOH, $CH_3(CH_2)_nOH$ PVA	1) ligand-controlled nucleation; 2) size enlargement by seeding steps	spheres 6–20 nm $\sigma = 9$–20%	< 1 min 64–82 °C 1 atm	[105,106,108]
Ag	$AgNO_3$	EG-driven Ag^+ reduction	EG PVP $H_2[PtCl_6]$	1) Pt-seeded nucleation 2) polymer-assisted shape evolution	rods/wires: 40–60 nm × 0.1–3 μm cubes: 40–50 nm $\sigma = 10$–30% (contaminating shapes)	2–8 min 198 °C 1 atm	[109,110]

Table 2: (Continued)

Metal	Precursors	Reaction type	Solvent additives	Formation Mechanism	Relevant NC features (morphology size, size variance)	Reaction time, temperature pressure	Ref.
Ag	$AgNO_3$	Na_3Cit-driven Ag^+ reduction	H_2O Na_3Cit Au seeds	1) Au-seeded growth 2) ligand-assisted shape evolution	nanorods 10–20 nm × 50–200 nm polydisperse	10 min 100 °C 1 atm	[100, 102]
Ag	$AgNO_3$	Na_3Cit (FA; PVP)-driven Ag^+ reduction	H_2O Na_3Cit/FA, PVP	ligand-assisted growth	spheres prisms 10–130/200–380 nm polydisperse	1–75 min 100 °C 1 atm	[99, 101]
Ag	$AgNO_3$	EG-driven Ag^+ reduction	EG PVP	polymer-assisted growth	irregular clusters 0.1–1.8 μm polydisperse	0.5–4 h 100–200 °C 1 atm	[111, 112]
Ag	$AgNO_3$	EtOH-driven Ag^+ reduction	EtOH PVP	polymer-assisted growth	spheres 10 nm polydisperse	5 s–60 min > 60–88 °C > 1 atm	[113, 114]
Ag Au	$AgClO_4$ $AgNO_3$ $H[AuCl_4]$	DMF/PVP-driven Ag^+/Au^{3+}reduction	DMF, Pyr, NMP PVP, β-CD NaOH or HCl	polymer-assisted growth	spheres 3–7 nm (20–30 nm, < 3%) σ = 25–30%	10 s–5 min (10 s pulses) 156 °C 1 atm	[116, 118, 119]
Ag	Ag_2O	dithiol-induced Ag_2O reduction	1,2-ethanedithiol None	ligand-assisted anisotropic growth	nanorods/nanowires 40–120 nm × 1–8 μm polydisperse	10 min 80–140 °C 1 atm	[148]
Ag	$AgNO_3$	EG-driven Ag^+ reduction	EG NaCl/PVP/O_2	1) polymer-assisted dissolution/deposition anisotropic growth 2) selective dielectric superheating	nanowires 40–50 nm × 4–12 μm σ = 5–10% (diameter)	3.5 min 170 °C 1 atm	[98]
Ag Fe Co Ni Pd Cu Ru Ir Rh FePt	$AgNO_3$ $Fe(acac)_3$ $Co(CH_3CO_2)_2$ $Ni(CH_3CO_2)_2$ $PdCl_2$ $CuSO_4$ $RuCl_3$ $H_2[IrCl_6]$ $RhCl_3$ $Fe(CH_3COO)_2$ $PtCl_2$	EG-driven metal-ion reduction	EG PVP PVP/DDA/TOP/OA PVP/NaH_2PO_4 NaOH	polyol-, polymer- and/or surfactant-assisted growth	faceted spheres irregular polyhedrons, rods, platelets 1–80 nm polydisperse	20 s–20 min (or MW cycles) 100–200 °C > 1 atm	[56, 86, 105, 126–134]
Ag	$AgNO_3$	EG-driven Ag^+ reduction	EG/toluene DDT	1) growth confined at liquid/liquid interfaces 2) ligand-assisted growth	spheres or cubes 10 nm σ = 5%	3 h 160–170 °C > 1 atm	[120]
Ag Pd Pt Au	$AgNO_3$ $Na_2[PdCl_4]/PdCl_2$ $Na_2[PtCl_6]/PtCl_4$ $H[AuCl_4]$	GSH-/sugar-driven $Ag^+/Pd^{2+}/Pt^{4+}/Au^{3+}$ reduction	H_2O GSH or sugars	ligand-assisted growth	spheres: 5–10 nm prisms/plates 1–4 μm polydisperse	30 s–5 min 34–60 °C 1 atm	[138, 140]
Ag	$AgNO_3$	CMC-driven Ag^+ reduction	H_2O NH_3 CMC	ligand-assisted growth	spheres > 5 nm σ = 10–20%	1–5 min reflux	[139]
Ag Au Pt Pd Cu Ni Ru Rh alloys	$Ag(CH_3CO_2)_2$ $H[AuCl_4]$ $PtCl_4$ $Pd(acac)_2$ $Cu(acac)_2$ $Ni(HCO_2)_2$ $RuCl_3$ $Rh(CH_3CO_2)_3$	DMF-/OLAM-/dioleamide-driven metal-ion reduction	none DMF, H_2O OLAM/OLAC	surfactant-assisted growth	spheres, cubes, polyhedrons 5–100 nm σ = 5–10%	1–35 MW cycles (30 s on/5 s off) < 150 °C 1 atm	[136, 137]

Table 2: (Continued)

Metal	Precursors	Reaction type	Solvent additives	Formation Mechanism	Relevant NC features (morphology size, size variance)	Reaction time, temperature pressure	Ref.
Ni	$Ni(CH_3CO_2)_2$	EG-driven Ni^{2+} reduction	EG $H_2[PtCl_6]$, PVP, DDA	1) Pt-seeded nucleation and growth of Ni 2) ligand-controlled growth	irregular polyhedrons 40–100 nm polydisperse	45 min 195 °C >1 atm	[151]
Ag	$AgNO_3$	EG-driven Ag^+ reduction	EG $H_2[PtCl_6]$/PVP	1) Pt-seeded nucleation and growth of Ag 2) polymer-assisted anisotropic growth 3) crystal-oriented attachment	spheres: 30–90 nm polyhedrons: 60–120 nm rods/wires:50 nm–1 μm polydisperse	2–7 min 198 °C 1 atm	[150]
Au@Ag	$H[AuCl_4]$ $AgNO_3$	EG-/DMF-driven Ag^{3+} and Ag^+ reduction	EG; DMF PVP NaCl	1) Au-seeded nucleation/growth of Ag shell 2) polymer-assisted shell shaping 3) selective oxidative etching of the shell	prisms, bipyramids, cubes, polyhdrons, plates, rods, wires 20–500 nm polydisperse	2–4 min (+ 3 h, 140 °C in oil bath) 198 °C 1 atm	[152–154]
Au@Pd	$H[AuCl_4]$ $PdCl_2$	EG-driven Au^{3+} and Pd^{2+} reduction	EG none	1) Au-seeded nucleation/growth of the Pd shell 2) polymer-assisted shell shaping	irregular spheres 12 nm polydisperse	MW cycles 21 s on/9 s off 198 °C 1 atm	[155]
Au	$H[AuCl_4]$	PAH-driven Au^{3+} reduction	H_2O PAH	1) Au-seeded growth; 2) polyelectrolyte-assisted growth and assembly	chain-like aggregates of ca. 22 nm spheres σ_{sphere} = 10–15 %	10–60 s 1 atm	[115]
Au	$H[AuCl_4]$	EtOH-driven Au^{3+} reduction	ethanol/*n*-heptane $CH_3(CH_2)_nNH_2$ NaOH	ligand-assisted growth	spheres 3–8 nm σ = 5–10 %	45 s 70 °C 1 atm	[135]
Au	$H[AuCl_4]$	EG-, PVP-, or DHN-driven Au^{3+} reduction	H_2O, EG, acetone PVP Na_3Cit//TOAB PVP/SDS MCl (M = H, Na, K) PPI G3 NaOH/TNMR CTAB	1) polymer- or ligand-assisted growth 2) selective oxidative etching	spheres, polyhedrons, prisms, platelets, rods 5–90 nm σ = 10–40 %	1–8 min 100–198 °C 1 atm	[97, 103, 117, 121–125]
Au	$H[AuCl_4]$	DNA-driven Au^{3+} reduction	H_2O DNA, EDTA	polymer-templated growth	nanowires 20 nm × 1–3 μm polydisperse	3 min (intermittent) <100 °C 1 atm	[149]
Au, Ag alloys	$AgNO_3$ $H[AuCl_4]$	N_2H_4/Na_3Cit-driven reduction	H_2O PAA Na_3Cit or N_2H_4	polymer-assisted growth	aggregated spheres 5–50 nm polydisperse	1–10 min <100 °C 1 atm	[104]
FePt FePd	$Pt(acac)_2$ $Pd(acac)_2$ $Na_2[Fe(CO)_4]$	$Na_2[Fe(CO)_4]$ driven Pt^{2+}/Pd^{2+} reduction	*n*-nonadecane dioctyl ether OLAM, OLAC	surfactant-assisted growth	spheres 2.5–8 nm σ = 5–10 %	<6 min 130–215 °C <17 atm	[141]
Pt, Pd on carbon	$K_2[PtCl_4]$ $Na_2[PdCl_4]$ $[\{(\eta\text{-}C_2H_4)PtCl_2\}_2]$ air N_2/H_2	MW-promoted H_2-driven Pt^{4+}/Pd^{2+} reduction	none	solventless solid-state reduction	spheres 3–9 nm	MW cycles 10–30 s on/45 s off 390–545 °C 1 atm	[147]
PtNi on carbon	$K_2[PtCl_4]$ $NiCl_2$ carbon	N_2H_4-driven Pt^{4+}/Ni^{2+}reduction	H_2O N_2H_4 NaOH/PVP	1) Pt-seeded nucleation and growth of PtNi; 2) polymer-assisted growth	spheres 3–6 nm polydisperse	10 min 60 °C 1 atm	[145]

Table 2: (Continued)

Metal	Precursors	Reaction type	Solvent additives	Formation Mechanism	Relevant NC features (morphology size, size variance)	Reaction time, temperature pressure	Ref.
Pt, Ru on carbon	$H_2[PtCl_6]$ $RuCl_3$	EG-driven Pt^{4+}/Ru^{3+} reduction	EG KOH	carbon-seeded nucleation	spheres 2–3 nm polydisperse	50 s 160–170 °C 1 atm	[146]
Rh, Pd or Pt on ZrO_2	$RhCl_3$ $PdCl_2$ $PtCl_4$ ZrO_2	EtOH-/ZrOH-driven metal-ion reduction	EtOH None	ZrO_2-seeded growth	nanoflowers 15–100 nm polydisperse	10 min 96 °C >1 atm	[142]
Cu on ZrO_2	$CuNO_3$ $CuCl_2$ TEOS	TEOS hydrolysis DDA-driven Cu^{2+} reduction TEOS	H_2O/ACN DDA	SiO_2 and Cu co-nucleation and growth	spheres/nanorods of 5–7 nm × 100 nm polydisperse	3 min 80 °C >1 atm	[142]
Ni on Me_xO_y (Me_xO_y = TiO_2, Al_2O_3 Fe_3O_4, ZrO_2 SiO_2)	$NiSO_4$ KBH_4 Me_xO_y/Ag	KBH_4-driven Ni^{2+} reduction	H_2O/EG NaOH	Me_xO_y/Ag-seeded growth	spheres 10–10 nm polydisperse	20–40 min 80 °C >1 atm	[143]
Pt, Au on SiO_2	$H_2[PtCl_6]$ $H[AuCl_4]$	alcohol-driven Pt^{4+} reduction	H_2O/EtOH/ *i*PrOH	SiO_2-seeded growth	spheres 3–30 nm polydisperse	15 min 50 °C 1 atm	[144]
Cu@Ni	$Ni(CO_2H)_2$ $Cu(CO_2H)_2$ OLAM	intramolecular Ni^{2+}/Cu^{2+} reduction	$CH_3(CH_2)_7OH$ OLAM	1) Cu-seeded nucleation/growth of Ni shell 2) surfactant-assisted growth	oblate spheroids 12 nm σ = 10–15 %	10 min 160–190 °C 1 atm	[157]
Pd@Pt	$K_2[PtCl_4]$ $PdCl_2$	AA-driven Pt^{4+}/Pd^{2+} reduction	H_2O CTAB, AA	1) Pd-seeded nucleation/growth of Pt shell 2) surfactant-assisted growth	cubes 10–30 nm σ = 10–15 %	3 min 100 °C 1 atm	[156]
Ag@SiO_2	$AgNO_3$/$NaBH_4$ TEOS	DMA-catalyzed hydrolysis of TEOS	H_2O/EtOH DMA	Ag-seeded nucleation/growth of SiO_2 shell	spheres 10–80 nm σ = 10–15 %	2 min 50 °C 1 atm	[158]

[a] PVP = poly(*N*-vinyl-2-pyrrolidone); PVA = polyvinyl alcohol; Na_3Cit = trisodium citrate; FA = formaldehyde; EG = ethylene glycol; PEG = polyethylene glycol; PAH = polyallylamine hydrochloride; PPI G3 = poly(propyleneimine) dendrimer; β-CD = β cyclodextrin; TNMR = 2,8,14,20-tetranonyl-4,6,10,12,16,18,22,24-octa(1-aminoethylcarbamoyl)-methoxyresorcinarene; AA = ascorbic acid; CTAB = cetyltrimethylammonium bromide; PAA = polyacrylamide; TEG = tetraethylene glycol; Pyr = Pyridine; NMP = *N*-methyl-2-pyrrolidone ; MeOH = methanol; EtOH = ethanol; *i*PrOH = 2-propanol; *t*BuOH = *tert*-butyl alcohol; DMF = *N*,*N*-dimethylformamide; DDA = dodecylamine; TOP = trioctylphosphine; OLAC = oleic acid; DDT = dodecylthiol; GSH = glutathione; acac = acetylacetonate; OLAM = oleyl amine; SDS = sodium dodecylsulfate; TOAB = tetradecylammonium bromide; PADA = polydiacetylene [10,12-heptacosadiynoic acid]; DNA = double-stranded sodium salt of deoxyribonucleic acid; DHN = 2,7-dihydroxynaphthalene; CMC = carboxymethylcellulose; TEOS = tetraethoxysilane; DMA = dimetylamine.

absorption and catalytic activity, have attracted a great deal of interest and, hence, have reached a comparatively higher level of advancement and practical application in diverse nanotechnology fields.[7,93–95]

Earlier MW-assisted syntheses have traditionally been based on hot reduction reactions of metal salts in H_2O media loaded with some reductants serving as weak stabilizers,[99–104] or in alcohols, the latter acting as both solvents (or chelating ligands in the case of polyols) and reducing agents, often with the assistance of some size/shape-regulating additives, such as polymers or surfactants.[105–115] MW irradiation of these liquids can result in extremely rapid (< 1 min) heating of the reaction mixture to the boiling point of the solvent or to higher temperatures (< 200 °C) under solvothermal conditions in sealed vessels, leading to fast nucleation and shortening of the overall time required for completing precursor conversion. The simultaneously reducing and coordinating environment offered by polyols provides a favorable basis to exert a certain degree of size and shape control, compared to that achievable in aqueous or monofunctional alcohol media.[99–102,107–113] Another aspect deserving emphasis is that, as opposed to conventional "hot-injection" based experiments, whereby fast metal reduction is induced upon rapid addition of a metal ion precursor solution to a preheated coordinating medium, MW protocols generally involve mixing all of the necessary reaction ingredients at low temperature prior to MW application. A strong modulation of the reduction dynamics can therefore be achieved due to the existence of a significant

fraction of metal ions that are strongly complexed with ligands or surfactants, rather than being simply solvated. Such circumstances, combined with more uniform heating conditions realized by MW irradiation, are believed to benefit controllable growth by circumventing undesired Ostwald ripening or retarding particle coalescence phenomena.[99–102,107–113,116]

Ag NCs in the narrow 4.9–7.4 nm range were prepared by reduction of fatty acid silver salts in alcoholic media under short MW irradiation times (1–5 min) at 140–155 °C under ambient pressure.[107] Relatively monodisperse ($\sigma = 9$–$12\,\%$) Ag NCs with gradually larger diameters were obtained on selecting carboxylate anions with proportionally longer alkyl chain lengths, as well as by increasing the reaction temperature and/or heating time. The results of this size tuning indicated that carboxylate anions not only acted as surface stabilizers against premature aggregation, but also as moderators of the alcohol-driven reduction reaction, regulating the extent of precursor consumption in the nucleation stage. On the other hand, the reaction temperature, which was dictated by the boiling point of the alcohol solvent, controlled the rate at which subsequent growth of nuclei took place.[107] It is notable that a similar dynamics can satisfactorily explain the evolution of NC size and size distribution observed in other systems in largely varying dimensional regimes.[99,101,111,112]

Other examples concern Au, Ag, and Pt NCs produced in heterogeneous systems of short-chain alcohols or H_2O loaded with surfactants, polyvinyl alcohol (PVA), or polyelectrolytes, with the PVA and polyelectrolytes serving as both stabilizers and reductants.[105,112–115,117] Spherical polyvinylpyrrolidone (PVP)-stabilized Ag nanoparticles with diameters on the order of around 3.5 nm ($\sigma = 20$–$30\,\%$) were achieved by reducing Ag^+ ions in *N*,*N*-dimethylformamide (DMF).[116,118,119] As opposed to what occurred in conventional hot-injection-based syntheses, whereby an aqueous Ag^+ precursor solution was rapidly added to a refluxing a PVP solution (156 °C), in this approach PVP complexation of Ag^+ ion precursor prior to MW application favored Ag^+ reduction on the polymer chains rather than in the bulk solvent, with PVP additionally inhibiting premature cluster aggregation in the early reaction stages. In the absence of additives (NaOH, HCl) this mechanism may be responsible for the almost fixed size regime in which the NCs can ultimately be obtained regardless of the reaction parameters.[116] Differently, the combination of aqueous cetyltrimethylammonium bromide (CTAB) surfactant molecules capable to assemble into shaped micellar templates as a function of their concentration, under mild pH-dependent reduction condition, such as those achieved with 2,7-dihydroxy naphthalene, allowed delicate switching among different growth regimes in which moderately polydisperse spherical, prismatic, or rod-like Au NCs could be obtained in appreciable yields (Figure 5 a–c).[117]

In another approach, dodecylthiol (DDT) was used as both capping agent and self-assembly promoter for monodisperse Ag NCs that were formed at the interface between partially miscible solvents, namely ethylene or polyethylene glycol (EG, PEG) and toluene, under MW irradiation (Figure 5 d,e).[120] Specifically $AgNO_3$ was reduced in EG in the presence of DDT and toluene upon prolonged heating at 160–170 °C. A phase separation took place between EG, which contained the metal salt while also preferentially dissolving the polar head groups of DDT molecules, and toluene, which accommodated the alkyl chains of DDT. By tuning the EG to DDT molar ratio, 10 nm spherical or cubic-shaped NCs were generated upon Ag^+ reduction confined at the liquid/liquid interface. Due to their high monodispersity ($\sigma < 5\,\%$) the NCs tended to spontaneously arrange in hexagonal or cubic "superlattices" after solvent evaporation. The effectiveness of the procedure was further demonstrated on replacing EG with an aqueous solution of thiourea as an S precursor, which afforded monodisperse spherical Ag_2S NCs that assembled in ordered superstructures.[120]

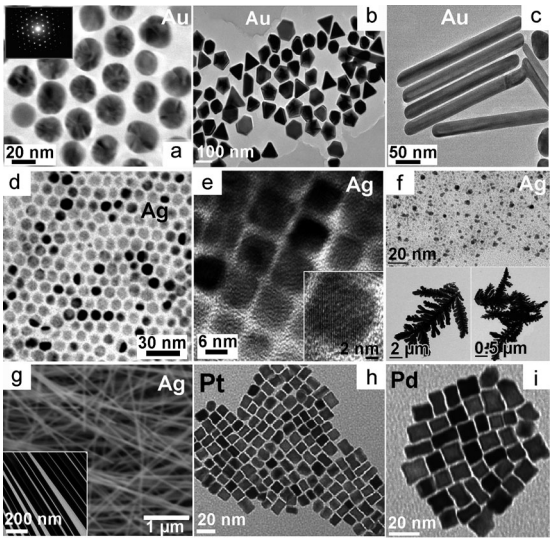

Figure 5. Examples of single-composition metal NCs grown under MW exposure: a)–c) Transmission electron microscopy (TEM) pictures of nearly spherical multiply twinned, variously faceted, and rod-shaped Au NCs, respectively, synthesized according to Ref. [117]; d),e) TEM pictures of monodisperse spherical and cubic Ag NCs, respectively, prepared according to Ref. [120] (inset in (e) shows a high-resolution TEM detail of an individual cubic particle); f) TEM images of polydisperse Ag NCs (top) and microstructures thereof (bottom), synthesized according to Ref. [138]; g) Scanning electron microscopy (SEM) image of uniform-diameter Ag nanowires prepared according to Ref. [98] (inset: a representative TEM image of the same sample); h),i) TEM images of single-crystalline Pt and Pd cube-shaped NCs obtained according to Ref. [136].

A MW-assisted polyol-based reaction scheme was applied to the preparation to size- and shape-modulated Au NCs in hot EG/PEG (100–198 °C) with the assistance of polymers or surfactants.[97,103,121–125] The concentration of $H[AuCl_4]$ was identified to be a sensitive parameter in dictating shape and size of the NCs. Comparative synthesis experiments carried out in the presence of suitably calibrated PVP amounts by either convective oil-bath heating or variable-rate MW heating (under continuous or pulsed irradiation) showed that the formation of polygonal nanoplatelets was found to be always preferred over the generation of spherical NCs under MW irradiation.[97,123] While PVP molecules undoubtedly played a role in governing the NC evolution by adhering to the solution-exposed Au NC facets with different bonding

strength, the observed shape preference was deduced to be a genuine result of MW irradiation, regardless of the heating rate realized.[97] In the presence of MCl (M = Na, K, H) additives, a fast EG-driven reduction of $H[AuCl_4]$, which led to nucleation and growth of PVP-capped Au NCs, competed with etching caused by the change in the redox oxidation potential of $[AuCl_4]^-$ proportional to the concentration of the Cl^- additive that was realized in the synthesis.[124] Owing to its remarkable dependence on the NC geometric features and crystal structure, the oxidative etching process was concluded to be responsible for the largely varying size and shape regimes in which the NCs could ultimately be obtained as a function of the MCl concentration.[124] Apart from a general acceleration of the synthesis rate, no specific interplay of MW irradiation was reported,[121–125] although it could accelerate the $[AuCl_4]^-/Cl^-$ oxidation pathways to a great extent.

Various synthetic efforts to other transition-metal (Ag, Co, Ni, Pd, Pt, Ru, Rh, Ir) and alloy (FePt, PtRu) nanostructures by hot reduction in complex surfactant/polymer/EG media were put forward, which however resulted in hardly any size-/shape-tuneable NCs and a broad variance of geometric parameters and/or a tendency to uncontrollable aggregation.[86,126–134] First attempts to implement these methods into a continuous-flow MW reactor systems have been also made.[56]

An organic-phase approach to hydrophobic-capped Au NCs featured by good size monodispersity ($\sigma < 10\,\%$) in the 4–10 nm range is worth mentioning.[135] The NCs were synthesized by fast ethanol/amine co-driven reduction of $H[AuCl_4]$ dispersed in reverse micelle systems of *n*-heptane/ethanol/alkylamines, whereby ethanol acted as strong MW absorber. The colloidal stability as well as the dimensions and size variance of the amine-capped NCs were highly dependent on concentration and alkylamine chain length, although no monotonic trend could be indentified.[135]

Recently, a broad selection of uniformly sized and shaped metallic NCs, such as of Au, Ag, Pt, Pd, Ru, Rh, Cu, Ni, and diverse combinations thereof in the form bimetallic alloys, were demonstrated by means of a general MW-assisted surfactant-based approach.[136,137] The method involved combining suitable metal salt precursors with oleic acid (OLAC) and oleylamine (OLAM) in calibrated proportions, in some cases diluted with a solvent (DMF, H_2O), and then subjecting the resulting mixture to intermittent MW irradiation for a total MW irradiation time of 30 s to 15 min. Single-size families of monodisperse MCs with morphologies as diverse as cubes, rods or faceted spheres were selectively achieved in the scale range of 5–100 nm (Figure 5 h,i). It was determined that the evolving metal clusters could catalyze the formation of dioleamide from the reaction of the two surfactants, which, in turn, propelled the growth process acting as a reductant jointly with free OLAM.[137] Excess free OLAC modified the relative surface energies of the NC facets, dictating their morphological evolution.[136,137] Interestingly, these metal NCs supported on nanoporous CeO_2 manifested high catalytic activity in low-temperature CO oxidation.[136]

A few relatively "greener" MW-assisted protocols to coinage metals have been devised. An environmentally benign tripeptide, glutathione, was successfully used as both reducing and capping agent in aqueous medium to prepare irregularly sized, polydisperse Ag NCs in the 5–10 nm range under MW irradiation within 30–60 s at 34–60 °C.[138] Dendritic nanostructures were observed for samples quenched at intermediate reaction stages (when the initial $AgNO_3$ precursor concentration had not been yet depleted completely), the origin of which remained unclear (Figure 5 f). It was found that increasing the MW irradiation power from 50 to 100 W, the reaction time as well as NC size could be reduced to some extent. Furthermore, corresponding reactions performed under conventional convective heating at 60 °C, while keeping all other conditions constant, did not yield any NC product even after 24 h. These results suggested the interplay of some MW effect in enhancing the reducing power of glutathione and the growth rate of Ag NCs. The synthesis procedure was successfully extended to other coinage metals, such as Pd, Pt, and Au, which could be accessed with larger particle sizes (ca. 100 nm).[138] In another potentially scalable approach, the reduction of aqueous $[Ag(NH_3)_2]^+$ complexes with carboxymethyl cellulose was found to open access to sub 5 nm Ag NCs with narrow size distributions.[139]

The rapid synthesis of Au NCs with broadly spread shapes, such as prisms, cubes, and hexagons was realized by MW-assisted spontaneous reduction of $H[AuCl_4]$ in an aqueous solution of α-D-glucose, sucrose, and maltose.[140] Also in this case the sugars served as reducing agents, while simultaneously performing a surface-protecting action against uncontrollable aggregation and influencing the NC shape evolution. It was found that the MW-assisted reaction reached completion in significantly shorter time (30–45 s) than that required under conventional convective heating conditions. Additionally, the method could be extended to the fabrication of Ag, Pd, Pt NCs.[140]

MW dielectric heating was used to accomplish the high-temperature surfactant-assisted synthesis of single size families of alloy fcc FePt and fcc FePd NCs with diameter smaller than 3 nm using $Na_2[Fe(CO)_4]$ as both Fe source and reducing agent for the Pt^{II} acetylacetonate or Pd^{II} acetylacetonate precursors.[141] A wide range of reaction regimes (120–215 °C) was explored upon varying the solvent media (nonadecane, octyl ether) and the surfactant composition (OLAM, OLAC or both), in closed vessels (pressure up to 17 atm). The MW irradiation allowed the rapid production (≤ 6 min) of reasonably monodisperse stoichiometrically controlled NCs ($\sigma = 5$–$10\,\%$) in the disordered fcc phase at temperatures significantly lower than those required with conventional hearing methods (150 °C vs. 330 °C). Interestingly, annealing the initially superparamagnetic fcc NCs in the solid state under reducing atmosphere converted them into comparatively larger fct FePt NCs in the ferromagnetically ordered Ll_0 phase exhibiting strong coercitivity at temperatures as low as 364 °C.[141]

MW-based methodologies based on all of the approaches described above or variously modified combinations thereof were extended to the preparation of tailored metal NCs (such as Ru, Rh, Pt, and Cu) dispersed directly on diverse mesoporous inorganic or organic solid supports (e.g., metal oxides, carbon), which are in great demand as functional nanocomposite platforms with high catalytic activity in a

number of reactions (e.g., hydrogenation of nitrobenzene, CO oxidation).[142–147]

Examples of MW syntheses of one-dimensional NCs have also been reported. In this context, a polydisperse mixture of single-crystalline Ag nanorods and nanowires, contaminated with a small percentage of twinned nanostructures, was achieved through MW-assisted reduction of Ag_2O in hot 1,2-ethanedithiol at low temperatures (80–140 °C) for a short reaction time (10 min).[148] The fact that substitution of 1,2-ethanedithiol for EG led to spherical NCs indicated that the dithiol ligands not only acted as reductants, but also facilitated anisotropic growth by facet-selective surface adhesion.

High-quality Ag nanowires with uniform 40–50 nm diameter were synthesized under aerobic conditions by MW irradiation of mixtures of $AgNO_3$, PVP, and NaCl in EG at 160–170 °C (Figure 5g).[98] The introduced Cl^- ions played a "buffering" action, interfering with the conversion of Ag^+ into Ag^0. Indeed, transient AgCl formation in the bulk solution and/or on the surface of the growing metal clusters decreased the concentration of free Ag^+ ions, which cathodically shifted the relevant reduction reaction. Concertedly, one-dimensional Ag growth was explained as originating from a metal deposition/redissolution dynamics, according to which cooperatively induced Cl^-/O_2 oxidative etching of the primary Ag particles at preferential sites competed with spatially unselective Ag deposition, ultimately leading to anisotropic lattice development facilitated by facet-selective PVP binding. Additionally, it was shown that extended MW irradiation times (> 3.5 min) induced welding of the purified Ag nanowires dissolved in EG into wire-built networks, a results that could not be reproduced under conventional heating.[98]

Au nanowires were synthesized under MW heating in water within 120–180 min using double-stranded DNA molecules as both reducing agents for $H[AuCl_4]$ and soft scaffolds guiding the growth of nanowires. The nanowires formed with a diameter of 10–20 nm and irregular morphologies, and exhibited resistivity comparable to that of pure metals.[149]

Seed-catalyzed approaches were exploited for various purposes, such as to bypass the otherwise kinetically hindered homogeneous nucleation of the target metal under the selected reaction conditions, to generate proportionally larger NCs, or to facilitate formation of anisotropically shaped nanostructures starting from smaller NC seeds acting as redox catalysts.[102,108–110,115,142–145,150,151] In one instance, MW-assisted $H[AuCl_4]$ reduction with stabilizing polyelectrolyte molecules allowed polydisperse 4 nm citrate-capped Au seeds to be converted into nearly monodisperse 22 nm Au NCs that tended to assemble into chain-like aggregates.[115]

Variable-shaped Ag nanostructures were synthesized by one-pot EG-driven sequential reduction of $H_2[PtCl_6]$ and $AgNO_3$ in the presence of polyvinylpyrrolidone (PVP) under ambient-pressure MW heating.[109,110] In this system, due to the more favorable reduction conditions, tiny (< 3 nm) Pt NCs were assumed to be initially generated, which then acted as preferential catalyst seeds on which subsequent Ag^+ ion reduction could take place, leading to heterogeneous Ag deposition with high selectivity. Within the reactant concentration range investigated, moderate Pt and PVP concentrations at increasingly higher $AgNO_3$ loadings were found to be beneficial toward formation of nanorods and nanowires (40–60 nm × 0.1–3 μm) in appreciable yield from multiple-twinned decahedral Ag NCs attained at the early reaction stages. On the other hand, at high PVP content and comparatively lower $AgNO_3$ supply more isotropic cubic-shaped NCs were favored, although they co-existed with other polyhedral shapes. The temporal evolution of the NCs and the detection of sheet-like Ag intermediates suggested that the Pt seeds and the complexing effect of PVP ligands on the Ag^+ ions governed the nucleation stage under rapid MW heating, while anisotropic growth was promoted by the delicate interplay of surface-selective adhesion of PVP molecules and sufficient supply of Ag^+ precursors.[109,110]

On the basis of control experiments carried out in the absence of $H_2[PtCl_6]$, in which only faceted spherical particles resulted, it was reported that ultimately two competing growth pathways could be delineated: a Pt-independent route, whereby PVP assisted homogeneous nucleation of Ag, followed by the isotropic evolution of the primarily formed embryos; a Pt-catalyzed route, whereby the initial in-situ generation of Pt seeds triggered heterogeneous nucleation of Ag, resulting in mixtures of differently sized flat plates with triangular or hexagonal profile, cubooctahedrons or multiply twinned NCs that could further evolve into bipyramidal-shaped or one-dimensional nanorods/wires.[150] Shape modulation likely arose from kinetically controlled processes, such as the relative rates of Ag^+ ion diffusion toward the available facets on the Pt seeds and rate of Ag^0 growth out of such sites.[97] More detailed time-dependent studies on the formation of Ag nanorods/wires showed that additional small Ag spheres could be nucleated on the fully-grown wires/rods upon prolonging the MW irradiation time, a fact that could be expected to be promoted by local heating of the concerned metallic surfaces.

Alternatively, application of a two-step seeding sequence opened access to various families of elongated Ag NCs with progressively larger thickness and higher aspect ratio, along with curved nanostructures derived from selective end-to-end crystal-oriented attachment of shorter nanorods.[150] Attempts to produce Ag nanorods by Au-seed-assisted $AgNO_3$ reduction in aqueous sodium citrate (Na_3Cit) solutions were less successful.[100,102]

The fabrication of polydisperse Ni NCs in the size range of 30–100 nm was realized under prolonged MW irradiation of Ni^{II} acetate in binary EG-diluted mixtures of PVP and dodecylamine (DDA) ligands at 195°,[151] although more complex surfactant combinations were also exploited.[127] Small amounts of $H_2[PtCl_6]$ were added, which guaranteed earlier nucleation of tiny Pt clusters that acted as catalyst substrates for heterogeneous deposition and growth of Ni upon EG-driven reduction of the relevant precursor.[151] It was found that the morphology of Ni NCs depended on the DDA concentration, while the NC size and size distribution were modulated by the precursor to DDA to PVP molar ratio. The MW-assisted polyol process was assessed to be much faster than the corresponding reaction carried out under convective heating (45 min vs. 2–17 h).[151]

Unfortunately, in all of the aforementioned reports, no direct proof for the incorporation of the foreign Pt or Au seeds into the final metal nanostructures was provided.[100,102,109,110,150,151]

3.1.2. Core–Shell HNCs

Seeded-growth approaches were employed for the development of bimetallic core–shell HNCs made of individually distinguishable inner core and outer shell domains. Depending on the particular reaction system devised, the starting core seeds could either be generated in situ in the same reaction mixture during the earlier synthesis stages, or prepared in an independent step and then added to the shell growth environment.

The synthesis of shaped Au@Ag (core@shell) core–shell HNCs was accomplished by a one-pot, two-stage procedure.[152,153] First, PVP-assisted $H[AuCl_4]$ reduction in EG under MW irradiation originated a mixture of single-crystal triangular, square, rhombic and pentagonal Au NCs surrounded by low-energy facets; subsequently, $AgNO_3$ was added to the seed-containing mixture to sustain epitaxial growth of an Ag shell. Depending on the original Ag^+:Au^{3+} molar ratio, a variety of shaped core–shell HNCs could be produced (Figure 6a–d).[152] More in detail, Ag overgrowth on Au triangular twinned plates generated HNCs shaped as truncated trigonal bipyramids (ca. 50–100 nm) at Ag^+:Au^{3+} molar ratios smaller than around 5:1 whereas thicker HNCs with regular bipyramidal shape were formed at Ag^+:Au^{3+} ratios approaching 30:1 (ca. 200–300 nm). In contrast, Ag deposition on octahedral Au seeds generated HNCs with a cube habit, which grew progressively larger (up to ca. 200 nm) with increasing the Ag^+ concentration. Finally, upon Ag shell coating multiply twinned decahedron Au seeds with a pentagonal cross-section evolved into approximately spherical HNCs at low Ag^+:Au^{3+} molar ratios, while they converted to nanorods (ca. 50×100 nm) and pentagonal wires (up to 4 μm long) under proportionally higher Ag^+ supply. Detailed TEM analyses allowed clarifying that the morphological changes observed were unequivocally attributable to selective PVP adsorption on different crystallographic facets exposed to the EG solvent environment. Further proof in support of this mechanism was provided by manipulating the conditions in which the Ag shell was generated. In a solvent-modified method,[153] shape-controlled Au seeds synthesized in an independent MW-assisted step were injected into a DMF solution containing $AgNO_3$ and PVP in suitable proportions and processed at 140 °C under conventional oil-bath heating. In contrast to the results achieved in the MW-irradiated EG environment, the resulting Au@Ag core–shell HNCs embodied Ag shell with shapes conformal to those of the Au core seed underneath.[153] In yet another case,[154] the Ag shell-deposition step was controlled by calibrating the content of extra Cl^- ions, which yielded AgCl, thus depressing the concentration of free Ag^+ ions, and promoting facet-selective oxidative etching of the shell by $[AuCl_4]^-$ species, analogous to that achieved in the morphological selection of Au NCs.[124] This mechanism led to polydisperse Au@Ag core–shell HNCs with tunable shell shapes.

Further attempts to the MW-assisted fabrication of core–shell HNCs relied on one-pot, single-step reaction schemes allowing the temporally separated formation of the core and shell materials along the synthesis course. Such self-regulated dynamics can arise from the remarkably large differences in the energy activation barriers that need to be surpassed for triggering the homogeneous nucleation of the respective materials. One of such mechanism was involved in the generation of Au@Pd HNCs made of 9 nm Au spherical core NCs coated with 3 nm thick Pd shells[155] (Figure 6e). These heterostructures resulted from the sequential EG-driven reduction of $H[AuCl_4]$ and $PdCl_2$ precursors, which led to initial selective homogenous nucleation of Au seeds onto which otherwise kinetically hindered Pd formation occurred via heterogeneous growth. A similar dynamics was involved in the formation of spherical or cubic-shaped Pd@Pt HNCs bearing a porous shell made of tiny Pt domains upon ascorbic-acid driven consecutive reduction of $PdCl_2$ and $K_2[PtCl_4]$ in aqueous CTAB solutions at reflux[156] (Figure 6f). In the latter case dihydrogen adsorption measurements were used to indirectly prove attainment of the core–shell geometry. Accordingly, proper adjustment of the heterostructure composition demonstrated to be an effective tool to tailor the electrocatalytic performances of the HNCs.[156]

Another interesting example concerns uniformly sized 12 nm Cu@Ni HNCs that were derived upon MW irradiating OLAM-modified nickel(II)- and copper(II) formate complexes co-dissolved in 1-octanol at 190 °C for about 10 min. Profiting from the divergence in the intermolecular reduction potentials of OLAM-modified nickel(II)- and copper(II) formate complexes, and from their different temperature dependence, the Cu core seeds were first produced in the solution at temperatures lower than 160 °C, after which the Ni shell nucleated and developed upon prolonged heating at 190 °C. The fast kinetics of HNC formation under MW irradiation minimized atomic interdiffusion, ultimately leading to a thin interfacial region with mixed Cu:Ni composition between the core and shell section, rather than to full conversion of the Cu@Ni core–shell heterostructures into corresponding fully alloyed CuNi NCs. Under ambient conditions the Cu@Ni HNCs showed ferromagnetic behavior at low temperature with asymmetric hysteresis cycles, which manifested magnetic exchange coupling between the Ni shell and its surface passivating layer of antiferromagnetic NiO attained upon air exposure.[157]

Finally, a straightforward MW technique has been recently developed for preparing monodisperse $Ag@SiO_2$ HNCs with SiO_2 shell thickness tuneable in the 10–80 nm range.[158] Unlike in traditional silica coating procedures based on the Stöber method,[15,36] which typically require pre-activation of the core seeds for silanization with a silane coupling agent and long hydrolysis times (4–24 h), in this case $Ag@SiO_2$ HNCs were efficiently prepared by MW irradiating a mixture of colloidal Ag seeds and tetraethoxysilane (TEOS) precursor dissolved in hydroalcoholic media in the presence dimethylamine as catalyst for only 2 min at 50 °C. The thickness of SiO_2 shell, which could be conveniently controlled solely by changing the concentration of TEOS, was

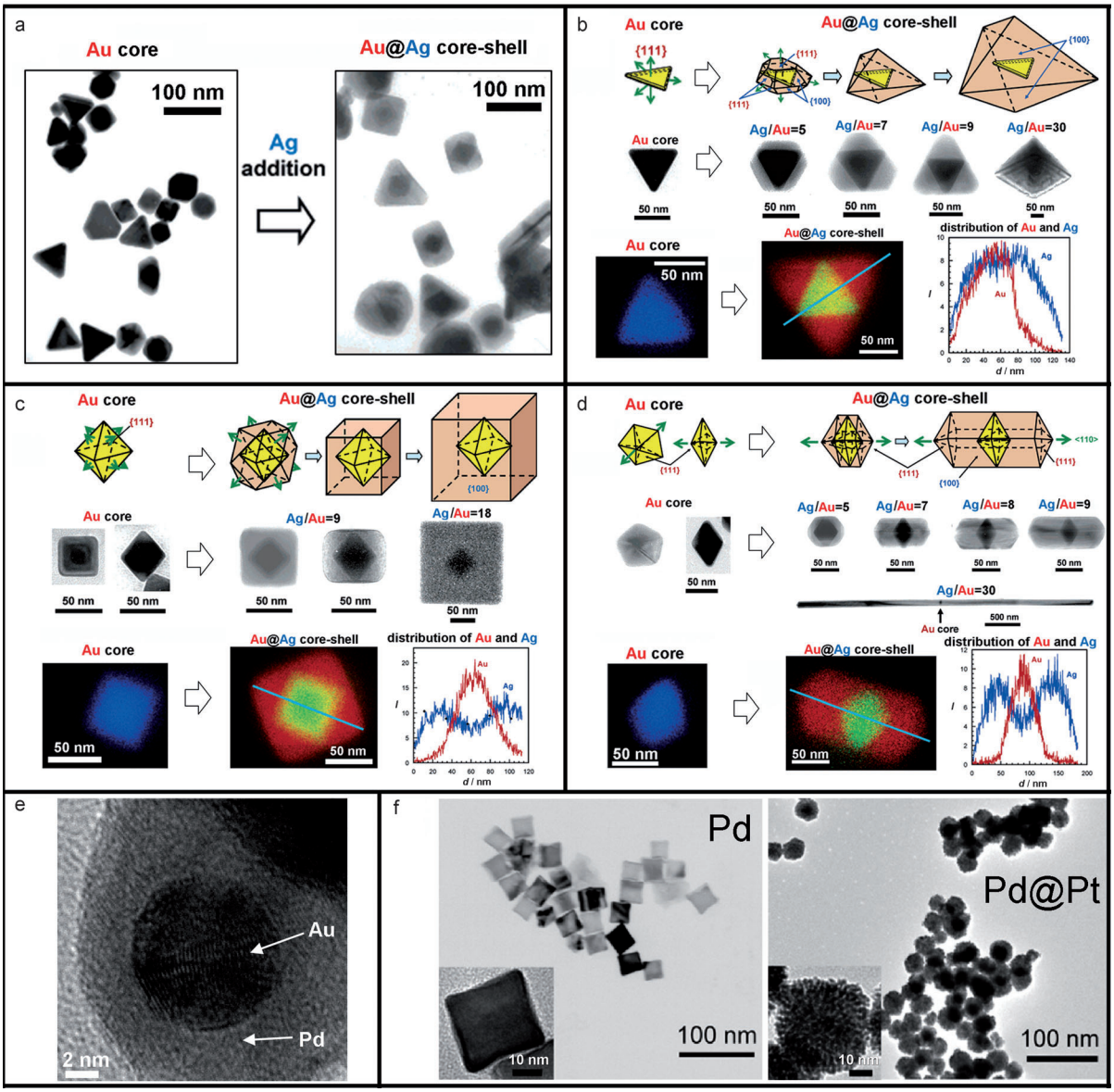

Figure 6. Examples of bimetallic HNCs grown under MW irradiation. a) TEM images showing the conversion of a sample of shape-polydisperse Au NC seeds into corresponding Au@Ag core–shell HNCs with variable morphologies, prepared according to Ref. [152]; b)–e) Detailed shape evolution of triangular platelet-like, octahedral and dodecahedral Au seeds to corresponding Au@Ag core–shell HNCs with truncated bipyramidal, cubic and rod-like shell shapes, respectively, corresponding to those shown in panel (a). The evolution is illustrated through mechanistic sketch (top part), relevant TEM images of individual particles as a function of the Au:Ag molar ratio realized in the synthesis (middle part), and representative Ag–Au compositional maps of individual seeds and HNCs obtained by energy-dispersive X-ray spectroscopy analysis in a TEM microscope; e) high-resolution TEM of a single spherical Au@Pd core–shell HNC prepared according to Ref. [155]; f) TEM images of cube-shaped Pd NCs (left) and Pd@Pt core@shell HNCs (right) derived upon Pt decoration of the Pd cubes, according to Ref. [156].

amenable to further chemical functionalization with either amino or carboxyl moieties.[158]

3.2. Transition-Metal Oxides

Nanostructured transition-metal oxides constitute a rather broad category of valuable materials exploited in many technological areas.[11,159] At the nanoscale, unique effects, such as surface- and strain-induced lattice distortion, changes in electronic structure due to composition and charge distribution variation systematically evolve with size and shape, influencing the ultimate optoelectronic behavior and catalytic responses. The properties of oxide nanomaterials cover almost all aspects of materials science and solid-state physics, and find applications in a number of fields, for example, in environmental purification, fuel production, ceramics fabrication, energy storage and conversion, sensing, catalysis, and biomedicine.[11,159]

The severe requirements in terms of controlled structural, dimensional and compositional features, which oxide NCs have to meet in order to be practically useful, have stimulated

development of a number of wet-chemical preparation approaches, whereby the application of MW dielectric activation in place of conventional heating has attracted a great deal of interest in the pursuit of shortened crystallization and growth times, as well as increased product selectivity and yield.[11,46,160] In this Section we will review the MW-assisted growth of transition-metal oxide NCs belonging to the main subclasses of binary or multi-metal based compounds. In Sections 3.2.1 and 3.2.2 a selection of cases of NCs produced by hydrothermal processes under assistance of the sole solvent molecules or specific template additives, such as organic molecules and/or surfactant agents as both reactivity moderators and particle stabilizers, is presented. In addition, a concise illustration of the pioneering utilization of ionic liquids as strong MW-absorbing media is offered. The relevant reaction conditions, product quality features, and NC formation mechanisms (whenever clearly proven or discussed) are summarized in Tables 3–5 for each material subfamily. Selected TEM demonstrations of the as-synthesized NCs can be found in Figure 7.

3.2.1. *Solvent-Assisted Hydrolytic Synthesis*

A glimpse into the collected examples indicates the hydrothermal method as one of the most commonly used approaches to generate oxides in liquid media in sealed high-pressure vessels. The general mechanistic pathways involve the initial hydrolysis of metal salts dissolved in H_2O to form hydroxylated, aqua- and/or oxo-complexes that represent the actual molecular monomer species from which the inorganic metal-oxygen network is progressively built upon successive polycondensation reactions under supersaturation conditions.[11,161,162] The suspended NCs usually experience an aging process during which they may continue to grow driven by aggregation and/or Ostwald ripening phenomena, depending on the presence of distinct anions, pH, and size-

Table 3: Synthesis of binary transition-metal oxide NCs under MW dielectric heating. The Table lists the main experimental conditions, size-morphological features of the resulting nanostructures, mechanistic pathways involved, and growth-governing factors.[a]

Metal oxide	Precursors	Reaction type	Solvent additives	Formation mechanism	Relevant NC features (morphology size range, size variance)	Synthesis time temperature pressure	Ref.
MgO, NiO, ZnO, ZrO_2, Fe_2O_3, Al_2O_3	$Mg(OAc)_2$, $Ni(Oac)_2$ $Zn(OAc)_2$, $Zr(iPrO)_4$ $Fe(OAc)_3$, $Al(OBu)_3$	thermal decomposition	H_2O EtOAc, PVP	polymer-assisted growth (crystallization requires calcination at 800–1200 °C)	amorphous powders; 3.2 nm particles after annealing	30 min	[163]
Bi_2O_3	$Bi(NO_3)_3$	alkaline hydrolysis	H_2O PVP, NaOH	polymer-assisted growth	rods (2×30 μm)	6 min reflux	[206]
CeO_2	$Ce(NO_3)_2$	hydrolysis	H_2O Urea	ligand-assisted growth self-aggregation	14 nm spheres assembled in hollow spheres (range 260 nm)	>30 min 170 °C	[207]
CeO_2	$(NH_4)_2Ce(NO_3)_6$ $CeCl_3$	alkaline hydrolysis	H_2O NH_3, NaOH, Urea, EDA, or FA	ion-assisted growth	spheres, 1.5–20 nm rods 7.5×30 nm	>60 min 160 °C	[208]
CeO_2	$(NH_4)_2Ce(NO_3)_6$	hydrolysis	H_2O PEG, NaAc	polyol-assisted growth	spheres average 2 nm	10 min 30 s MW cycles (9 s on/21 s off)	[209]
CeO_2	$(NH_4)_2Ce(NO_3)_6$	hydrolysis	H_2O PEG, HMT	polyol-assisted growth	spheres 2–3 nm	10 min 30 s MW cycles (9 s on/21 s off) 100 °C 1 atm	[210]
CeO_2	$(NH_4)_2Ce(NO_3)_6$	hydrolysis	H_2O NaOH	co-precipitation	spheres 5.1 ± 0.1 nm	5–240 min 194 °C 3–14 atm	[211]
$Cd(OH)_2$	$Cd(NO_3)_2$	alkaline hydrolysis	H_2O NH_3	oriented aggregation	nanowires 5–30 nm×0.3 μm	5 min	[212]
Co_3O_4	$Co(NO_3)_2$	hydrolysis	H_2O Urea	ligand-assisted growth	nanocrystals no singular shapes	15 min	[213]
Co_3O_4	$CoCl_2$	hydrolysis	H_2O Urea	ligand-assisted growth (crystallization requires annealing at 300 °C required)	nanowires 80 nm×2 μm	6 h 110 °C	[164]

Table 3: (Continued)

Metal oxide	Precursors	Reaction type	Solvent additives	Formation mechanism	Relevant NC features (morphology size range, size variance)	Synthesis time temperature pressure	Ref.
Co_3O_4	$Co(NO_3)_2$	hydrolysis	H_2O EG, Urea	ligand-assisted growth	flakes arranged in Flower-like shapes 2–3 μm	15–90 min 85 °C	[214]
CuO	$Cu(OAc)_2$	EtOH- and NaOH-driven CuO formation	EtOH NaOH, PEG	ligand-assisted growth	spheres average 4 nm	10 min 30 s MW cycles (6 s on/24 s off) reflux	[215]
CuO	$CuCl_2$	hydrolysis	[omim][TFA], NaOH	ion-assisted growth	flower-like or leaf-like nanocrystals	10 min 80 °C	[201]
CuO	$CuCl_2$	alkaline hydrolysis	H_2O NH_4OH	oriented attachment	urchin-like structures	15 min 100 °C	[216]
CuO Cu_2O Cu	$Cu(OAc)_2$	hydrolysis	H_2O EG	ligand-assisted growth	wiskers: 80 nm × 10 nm Cubes: 50 nm; Spheres: 100–120 nm	15 min 100–197 °C	[217]
Cu_2O	$Cu(OAc)_2$	glucose-driven reduction	H_2O/glucose	Ostwald ripening	ellipsoids ca. 300 nm	30 min 70 °C	[218]
α-Fe_2O_3	$FeCl_3$	pH-controlled hydrolysis	H_2O $NH_4H_2PO_4$	ion-assisted oriented attachment	nanorings outer diameter 100 nm cubes, spindles	25 min 220 ± 1 °C	[219, 220]
α-Fe_2O_3	$FeCl_3$	In-situ H_2O generation by an esterification reaction forced hydrolysis	EtOH AcOH	solvent-assisted growth	spheres 14.7–40 nm polydisperse and agglomerated	1–150 min 150 °C > 1 atm	[175]
CoO MnO ZnO Fe_3O_4 $BaTiO_3$	Benzyl alcohol $Co(OAc)_2$ $Mn(OAc)_2$, $Mn(acac)_2$ $Zn(OAc)_2$, $Zn(acac)_2$ $Fe(OAc)_2$, $Fe(acac)_3$ Ba, $Ti(OiPr)_4$	alcolysis and ester elimination	Benzyl alcohol	solvent-assisted growth	spherical 4–9 nm polydisperse and agglomerated	30 s–3 min 200 °C > 1 atm	[187, 188]
α-Fe_2O_3	$FeCl_3$	pH-controlled hydrolysis	H_2O HCl	solvent-assisted growth	spheres 31–66 nm	2–8 h 100–160 °C	[221]
α-Fe_2O_3	$FeCl_3$	pH-controlled hydrolysis	PAM Urea	ligand-assisted growth	spheres 400–800 nm	20 min reflux	[222]
α-Fe_2O_3	$FeCl_3$	pH-controlled hydrolysis	PEG N_2H_4, H_2O_2	polymer-assisted oriented attachment	ellipsoids 100 × 200 nm	10 min 100 °C	[223]
α-Fe_2O_3	$FeCl_3$	pH-controlled hydrolysis	PEG Urea	polyol-assisted growth	amorphous 3–5 nm particles	10 min 30 s MW cycles (15 s on/15 s off)	[224]
α-Fe_2O_3	$Fe(NO_3)_3$	hydrolysis	PVP $BaCl_2$	polymer-assisted growth	octahedral 300 nm	24 h 200 °C	[225]
α-Fe_2O_3	$FeCl_3$	hydrolysis (in situ generated H_2O)	EtOH AcOH	solvent-assisted growth	< 20 nm	15 min 150 °C	[175]
α-Fe_2O_3	$Fe(NO_3)_3$	hydrolysis	H_2O	solvent-assisted growth	rhombic-shaped 18–38 nm	0.5–48 h 100–120 °C	[226]
α-Fe_2O_3	$K_4[Fe(CN)_6]$	hydrolysis	H_2O	solvent-assisted growth	snowflake-like, pine-tree-like assemblies 2–4.5 μm polydisperse	0.5–3 h 120–220 °C > 1 atm	[169, 227]

Table 3: (Continued)

Metal oxide	Precursors	Reaction type	Solvent additives	Formation mechanism	Relevant NC features (morphology size range, size variance)	Synthesis time temperature pressure	Ref.
Cr_2O_3 MoO_2 CoO Mn_2O_3	$K_3[Cr(CN)_6]$ $K_3[Mo(CN)_8]$ $K_3[Co(CN)_6]$ $K_3[Mn(CN)_6]$	hydrolysis	H_2O	solvent-assisted growth	octahedral-, spherical-, rod-, pinetree-, snowflake-like assemblies 1–5 μm polydisperse	3 h 180 °C > 1 atm	[168]
$MeFe_2O_4$ (Me=Ni, Co, Mn)	$Fe(NO_3)_3$ $Ni(NO_3)_2$ $Co(NO_3)_2$ $Mn(NO_3)_2$	hydrolysis	H_2O/toluene OLAC	solvent-/surfactant-assisted growth surfactant-driven phase transfer	spherical 4–9 nm σ = 10–30%	1 h 160 °C > 1 atm	[170]
Fe_3O_4	$FeSO_4$	alkaline hydrolysis	H_2O NH_4OH	Solvent-assisted growth	aggregates of ca. 35 nm particles	8 min 80 °C	[228]
Fe_3O_4	$FeSO_4$	hydrolysis	H_2O PEG	polyol-assisted anisotropic growth	wires 30–50 nm × > 1 μm	15 min 180 °C > 1 atm	[181, 182]
Fe_3O_4	$FeCl_3$	alcolysis	EG NaOAc P123 copolymer NaBDS	polyol-assisted or surfactant-assisted growth by oriented attachment	clusters made of < 20 nm NCs 100 nm–5 μm σ = 20–30%	15–60 min 160–210 °C > 1 atm	[192, 193]
Fe_3O_4	$Fe(acac)_3$	nonhydrolytic condensation	Phenyl ether OLAC 1,2-hexadecandiol $[bmim][BF_4]$	surfactant-assisted growth	spheres 6 nm σ = 30%	5–10 min 250 °C	[198]
In_2O_3	$InCl_3$	alkaline hydrolysis	NH_4OH	NH_4OH-assisted $(In(OH)_3$ converted into In_2O_3 after calcination at 700 °C)	hexagons 22 nm σ = 10%	60 min (MW cycles: 12 s on/7 s off) reflux	[165]
Mn_3O_4	$Mn(OAc)_2$	alkaline hydrolysis	H_2O HMT	Ostwald ripening	cubes rhombohedra 15–40 nm	10–60 min 80 °C	[229]
MnO_2	$KMnO_4$	hydrolysis	H_2O OLAC	growth confined in oil-in-water microemulsions Ostwald ripening	nanowires/belts polydisperse	8 min reflux	[230]
MnO	$Mn(OAc)_2$ $Mn(acac)_2$	alcolysis	$C_6H_5CH_2OH$	solvent-assisted ester elimination	cube-like 30–50 nm	0.5–3 min 200 °C	[187]
PdO	$H_2[PdCl_4]$	pH-dependent hydrolysis	H_2O PVP, NaOH NaOAc, $C_6H_5CO_2Na$	polymer-assisted growth	spheres 1.8–3.2 nm σ = 25%	8 min reflux	[231]
PtO_2	$H_2[PtCl_6]$	pH-dependent hydrolysis	H_2O PVP, NaOH, NaOAc	polymer-assisted growth	spheres average 1.68 nm	10 min reflux	[232]
SnO	$SnCl_2$	pH-dependent hydrolysis	H_2O HCl, NH_3	solvent-assisted growth	crystalline powders	10–15 min reflux	[233]
SnO_2	$SnCl_4$	hydrolysis	H_2O Urea	solvent-assisted growth	spheres 3 nm polydisperse	15 min reflux	[166]
SnO_2	$SnCl_4$	acidic hydrolysis	H_2O HCl	solvent-assisted growth	average 5 nm	1–2 min 180 °C ca. 0.9 atm	[234]
SnO_2	$SnCl_4$	pH-dependent hydrolysis	H_2O HCl, NH_4OH or Urea	solvent-assisted growth	average 3 nm	0.5–4 h 100–200 °C	[235]

Table 3: (Continued)

Metal oxide	Precursors	Reaction type	Solvent additives	Formation mechanism	Relevant NC features (morphology size range, size variance)	Synthesis time temperature pressure	Ref.
TiO_2	$Ti(OBu)_4$ $TiCl_4$	hydrolysis	Toluene poly(ethylene oxide) block copolymer poly(ethylene oxide) HCl, NH_4OH	growth confined in polymer micelles (crystallization required calcination at 400 °C)	spheres 5 nm $\sigma = 5\%$ rods 30–50 nm × 0.5–1 μm	5 min–8 h 25–80 °C 1 atm	[179, 236]
TiO_2	$Ti(OBu)_4$ $Ti(OiPr)_4$	hydrolysis glycolysis	H_2O, EtOH, *i*PrOH, BuOH, 1,5-pentanediol or 1,6-hexanediol EG or TEG	solvent-assisted growth, (crystallization required calcination at 500–900 °C)	spherical aggregates ca. 200 nm 4.5–10 nm anatase/rutile rods 0.4 × 5 μm	2–30 min 240–285 °C	[237–239]
TiO_2	$Ti(OiPr)_4$	hydrolysis	H_2O	MW-induced recrystallization of TiO_2 colloidal solutions previously prepared	3–5 nm	5–10 min 121–145 °C 2–4 atm	[240]
TiO_2	$TiCl_4$	hydrolysis	H_2O	solvent-assisted growth	aggregates 150 nm polydisperse	5–15 min 100 °C	[241]
TiO_2	$TiCl_4$	hydrolysis	HCl	solvent-assisted growth	aggregates 70 nm polydisperse	30 s ca. 0.4 atm	[242]
TiO_2	$TiCl_4$	hydrolysis	HCl	solvent-assisted growth	< 100 nm	5–120 min 100–160 °C	[167]
TiO_2	$TiCl_4$	hydrolysis	H_2O HCl, H_2SO_4	solvent-assisted growth	aggregates 800 nm polydisperse	30–120 min 120–180 °C	[243]
TiO_2	$TiCl_3$	pH-dependent hydrolysis	H_2O NH_3 or NaCl or NH_4Cl	ion-assisted growth	cubes: 25 nm rods: 4 × 17 nm spheres: 8 nm	20–60 min	[244]
TiO_2	$TiOCl_2$	hydrolysis	H_2O	solvent-assisted growth	spheres (10 nm), rods (10×100 nm)	5–60 min 195 °C	[245]
TiO_2	$(NH_4)_2TiF_6$	hydrolysis	H_2O H_3BO_3	solvent-assisted growth	spheres 20–200 nm	10–60 min 70 °C	[246]
TiO_2	$Ti(OiPr)_4$	thermal decomposition	[bmim][BF_4]	solvent-assisted growth MW-driven crystallization of amorphous hydroxide particle precursors	truncated cubes 8–10 nm	40 min 1 atm	[196]
TiO_2	TiF_4	forced hydrolysis	[bmim][BF_4]	solvent-assisted growth MW-driven crystallization	sheets 2 μm × 2 μm	90 min 210 °C > 1 atm	[197]
WO_3	WCl_6	alcolysis	$C_6H_5CH_2OH$	solvent-assisted growth	aggregates of 5–30 nm particles	5–15 min 210 °C	[247]
WO_3	Na_2WO_4	hydrolysis	H_2O $(NH_4)_2SO_4$, HCl	ion-assisted anisotropic growth	nanowires 20–30 nm × > 1 μm	20 min–3 h 150 °C > 1 atm	[176]
ZnO	$Zn(OAc)_2$	alcolysis dehydratation/ ester elimination	EG	polymer-assisted oriented attachment sequential seeding	clusters of 8 nm NCs 50–275 nm	1–5 min steps 120–180 °C 1 atm	[190]
ZnO	zinc oximate $Zn(acac)_2$	alcolysis	ROC_2H_4OH (R = CH_3, C_2H_5, *n*-CH_4H_9)	solvent-assisted oriented attachment	clusters of 10–30 nm NCs 50–180 nm	4 min > 1 atm	[191]
ZnO	$Zn(OAc)_2$ $Zn(acac)_2$	alcolysis ester elimination	$C_6H_5CH_2OH$	solvent-assisted growth	aggregates of 20–30 nm particles	0.5–3 min 200 °C	[187]
ZnO	$Zn(NO_3)_2$	alkaline hydrolysis	H_2O HMT	oriented attachment	rods:100 nm × 1 μm bipods, tripods, multipods	2–30 min 90 °C	[248]

Table 3: (Continued)

Metal oxide	Precursors	Reaction type	Solvent additives	Formation mechanism	Relevant NC features (morphology size range, size variance)	Synthesis time temperature pressure	Ref.
ZnO	$Zn(NO_3)_2$ $Zn(OAc)_2$	alkaline hydrolysis	H_2O HMT HMT + EDA HMT + TEC NH_4OH or NH_4OH + TKC	ligand-assisted growth	rods or needles or stars or disks or balls range 0.4–5 μm	15 min 90 °C	[249]
ZnO	$Zn(NO_3)_2$	alkaline hydrolysis	NaOH	solvent-assisted growth	rods range 1 μm	120 min 192 °C	[250]
ZnO	$Zn(NO_3)_2$, $Zn(OAc)_2$ $ZnSO_4$ $ZnCl_2$	pH-dependent hydrolysis	H_2O Urea	ion-assisted growth	needles 11 μm σ = 20–30%	> 15 min	[251, 250]
ZnO	$Zn(OAc)_2$	hydrolysis	H_2O N_2H_4	solvent-assisted growth	rods diam. 25–7 nm len. 0.5–1.5 μm	10 min	[253]
ZnO	$Zn(OAc)_2$	hydrolysis	H_2O NH_4OH	solvent-assisted growth	dumbbells 2 × 5 μm	5–10 min	[254]
ZnO	$Zn(OAc)_2$	hydrolysis	H_2O EG	polymer-assisted seeded growth	rods packed in micromer-sized bundles, spheres or flowers	different MW cycling modes 60–90 min	[255]
ZnO	$Zn(OAc)_2$	alkaline hydrolysis	H_2O NaOH, PEG, EtOH	polymer-assisted growth	rods 50–250 nm diameter × 70–300 nm length	30 min 140 °C	[256]
ZrO_2	$Zr(NO_3)_4$	alkaline hydrolysis	H_2O NaOH, PVA	polymer-assisted growth	aggregates of 2 nm particles	6 min (MW cycles: 10 s on/20 s off) 320 °C	[257]
ZrO_2	ZrOCl	alkaline hydrolysis	H_2O NaOH	Solvent-assisted growth	spheres 10–20 nm	120 min 194 °C 14 atm	[258]
ZrO_2	$Zr(OiPr)_4$	hydrolysis	H_2O/EtOH Caproic acid	ligand-assisted growth	spheres 100 nm	50–100 mL min^{-1} 60 °C 15 atm	[184]

[a] EDA = ethylenediamine; ODA = *n*-octadecylamine; FA = formamide; HMT = hexamethylenetetramine; OAc = acetate AcOH = acetic acid; EtOH = ethanol; *i*PrOH = 2-propanol; BuOH = 1-butanol; acac = acetylacetonate; [omim]TFA = 1-octyl-3-methylimidazolium trifluoroacetate; EG = ethylene glycol; TEG = triethylene glycol; PEG = polyethylene glycol; PAM = polyacrylamide; PVP = polyvinylpyrrolidone; TEC = triethyl citrate; TKC = tripotassium citrate monohydrate; PVA = Poly (vinyl alcohol); MPA = mercaptopropionic acid.

Table 4: Synthesis of multimetal oxide NCs under MW dielectric heating. The Table lists the main experimental conditions, size-morphological features of the resulting nanostructures, mechanistic pathways involved, and growth-governing factors.[a]

Metal oxide	Precursors	Reaction type	Solvent additives	Formation mechanism	Relevant NC features (morphology size range, size variance)	Synthesis time temperature pressure	Ref.
$NiFe_2O_4$ $ZnAl_2O_4$ Mo-V-Te-Nb-Pd-based oxides	Metal nitrates Ammonium vanadates and heptamolybdate Telluric acid Niobium ammonium oxalate Vanadyl sulfate	Alkaline Hydrolysis	H_2O NaOH Na_2CO_3	solvent-assisted growth (post-synthesis calcination required)	Agglomerated 6–20 nm spheres microcrystals polydisperse	5–10 min 1 atm	[83, 178]
$NiFe_2O_4$	$FeCl_3$ $NiCl_2$	Alcolysis	EtOH EtONa	solvent-assisted growth (post-synthesis calcination required)	4–5 nm	5 min 160 °C 11 atm	[259]

Table 4: (Continued)

Metal oxide	Precursors	Reaction type	Solvent additives	Formation mechanism	Relevant NC features (morphology size range, size variance)	Synthesis time temperature pressure	Ref.
$ZnFe_2O_4$ β-FeOOH	$Fe(NO_3)_3$ $Zn(OAc)_2$	Hydrolysis	H_2O [bmim][BF_4] Urea	ion-assisted	Plates average 40 nm	30 min 120–200 °C	[204]
Co_3O_4	$CoCl_2$ $CoSO_4$ $Co(NO_3)_2$	Hydrolysis of a metal-ligand complex	H_2O MPA	ligand-assisted growth	Spheres, cubes 10–20 nm $\sigma = 20$–40%	10 min 100–140 °C >1 atm	[183]
$CoFe_2O_4$	$FeCl_3$ $Co(OAc)_2$	Hydrolysis	H_2O 1,2-propandiol NaOAc	ligand-assisted growth	Aggregates of 5 nm particles	>60 min 160 °C	[260]
$FeMoO_4$	$Fe(NO_3)_3$ $(NH_4)_6Mo_7O_4$	Glycolysis	H_2O, EG	bubble templating growth coupled with self-assembly	Hollow hierarchical spheres 0.5–1 μm monodisperse	30 s–10 min 100–130 °C	[261]
$MnZnFe_2O_4$	$Fe(NO_3)_3$ $Zn(NO_3)_2$ $Mn(NO_3)_2$	Alkaline hydrolysis co-precipitation	H_2O NaOH	solvent-assisted growth	Aggregates of 10 nm spherical particles	5–30 min 100 °C	[262]
$NiCuZnFe_2O_4$	$Fe(NO_3)_3$ $Ni(NO_3)_2$ $Cu(NO_3)_2$ $Zn(NO_3)_2$	Alkaline hydrolysis co-precipitation	H_2O NaOH	solvent-assisted growth	Aggregates of 20–60 nm particles	45–60 min 160 °C	[263, 264]
α-$Ni(OH)_2$	$Ni(NO)_3$ $NiCl_2$	Hydrolysis	H_2O/EtOH Urea	ligand-assisted growth	3D Flower-like 700 nm–1 μm	15 min 90 °C	[265]
α-$Ni(OH)_2$	$Ni(OAc)_2$	Alkaline hydrolysis	H_2O HMT, SDS	surfactant-assisted growth	Microspheres and nano-sheets 200–250 nm	60 min 95 °C	[266]
$Mg(OH)_2$	$Mg(NO_3)_2$	Alkaline hydrolysis	H_2O NaOH	solvent-assisted growth and local hot-spot enhancement	Fibre-like 20–40 nm × 100-150 nm	4 days 25 °C	[267]
$Ca(PO_4)_6(OH)_2$	$CaNO_3$ Na_2HPO_4	pH-dependent hydrolysis	H_2O EDTA, NaOH	ligand-assisted growth	Nanorods, bowknot-like and flower-like	30 min (cycles 6 s MW on/10 s MW off) reflux	[268]
$CaZn_2(OH)_6$	$Ca(NO_3)_2$ $Zn(NO_3)_2$	Alkaline hydrolysis	H_2O KOH	solvent-assisted Ostwald ripening	Microspheres and lozenge-like particles μm sizes	1–2 h 130 °C	[269]
$AgIn(WO_4)_2$	$In(NO_3)_3$ Na_2WO_4 $AgNO_3$	pH-dependent Hydrolysis	H_2O KOH/HCl	solvent-assisted growth	Caterpillar-like Hundreds of nanometers polydisperse	20 min 180 °C	[177]
$BaTiO_3$	$TiCl_4$ $BaCl_2$	Alkaline hydrolysis	H_2O KOH	solvent-assisted Anisotropic Growth via Ostwald ripening and coarsening	Polyhedrons 25–50 nm $\sigma = 20$–30%	10–60 min 140 °C 2.5 atm	[171, 173]
$BaTiO_3$	$Ti(OBu)_4$ $BaCl_2$	Alkaline hydrolysis or alcolysis	EG/EtOH KOH	solvent-assisted Ostwald ripening polyol-assisted growth	Spheres: 50 nm Wires: 45–50 nm × 2–5 μm $\sigma = 20$–40%	90 min 200 °C >1 atm	[174]
$BaTiO_3$	$Ti(OiPr)_4$ $BaCl_2$	Alkaline glycolysis	EG KOH	polyol-assisted (crystallization required annealing at 700 °C)	Aggregates of 10 nm particles	5 h reflux	[270]
$BaTiO_3$	$Ti(OiPr)_4$ $BaCl_2$	pH-dependent hydrolysis	H_2O HCl, NaOH	Ostwald ripening	Spheres 50–60 nm polydisperse	2–40 h sweep time 1–5 s 170 °C	[172]
$BaTiO_3$	$TiCl_4$ $Ba(OH)_2$	Alkaline hydrolysis	H_2O NH_3	solvent-assisted growth	Tetragonal prisms 100–250 nm	12 h 220–240 °C	[271]
$BaTiO_3$	$TiCl_4$, $BaCl_2$	Alkaline hydrolysis	H_2O, KOH	solvent-assisted growth	Spheres 30 nm	>30 min 180 °C	[272]
$BaWO_4$	$BaCl_2$ Na_2WO_4	Hydrolysis	H_2O PVP	polymer-assisted growth	Sheets/nanobelts 50–800 nm × 2–3 μm polydisperse	100 °C	[180]

Table 4: (Continued)

Metal oxide	Precursors	Reaction type	Solvent additives	Formation mechanism	Relevant NC features (morphology size range, size variance)	Synthesis time temperature pressure	Ref.
$BaFe_{12}O_{19}$	$Ba(NO_3)_2$ $Fe(NO_3)_3$	Acidic hydrolysis	H_2O Citric acid, EDTA	ligand-assisted growth	Spheres/ellipsoids 50–100 nm	15 s	[273]
$La_{0.75}Sr_{0.25}Cr_{0.93}$--$Ru_{0.07}O_{3-\delta}$	$SrCl_2$ CrN_3O_9 $RuCl_3$	Alcolysis	EtOH EtONa	ion-assisted growth	Agglomerates of 10 nm clusters polydisperse	2–3 min 160 °C 1300 kPa	[189]
$BiVO_4$	V_2O_5, $Bi(NO_3)_3$	Acidic hydrolysis	H_2O NaOH, HNO_3, CTAB	surfactant-assisted growth	Sheets or belts 10–30 nm × 2–3 μm	10–40 min reflux	[274]
$NaNbO_3$, $Na_2Nb_2O_6$	$NH_4Nb(C_2O_4)_2$	pH-dependent hydrolysis	H_2O NaOH	$Nb_2O_5{\cdot}n\,H_2O$ precipitation	Cubic-like and fibers μm range	100–40 min 200 °C	[275]
$LnVO_4$ (Ln=Ce, Pr, Nd)	NH_4VO_3, $Ln(NO_3)_3$ (Ln=Ce, Pr, Nd)	Hydrolysis	H_2O PEG	PEG-assisted	Aggregates of 20–30 nm particles	15 min	[276]
$CeVO_4$	V_2O_5, $Ce(NO_3)_3{\cdot}6\,H_2O$	pH-dependent hydrolysis	NaOH, AcOH or NH_4OH,	solvent-assisted hydroxylation	Aggregates of 6–18 nm particles	10 min (cycles 6 s MW on/10 s MW off) reflux	[277]
$ZnWO_4$	H_2WO_4, $Zn(OAc)_2$	Acidic hydrolysis	H_2O, citric acid	solvent-assisted hydroxylation then annealing at 300–600 °C	Aggregates of 18–25 nm particles	30 min (cycles 30 s on/30 s off)	[278]
Zn(OH)F	$Zn_5(OH)_8(NO_3)_2$	Hydrolysis	H_2O [tmim][BF_4]	ion-assisted growth	Nanofibers 80–200 nm × a few μm	60 min	[203]

[a] EtOH = ethanol; EtONa = sodium ethoxide; EDTA = ethylenediaminetetraacetic acid; OAc = CH_3COO^-; [bmin][BF_4] = 1-*n*-butyl-3-methyl imidazolium tetrafluoroborate; [tmim][BF_4] = 1,2,3-trimethylimidazolium tetrafluoroborate; NaOAc = sodium acetate; EG = ethylene glycol; CTAB = cetyltrimethyl ammonium bromide; PEG = poly-ethyleneglycol; AcOH = acetic acid; HMT = hexamethylenetetramine; SDS = sodium dodecyl sulfate; Ti(O*i*Pr)$_4$ = titanium tetraisopropoxide; Ti(OBu)$_4$ = titanium tetrabutoxide; EtOH = ethanol; NaBDS = sodium dodecylbenzenesulfonate-6; P123 = Poly(ethylene glycol)-*block*-poly(propylene glycol)-*block*-poly(ethylene glycol)

Table 5: Synthesis of doped oxide NCs under MW dielectric heating. The Table lists the main experimental conditions, size-morphological features of the resulting nanostructures, mechanistic pathways involved, and growth-governing factors.[a]

Metal oxide	Precursors	Reaction type	Solvent additives	Doping level [mol %]	Formation mechanism	Relevant NC features (morphology size range, size variance)	Synthesis time temperature pressure	Ref.
Pr-doped CeO_2	$(NH_4)_2Ce(NO_3)_2$, $Pr(NO_3)_3$	Alkaline hydrolysis	NH_4OH	0–10	solvent-assisted growth	Polyhedrons ca. 30 nm	15–120 min 2–14 atm	[279]
Gd-doped CeO_2	$Ce(NO_3)_3$ Gd_2O_3	Alkaline hydrolysis	H_2O HNO_3, NH_4OH	19	oriented attachment	Rods 20–60 nm × 50–500 nm	30 min 130 °C 3 atm	[280, 281]
Cu-doped $ZnGa_2O_4$	$Ga_2(SO_4)_3$ $ZnSO_4$ $CuCl_2$	Alkaline hydrolysis	H_2O NH_4OH	5	solvent-assisted growth	Aggregates of spherical 10–20 nm particles	30 min 150 °C	[282]
Sn-doped In_2O_3	$InCl_3$ $SnCl_4$	Glycolysis	DEG $N(CH_3)_4OH$	5	polyolassisted growth; MW-driven crystallization of amorphous hydroxide particle precursors	Spheres 15–19 nm $\sigma < 10\%$	120 min 200 °C 1 atm	[186]
Sn-doped In_2O_3	$InCl_3$ $SnCl_4$	Alkaline hydrolysis	IL DMF/EtOH $N(CH_3)_4OH$	8	solvent-assisted crystallization of amorphous hydroxide particle precursors	Irregular polyhedrons 25 nm $\sigma = 20$–30%	3–15 s 300 °C	[195]
La-Zr-doped TiO_2	Ti(O*i*Pr)$_4$, $ZrCl_4$ $La(NO_3)_3$	Acidic hydrolysis	*i*PrOH AcOH, citric acid, PEG, H_2O		polyol-assisted growth (crystallization requires annealing at 500 °C)	Aggregates of 15–25 nm particles	4 min	[283]
Ce^{+3},Tb^{+3}-doped $LaPO_4$	$Ln(NO_3)_3$ (Ln=La, Ce, Tb)	Glycolysis	EG $NH_4H_2PO_4$		polyol-assisted growth in microfluidic reactor	Nanorods 60–70 nm	20 s 80–150 °C	[84]

Table 5: (Continued)

Metal oxide	Precursors	Reaction type	Solvent additives	Doping level [mol %]	Formation mechanism	Relevant NC features (morphology size range, size variance)	Synthesis time temperature pressure	Ref.
In-doped ZnO	$Zn(OAc)_2$ $InCl_3$	Glycolysis	H_2O DEG	10	polyol-assisted growth	Spheres 15 nm	30 min 200 °C	[284]
Au-doped ZnO	$Zn(NO_3)_2$, $H[AuCl_4]$	Alkaline hydrolysis	EtOH NaOH, PEG NaOH, PVP	10	polymer-assisted growth	Nanoods 10–15 nm × 100–600 nm	10 min (MW cycles: 10 s on/20 s off)	[285]
Al-doped ZnO	$Zn(OAc)_2$ $AlCl_3$	Glycolysis	H_2O DEG	10	polyol-assisted growth	Spheres ca. 12 nm	30 min 200 °C	[284]
Pr-doped ZrO_2	$ZrOCl_2$ $Pr(NO_3)_3$	Alkaline hydrolysis	H_2O NaOH	10	solvent-assisted growth	Aggregates of ca. 15 nm particles	120 min 14 atm	[286]

[A] IL = $[N(CH_3)(C_4H_9)_3][(N(SO_2CF_3)_2]$; DEG = diethylene glycol; DMF = dimethyl formamide; O*i*Pr = isopropoxide; *i*PrOH = 2-propanol; OAc = acetate; PEG = polyethylene glycol.

dependent particle solubility.[161] In such environment, H_2O molecules simultaneously act as ligand and solvent, whereas the use of MW radiation provides their dielectric activation along with breakage of hydrogen bonds, resulting in rapid and homogeneous heating, elevated temperatures and pressures. In many instances the as-synthesized oxide nanoparticles are amorphous in nature, therefore a further calcination step is required to convert them into a crystalline form.[163–167] A post-synthesis thermal air treatment may also be necessary to promote further oxidation and phase transformation of crystalline particles (e.g., in the case of CoO and MoO_2 converting to Co_3O_4 and MoO_3, respectively).[168]

Based on the high reactivity of metal salts (e.g., metal chlorides, nitrates, sulfates) or metal–organic compounds (e.g., metal alkoxides) in aqueous media, the control over the NC size and shape is generally rather arduous in the absence of any extra additives and/or capping agents.[167] However, some groups have reported moderate shape control of NCs by ligand-free synthesis under hydrothermal conditions. For instance, micrometer-sized α-Fe_2O_3 particles with a dendritic six-fold symmetry were obtained in moderate yield (ca. 40%) by heating $K_4[Fe(CN)_6]$ in water at 150 °C under MW irradiation for 3 h, without using any reducing or capping agent. The α-Fe_2O_3 objects formed in the rhombohedral crystal structure via hydrolysis of octahedral $[Fe(CN)_6]^{4-}$ ions, followed by condensation of the hydroxylated species and lattice growth along six equivalent crystallographic directions to give rise to morphologies reminiscent of pine trees. Mechanistic investigations revealed the crucial role played by the reactant concentration and growth temperature in smoothing the dendritic particle contour and influencing the ultimate growth rates.[168]

It was possible to extend the same synthesis approach to obtain micrometer-sized architectures made of either CoO, MoO_2, Cr_2O_3 or Mn_2O_3 primary particles that had assembled into uniform octahedral-, triangular-nanorod-shaped, or spherical-like aggregates at 180 °C in 1–3 h.[168] The accessed morphologies and crystal phase were proven to withstand high-temperature air calcination treatments (Figure 7 a–e). Interestingly, the metal ferrites, decorated with Pd clusters (linked to the ferrites by amine bridges), were exploited as valuable platforms for various heterogeneous catalytic organic transformations, such as carbon–carbon cross-coupling reactions.[168,169]

A high-yield route to monodisperse cubic-phase spinel ferrite ($MeFe_2O_4$, where Me = Ni, Co, Mn) and maghemite (γ-Fe_2O_3) NCs in immiscible H_2O/toluene media was also presented.[170] Heating at 160 °C for at least 1 h under MW irradiation was applied to an aqueous solution of nitrate or chloride metal salts, which had been combined with a toluene solution of OLAC, the latter serving as both stabilizer and organic-transferring agent for the NCs that evolved at the H_2O/toluene interface. The method afforded gram-scale production of uniform spherical NCs in the 4–9 nm size range. Comparative tests of MW versus conventional syntheses indicated that the MW approach required milder temperatures for NC formation.

A MW-assisted hydrothermal approach was implemented to produce pure tetragonal-phase $BaTiO_3$ NCs by irradiating stoichiometric amounts of $BaCl_2$ and either $TiCl_4$ or titanium isopropoxide in the presence of KOH at 140–170 °C.[171,172] The as-synthesized $BaTiO_3$ NCs exhibited a spherical morphology and a non-uniform size distribution, additionally showing an intense and broad photoluminescence green band at room temperature (Figure 7 f). The growth kinetics was subjected to theoretical and experimental investigations from which it was concluded that the NCs grew by coarsening controlled by a reversible interface reaction.[173] MW irradiation accelerates the $BaTiO_3$ growth rate by up to one order of magnitude compared to the conventional hydrothermal process. In addition, it was verified that, in contrast to the results achieved using conventional heating, MW treatment guaranteed formation of NCs with monomodal size variance. The crystal structure and size-morphological features of the NCs were influenced by the MW frequency (in the range 3–5.5 GHz) and bandwidth sweep time.[172]

A report on nanoscale $PbTiO_3$ dealt with the synthesis of 50 nm spherical perovskite nanospheres and 40–60 nm thick PX phase acicular microwires with an aspect ratio close to 90:1.[174] The nanostructures were achieved in hydroalcoholic media of H_2O/EG and H_2O/ethanol, upon MW treating of mixtures of lead acetate and titanium tetrabutoxide under

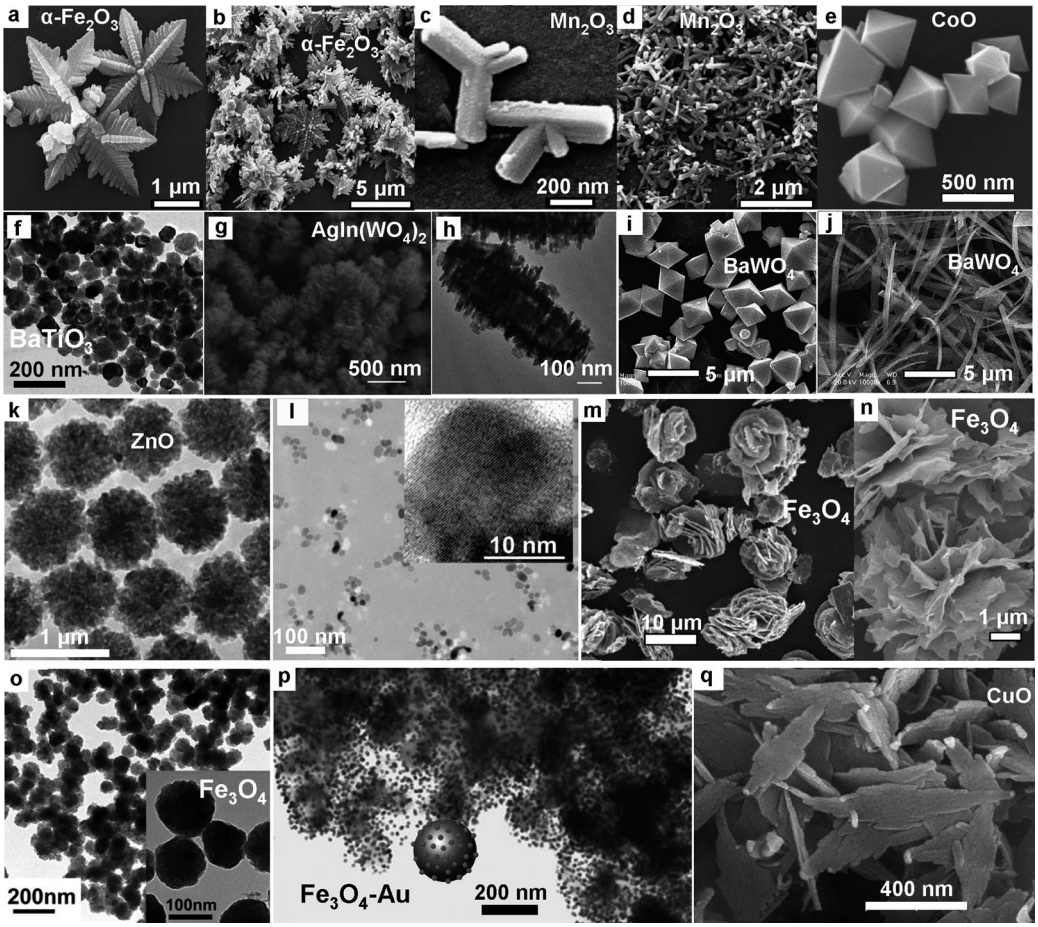

Figure 7. Examples of transition-metal oxide NCs and microstructures grown under is MW irradiation. a)–e) SEM images at different magnification of dendritic α-Fe_2O_3 particles, Mn_2O_3 multipods, and of octahedral CoO mesocrystals, synthesized according to Ref. [168]; f) TEM image of slightly aggregated spherical $BaTiO_3$ NCs obtained according to Ref. [172]; g),h) SEM and TEM images, respectively, of $AgIn(WO_4)_2$ caterpillar-like NCs prepared according to Ref. [177]; i),j) SEM images of $BaWO_4$ NCs in octahedral and belt-like shapes, respectively, prepared according to Ref. [180]; k) TEM pictures of blackberry-like clustered ZnO NCs, prepared according to ref. [191]; l) TEM picture of oblate ZnO NCs synthesized according to Ref. [188] (inset: a high-resolution TEM image of a single particle); m),n) SEM pictures of rose-like shaped Fe_3O_4 microparticles adapted from Ref. [192]; o),p) TEM pictures of spherical Fe_3O_4 NCs and Au-decorated hybrid counterparts thereof, respectively, synthesized according to Ref. [193]; q) SEM image of leaf-like CuO NCs prepared according to Ref. [199].

alkaline conditions for 90 min at 200 °C. Anisotropic growth presumably took place through coalescence of primary particles in the absence of tightly binding EG molecules. Groups of needle-shaped $PbTiO_3$ nanowires were observed to arrange parallel to each other into regular bundles along the $\langle 001 \rangle$ axis direction. Unexpected Raman modes were detected and interpreted as arising form from breakage of the translation lattice symmetry across contiguous unit cells.

One interesting strategy devised to decrease and/or to adjust the metal oxide precursor susceptibility towards the hydrolysis relied on realizing controllable in-situ H_2O production to allow for local control of the H_2O concentration. As an example, α-Fe_2O_3 NCs with average sizes ranging from 15–40 nm were synthesized by forced hydrolysis of $FeCl_3$ with H_2O released from MW-assisted esterification of ethanol and acetic acid 150 °C.[175] The as-synthesized NCs showed high-performance electrochemical sensing ability. Hexagonal-phase WO_3 nanowires with a diameter of 5–10 nm and length of up to several microns were synthesized by processing a solution containing Na_2WO_4 as molecular precursor and $(NH_4)_2SO_4$ as capping agent with MW radiation at 150 °C for 3 h.[176] From the investigation of the impact of several salt cations and anions on the crystal phase and morphology of the resulting nanostructures, it was concluded that ammonium ions worked as structure-directing stabilizers, whereas sulfate anions determined anisotropic growth. The nanowires exhibited distinctive electrocatalytic activity for hydrogen evolution from water.

There have also been studies on the formation of complex oxides incorporating multiple transition metals. Very recently, $AgIn(WO_4)_2$ mesocrystals were derived upon irradiating aqueous suspension of $AgNO_3$ and hydrated $In(NO_3)_3$ and Na_2WO_4 salts for 20 min at 180 °C.[177] The resulting objects, in the size range of a few hundreds of nanometers, showed exotic caterpillar-like shape made of an elongated core out of which rod-like stripes of the material had vertically grown (Figure 7 g,h). The pH value of the reaction solution was concluded to be the most critical parameter governing the crystal phase, morphology and the composition of the particle product. Concurrence of random oriented attachment and Ostwald ripening processes was invoked in order to explain the formation of the particular architectures observed. The $AgIn(WO_4)_2$ nanostructures were successfully utilized in the selective photocatalytic degradation of organic dyes under UV/Vis light excitation.

An elaborate ambient-pressure, continuous-flow method was proposed to synthesize rather agglomerated $NiFe_2O_4$ and $ZnAl_2O_4$ NCs with mean sizes within the 6–20 nm range.[83] The approach combined MW heating with in-situ precursor mixing achieved by an ultrasonic nozzle spray. The same research group investigated the influence of the vaporization

conditions on the average particle size as well as the effect of the MW irradiation on promoting diffusion and mixing of the reagents, thereby facilitating complete conversion of the starting materials to single-phase products. In a similar way they succeeded in synthesizing other complex micrometer-size multimetal oxides, such as, for instance, Mo-V-Te-based or Mo-V-Te-Nb-Pd-based oxides.[178]

3.2.2. Organic-Ligand-Assisted Hydrolytic Synthesis

Alternative routes to manipulate the precursor reactivity make use of organic additives like carboxylic acids, β-diketones, block copolymers or functional alcohols, which can either act as chelating ligands complexing the metal precursors or provide self-assembled nanoreactors in which the synthesis is physically constrained. For instance, monodisperse 5 nm TiO_2 nanoparticles were grown inside the inner aqueous pools of inverse polystyrene-*co*-poly(ethylene oxide) diblock copolymer micelles dispersed in toluene upon fast hydrolysis of titanium alkoxide under MW treatment at 80 °C.[236] The choice of the chemical structure of the diblock copolymer affected the micelle formation mechanism, in turn influencing the size of the TiO_2 nanoparticles and their propensity to assemble into larger superstructures. In a similar way, a triblock copolymer was used as a templating agent for the preparation micrometer-long anatase TiO_2 rods with 30–50 nm diameter upon hydrolysis of $TiCl_4$.[179] Mechanistic investigations revealed that these objects formed upon oriented attachment of small primary particles into pearl-necklace-shaped assemblies that evolved into progressively defined rod-shaped objects with a mesoporous structure. In the synthesis of single-crystalline $BaWO_4$ nanosheets and nanobelts upon MW-assisted hydrolysis of Na_2WO_4 and $BaCl_2$ in PVP-based micelles at 100 °C (Figure 7i,j), the PVP concentration had to be carefully adjusted to ensure formation of nanostructures with reproducible morphologies.[180]

Several reports have documented the specific use of surface-binding ligands and polymers as size and shape regulating agents. Using $FeSO_4$ as precursor, 20–50 nm thick Fe_3O_4 nanowires were obtained under MW-assisted hydrothermal conditions with PEG acting as a soft template. These nanostructures could subsequently be decorated with carbon via a MW-driven carbonization process, ultimately affording excellent charge cyclability and rate performance when used as anode in lithium-ion batteries.[181,182]

Moderately polydisperse water-soluble 10–20 nm Co_3O_4 NCs with either a spherical or cubic shape were prepared under MW irradiation of different types of Co salts complexed with 3-mercaptopropionic acid at 100–140 °C.[183] The experimental results pointed out that the temperature was the key variable dictating the NC habit, in agreement with the shape dependence of the thermodynamic stability order expected for cubic-phase materials. In another study, a continuous-flow reactor was utilized to achieve MW-stimulated sol-gel synthesis of amorphous ZrO_2 nanoparticles from a hydroalcoholic solution of zirconium tetraisopropoxide and caproic acid as stabilizer.[184] The reaction outcome manifested a flow-rate dependence, leading to severe effects on the particle size and dispersion. Specifically, low flow rates promoted formation of well dispersed 100 nm ZrO_2 spheres, whereas higher fluxes produced agglomerates made of smaller clusters.

3.2.3. Nonhydrolytic Approaches

Despite the simplicity of the hydrothermal method and its potential applicability to large-scale preparation, the inevitable temporal overlapping of the hydrolysis and condensation reactions, as well as the strong sensitivity of the latter to any slight changes in the synthesis conditions, make it hard to fully control the formation of metal oxides in aqueous media. Alternative powerful preparation routes to transition-metal oxide NCs rely on the exploitation of nonhydrolytic pathways in non-aqueous solvents, whereby organic molecules serve as both oxygen sources and capping agents under strict exclusion of H_2O.[11,17,18] These mechanisms generally allow a good control over the NC structure, size, shape, while ensuring an appreciable degree of liquid-phase dispersibility.[185] Alcohols and, particularly, polyhydroxy alcohols, which are characterized high $\tan\delta$ values, have proven to be convenient reaction media for non-aqueous MW-assisted synthesis.

Numerous examples have appeared in the recent literature. Sn-doped In_2O_3 (ITO) NCs were synthesized by a two-step polyol method based on the initial precipitation of amorphous indium tin oxide (ITO) from $InCl_3$ and $SnCl_4$ salts in DEG in the presence of $N(CH_3)_4OH$, followed by MW-induced crystallization at 200 °C. This procedure led to aggregation-free monocrystalline NCs with an average diameter of about 17 nm and good size variance.[186]

On several instances, small NCs were successfully produced, which frequently showed a strong tendency toward uncontrollable clustering into large micron-sized aggregates. For example agglomerates of sub-10 nm ZnO, CoO, Mn_xO_y, Fe_3O_4, and $BaTiO_3$ NCs were achieved by the ultrafast reaction of benzyl alcohol with various metal acetate and metal acetonate precursors by an ester elimination process in 0.5–3 min at 200 °C.[187] Reaction acceleration was initially suggested to be due to specific interactions of the MW field with the polar transition state resulting from the nucleophilic attack of benzyl alcohol on the acetate ligands (see Section 4.3).[187] In a later more detailed study, it was ascertained that MW irradiation not only increased the aforementioned esterification reaction, but also boosted the inherent rate of NC growth (Figure 7l).[188]

In the same size regime, $La_{0.75}Sr_{0.25}Cr_{0.93}Ru_{0.07}O_{3-\delta}$ NCs were obtained upon MW heating of an ethanolic solution of hydrated LaN_3O_9, $SrCl_2$, CrN_3O_9, $RuCl_3$, and sodium ethoxide at 160 °C.[189] In a different case, reiterated seeding steps based on MW processing of hydrated zinc acetate in EG led to the formation to rather monodisperse ZnO clusters composed of primary 8 nm NCs, which could be tailored with diameters in the 50–275 nm range.[190] Oriented attachment pathways in the presence of suitably balanced amounts of ZnO NC seeds and zinc acetate precursor were found to be responsible for the controllable formation of such nanostructures. Analogous features were observed upon MW decomposition of zinc oximate or zinc acetylacetonate complex precursors in various alkoxyethanols (RO-C_2H_4OH, R = methyl, ethyl,

butyl), which led to suspensions of sub-200 nm "blackberry"-like ZnO clusters consisting of irreversibly aggregated zincite crystallites (Figure 7k).[191]

Moderately uniform flower-like Fe_3O_4 assembled clusters were fabricated in EG upon MW treatment of $FeCl_3$, sodium acetate and either a selected triblock copolymer or surfactant species.[192,193] It was speculated that MW radiation set homogeneous conditions for the creation of the starting NC seeds in the precursor solution and accelerated subsequent clustering under assistance of the relevant stabilizers. The as-prepared Fe_3O_4 superstructures (Figure 7m,n) exhibited high sensitivity and good reversibility for sensing of ethanol vapor at room temperature,[192] while also demonstrating electrochemical and catalytic properties after functionalization with polypyrrole and Au nanoparticles (Figure 7o,p).[193]

An appealing class of reaction fluids that may coexist with or totally replace traditional molecular solvents in MW synthesis is represented by ionic liquids. These compounds are entirely formed by ions (one of which is organic with delocalized charge) that are poorly coordinated, and therefore behave as molten salts already at very low temperatures. Their ionic nature provides high absorption capabilities in the MW frequency range.[194] In some cases, ionic liquids may be able to coordinate to the growing NC surface, thereby acting as weak colloidal stabilizers that can influence the relevant nucleation and growth stages. In addition, the experimental combination of a nonvolatile aprotic solvents and MW irradiation allows reaching ultrafast heating rates up to very high temperatures (for example, up to 300 °C within 15 s) at relatively low autogenic pressures, which are favorable to access well-crystallized oxide NCs under anhydrous conditions. Ultimately, from the environmental and economical viewpoints, ionic liquids offer benefits related to the ease with which they can be recovered and reused in successive reactions.

Some examples are worth mentioning. Conductive 25 nm ITO NCs with faceted shape were produced by MW-induced crystallization of amorphous metal hydroxide particles resulting from alkaline co-hydrolysis of $SnCl_4$ and $InCl_3$ precursors in $[N(CH_3)(C_4H_9)_3][N(SO_2CF_3)_2]$ ionic liquid.[195] Size-controlled anatase TiO_2 NCs with a truncated cube-like profile were achieved by decomposing titanium isopropoxide in 1-butyl-3-methylimidazolium tetrafluoroborate ([bmim][BF_4]),[196] whereas single-crystalline microsheets of anatase TiO_2 were derived by treating titanium tetrafluoride at 210 °C in the same ionic liquid.[197] Minute amounts of [bmim][BF_4] added to nonpolar dibenzyl ether reaction medium were exploited as MW-coupling antenna to enable fast heating required for the OLAC-assisted synthesis of 6 nm Fe_3O_4 NCs from the nonhydrolytic reaction of iron acetylacetonate and 1,2-hexanediol at 250 °C.[198] Ionic liquids have also been employed in MW-hydrothermal synthesis of several other prototypes of metal oxide nanostructures with largely diversified shapes, such as of CuO,[199–201] (Figure 7q), ZnO,[202] $Zn(OH)_2$,[203] $ZnFe_2O_4$, and iron oxohydroxides.[204,205]

3.3. Non-Oxide Semiconductors

NCs and HNCs made of non-oxide semiconductors (transition-metal chalcogenides, fluorides, and nitrides, as well as metal phosphates) are widely acknowledged for the unique size dependence of their conduction and optical absorption/photoluminescence properties (related to quantum-confinement effects and the high probability of radiative carrier recombination from band-edge states), while many metal fluorides and phosphates are sought after as convenient host lattices in which rare-earth elements can be allowed to produce ultra-narrow light bands at fixed wavelengths. All these features are widely exploited in optoelectronic and sensing devices, as well as in biomedicine (e.g., optical labeling, tomographic imaging). On the other hand, materials, such as metal nitrides and metal phosphates exhibit thermal, electric and electrochemical properties relevant to energy storage and conversion applications.

This Section summarizes recent progress achieved in the MW-assisted preparation of semiconductor NCs and HNCs, with a major emphasis on metal chalcogenide materials, for which the highest level of synthetic control under conventional heating condition has already been reached. The results so far documented illustrate the remarkable synthetic flexibility afforded by MW-driven routes over the traditional ones. This transcribes, for example, into the possibility of: a) using a broader variety of precursors (even poorly soluble compounds that are normally unsuitable to be transformed into high-quality NCs by traditional colloidal approaches); b) promoting more efficient reactant decomposition and/or alternative reaction pathways; c) inducing the desired temporally short, spatially homogeneous nucleation event upon realization of abrupt volumetric heating; and d) accelerating growth. Table 6 summarizes reaction conditions, product characteristics, and main formation mechanisms of semiconductor NCs/HNCs processed under MW conditions. Representative TEM examples of the as-synthesized nanostructures are shown in Figure 8 and Figure 9.

3.3.1. Metal Chalcogenide and Metal Chalcogen NCs

The use of MW irradiation was considered within the frame of well-established organometallic approaches to synthesize fluorescent CdX (X = Se, S, Te) NCs in hot alkane and/or surfactant media at 180–280 °C.[287–291] In earlier studies on the formation of CdSe NCs, two approaches were comparatively examined: the pyrolysis of a single-source precursor, $Li_4[Cd_{10}Se_4(SPh)_{16}]$, in hexadecylamine (HDA) in the presence of a small aliquot of a ionic liquid additive, 1-hexyl-3-methylimidazolium chloride ([hmim][Cl]); and the reaction of cadmium stearate complex (obtained from CdO and stearic acid) with tetrabutylphosphine selenide (TBPSe) in mixtures of HDA and tri-*n*-octylphosphine oxide (TOPO).[287] The syntheses were performed in dedicated MW reactors equipped with pressurized vessels, to which active cooling with compressed air allowed the reaction temperature to be adjusted to a constant level after the initial ramp at any MW power applied, as well as the growth process to be rapidly quenched when desired, preventing Ostwald

Table 6: Synthesis of non-oxide semiconductor NCs and HNCs under MW dielectric heating. The table lists the main experimental conditions, size-morphological features of the resulting nanostructures, mechanistic pathways involved, and growth-governing factors.[a]

Material	Precursors	Reaction type	Solvent additives	Formation mechanism	Relevant NC features (morphology size range, size variance)	Synthesis time temperature pressure	Ref.
CdS	$CdCl_2$ TAA	Thermolysis	H_2O	solvent-assisted growth	aggregated spheres 9 nm polydisperse	20 min reflux	[331]
CdS	$Cd(OAc)_2$ thiourea	Thermolysis	DMF	solvent-assisted growth	spheres <5 nm polydisperse	18 s 1 atm 80 °C	[332]
CdS	$Cd(OAc)_2$ thiourea	Thermolysis	DMF 1-thioglyc	ligand-assisted growth	spheres <5 nm polydisperse	50 s 1 atm	[333]
CdS	$CdCl_2$ thioacetamide	Thermolysis	H_2O NaCT, KOH	solvent-assisted growth	aggregated spheres $\approx$20 nm	1 min 86 °C	[334]
CdS	$[\{Cd(APDTC)_2\}_2]$	Thermolysis	EDA	ligand-assisted growth	nanowires 5×50–100 nm polydisperse	1 min reflux	[335]
CdS	$Cd(ClO_4)_2$ thioacetamide	Thermolysis	H_2O DNA, Tris-EDTA	polymer-templated growth	nanowires 140–170 nm×8–12 μm	60 s (intermittent) 1 atm	[297]
CdS	Cadmium ethyl xanthate	Thermolysis	DMF Alkylamines	surfactant-assisted growth	nano-rds/wires 1–1.5 nm×5–450 nm $\sigma=10\%$	0.5–3 min (400 W) >1 atm	[293]
CdS	$CdSO_4$, Na_2S	co-precipitation	H_2O, Heptane, AOT	micelle-templated growth	spheres ca. 2.7 nm polydisperse	4–550 min 1 atm 30–35 °C	[298, 299]
CdSe	$Li_4[Cd_{10}Se_4(SPh)_{16}]$	Thermolysis	HDA [hmim][Cl]	surfactant-assisted, ionic-liquid-propelled growth	spheres ca. 2–5 nm $\sigma=10$–15%	30 s–10 min >1 atm 90 °C	[287]
CdSe	CdO-SA TBPSe	Thermolysis	TOPO, HDA	surfactant-assisted, TOPO-liquid-propelled growth	spheres ca. 2–5 nm $\sigma=10$–15%	30 s >1 atm 160–240 °C	[287]
CdSe	CdO-OLAC TOPSe	Thermolysis	Diesel, Glyc	surfactant-assisted growth	irregular spheres ca. 2 nm polydisperse	30 s–5 min 1 atm 50–140 °C	[336]
CdSe PbSe $Cu_{2-x}Se$,	$CdSO_4$ $Pb(OAC)_2$ $CuOAC)_2$ Na_2SeSO_3	Thermolysis	H_2O NTA	surfactant-assisted growth	agglomerated spheres ca. 5 nm polydisperse	0.5 min 1 atm reflux	[337]
CdX (X=S, Se, Te)	CdSA TOPS, TOPSe or TOPTe	Thermolysis	Pentane, heptane, octane, decane HAD	surfactant-assisted growth	spheres, ellipsoids 4–6 nm $\sigma=6$–12%	18 min >1 atm 220–240 °C	[288–290]
CdSe	$Cd(OAc)_2$ Se	Thermolysis	EG	polyol-assisted growth	spherical aggregates of tiny clusters 6–7 nm	60 min reflux	[338]
CdSe	$Cd(OAc)_2$ Se	Thermolysis Solvent-driven reduction	Cyclohexanone	solvent-assisted growth	aggregated spheres 3–6 nm	0.5–15 min 1 atm 145 °C	[339]

Table 6: (Continued)

Material	Precursors	Reaction type	Solvent additives	Formation mechanism	Relevant NC features (morphology size range, size variance)	Synthesis time temperature pressure	Ref.
CdSe	Cd $(OAc)_2$ Selenourea	Thermolysis	DMF Alkylamines	surfactant-assisted growth	nanords 2 nm×4 nm polydisperse	0.5–3 min >1 atm	[293]
CdSe	$Cd(NO_3)_2$ Se	Thermolysis	Glyc, OLAC, PVP, CTAB	ligand-/polymer-assisted growth	multipods 1–2 μm polydisperse	10 min 1 atm 150°C	[340]
CdTe	$CdCl_2$ Na_2TeO_3 $NaBH_4$	$NaBH_4$-, MPA-driven reduction	H_2O TSC, MPA	ligand-assisted growth	irregular spheres ≈3 nm	10–40 min >1 atm 80–140°C	[341]
CdTe	$CdCl_2$ NaHTe	Thermolysis	H_2O MPA or TGA	ligand-assisted growth	spheres <5 nm σ<10%	15–120 s/10–60 min >1 atm 80–120°C	[294, 295, 342]
CdTe	CdO TeTBP	Thermolysis	ODE TDPA	surfactant-assisted growth	Spheres ca. 4.4 nm σ=5–10%	1–90 min 1 atm 180–280°C	[291]
CdZnSe	$Cd(OAc)_2$ $Zn(OAc)_2$ Se	EG-driven reduction	EG NaOH	polyol-assisted growth	aggregated spheres ca. 6 nm polydisperse	60 min MW cycles (21 s on/9 s off) reflux	[343]
Mn:ZnSe@ZnS	Core: $Cd(OAc)_2$, Se, $NaBH_4$, $MnCl_2$ Shell: Na_2S, $Zn(OAc)_2$ hexamethyldisilathiane	Thermolysis Coprecipitation	H_2O Sodium oleate H_2O, MPA	surfactant-assisted two-step seeded growth	Spheres ca. 6 nm σ=15–20%	40 min 12 atm 170°C 5 min 1 atm 70°C	[329]
CdSe@ZnS	Core: CdSA, Se, Shell: $Zn(Un)_2$, CySCN	Thermolysis	TOPO, TOP, SA, HDA Octylamine	surfactant-assisted one-pot two-step seeded growth	spheres <5 nm polydisperse	30–120 s 1 atm MW 5 cycles (30 s on/2 min off)	[324]
CdSe@ZnS	Core: $Cd(OAc)_2$, Se, Shell: $Zn(Et)_2$ Haxamethyldisilathiane	Thermolysis	TOPO, TOP, HDA NMP, But-amine, MPA	ligand-assisted two-step seeded growth	spheres 2–6 nm σ=10–15%	1–5 min 1 atm 145–150°C 5 min 1 atm 70°C	[328]
CdSe@ZnS	Core: $CdCl_2$, Se, shell: HMTD, $ZnCl_2$,	Thermolysis	H_2O, MPA, NaOH, $NaBH_4$ H_2O, NH_4OH	ligand-assisted two-step seeded growth	aggregated spheres <5 nm polydisperse	10 s 45–120 min 140–170°C	[325]
CdTe@CdS	core: $CdCl_2$, NaHTe shell: $CdCl_2$, Na_2S	Thermolysis	H_2O, MPA H_2O, MPA	surfactant-assisted two-step seeded growth	spheres	1 min 100°C 5–3 min 100–120°C	[325]
CdTe@CdS@ZnS	core: $CdCl_2$, NaHTe shell1: $CdCl_2$, Na_2S shell2: $ZnCl_2$, Na_2S	Thermolysis	H_2O, MPA H_2O, MPA H_2O, MPA	ligand-assisted three-step seeded growth	spheres 3–5 nm	1 min, 100°C 5 min, 100°C 5 min, 60°C	[327]
Cu_9S_8	$Cu(NO_3)_2$ TAA	Thermolysis	H_2O SDS	ligand-assisted growth	nanorods 5×50 nm	20 min reflux	[344]
CuS	$Cu(OAc)_2$ thioacetamide	Thermolysis	H_2O FA	ligand-assisted growth	irregular spheres 5–10 nm	20 min reflux	[345]
$CuInS_2$	$CuCl_2$, $InCl_3$ Na_2S	Thermolysis	H_2O MAA	ligand-assisted growth	spheres 3 nm	30 min 90°C	[346]

Table 6: (Continued)

Material	Precursors	Reaction type	Solvent additives	Formation mechanism	Relevant NC features (morphology size range, size variance)	Synthesis time temperature pressure	Ref.
$CuInS_2$	CuI, $InCl_3$ S	Thermolysis	OLAM	surfactant-assisted growth	irregular spheres 3–10 nm polydisperse	20–30 min >1 atm 120–220 °C	[303]
$CuInS_2$	$[P(iBu)_3]_2CuIn(SEt)_4$ or $(PPh_3)_2CuIn(SEt)_4$	Thermolysis	DOP hexanethiol	ligand-assisted growth	spheres 3–5.2 nm	20–30 min 1 atm 140–170 °C	[302]
$CuInSe_2$	$CuCl_2$, $InCl_3$ Na_2Se	Thermolysis	H_2O MAA	ligand-assisted growth	spheres 4.5 nm	30 min 90 °C	[347]
$CuInSe_2$	CuCl, In, Se	TEG-driven reduction	TEG	ligand-assisted growth	Irregular spheres ca. 83 nm	60 min reflux	[304]
$CuInS_2$	$CuCl_2$, $InCl_3$ Se	Thermolysis	EDA	ligand-assisted or seed-assisted growth	platelets, rods 20–50 nm × 2–5 μm polydisperse	5–30 min 1 atm 180 °C	[300]
$CuInTe_2$	CuCl, In, Te	TEG-driven reduction	TEG	ligand-assisted growth	irregular spheres ca. 94 nm	60 min 1 atm reflux	[347]
$CuIn_xGa_{1-x}S_2$	$(Ph_3P)_2Cu(\mu\text{-}SEt)_2In(SEt)_2$, $(Ph_3P)_2Cu(\mu\text{-}SEt)_2\text{-}Ga(SEt)_2$	Thermolysis	Benzyl acetate, 1,2-ethanedithiol	ligand-assisted growth	aggregated spheres 2.9–4.3 nm polydisperse	60 min 1 atm 160–240 °C	[301]
Cu_2SnSe_4	$CuCl_2$ Sn, Se	polyol-driven reduction	PEG	polyol-assisted growth	irregular aggregates 30–50 nm polydisperse	120 min 1 atm reflux	[348]
PbS	$Pb(OAc)_2$ S	polyol-driven reduction	PEG	ligand-assisted growth	irregular spheres 20–30 nm polydisperse	20 min 1 atm reflux	[349]
PbS	$Pb(OAc)_2$ thiourea	Thermolysis	EtOH or H_2O EG or PEG	ligand-assisted growth	spherical or rectangular or ear-like or hexapod	30 min MW 30 s cycles (9 s on/21 s off) reflux	[350–352]
PbS	$Pb(OAc)_2$ S	Thermolysis	EtOH NaOH	solvent-assisted growth	roughly spherical ca. 10 nm	20 min MW 30 s cycles (6 s on/24 s off) reflux	[353]
PbSe	$Pb(OAc)_2$ selenourea	Thermolysis	phenyl ether, DMF OLAC	surfactant-assisted growth	polyhedrons, cubes 5–15 nm $\sigma = 5$–10%	1 min 3 bar 160 °C	[292]
ZnS	$Zn(OAc)_2$ TAA	Thermolysis	H_2O	solvent-assisted growth	clustered spheres <100–300 nm polydisperse	15 min reflux	[354]
ZnS	$Zn(OAc)_2$ thiourea	Thermolysis	DMF PVP	polymer-assisted growth	spheres ca. 7 nm polydisperse	1–12 min MW 30 s cycles (9 s on/21 s off) 1 atm	[355]
ZnS	zinc ethyl xanthate	Thermolysis	DMF Alkylamines	surfactant-assisted growth	nano-rods/wires 1–1.5 nm × 5–450 nm $\sigma = 5$–10%	0.5–3 min (400 W) >1 atm	[293]

Table 6: (Continued)

Material	Precursors	Reaction type	Solvent additives	Formation mechanism	Relevant NC features (morphology size range, size variance)	Synthesis time temperature pressure	Ref.
ZnSe	$Zn(OAc)_2$ Se	Thermolysis	TBP Alkylamines	surfactant-assisted growth	aggregated spheres/ellipsoids 20–500 nm polydisperse	20 min >1 atm 180°C	[356]
ZnSeS	$ZnCl_2$ NaHSe MPA	thermolysis	H_2O MPA	ligand-assisted growth	spheres ca. 5 nm	55 min >1 atm 140°C	[357]
ZnSe	$Zn(OAc)_2$ selenourea	Thermolysis	DMF Alkylamines	surfactant-assisted growth	nano-rods/wires 1–1.5 nm × 5–450 nm $\sigma = 6$–12%	0.5–3 min (400 W) >1 atm	[293]
$Zn_xCd_{1-x}S$	$Zn(OAc)_2$, $Cd(OAc)_2$, $(Et)_2NCS_2Na$	Thermolysis	H_2O EDA	ligand-assisted growth	nanorods 5–10 nm × 30–150 nm polydisperse	10 min >1 atm 140–160°C	[296]
HgS	$Hg(OAc)_2$ thiourea	Thermolysis	EtOH or THF or DMF or H_2O	solvent-assisted growth	aggregate spheres 8–23 nm polydisperse	10 min MW 30 s cycles (6 s on/24 s off) reflux	[358]
HgTe	$Hg(OAc)_2$ Te	Thermolysis	EDA	ligand-assisted growth	irregular shapes 40 nm polydisperse	120 min reflux	[359]
Bi_2S_3	$Bi(NO_3)_3$ Thiourea glutathione	Thermolysis	H_2O FA, proteins, peptite	ligand-/biomelecule assisted growth	nanorods/wires 10–30 nm × 200–900 nm polydisperse	20 min >1 atm 120–160°C	[307, 360]
Bi_2Se_3	$BiONO_3$ Se	EG-driven reduction	EG NaOH	polyol-assisted growth	cucumber-like 50 × 300 nm	30 min MW 30 s cycles (21-s on/9-s off) reflux	[361]
$MoSe_2$	$Mo(CO)_6$ Se	EG-driven reduction	EG	polyol-assisted growth	aggregates 100–400 nm	60 min 1 atm reflux	[362]
Se	Na_2SeO_3,	$NaBH_4$-driven reduction	EDA $NaBH_4$	ligand-assisted growth	nanorods 30–150 nm × 1–2 μm polydisperse	60 min >1 atm 80–160°C	[363]
Te	TeO_2 H_2TeO_3	additive-driven reduction	[hmim][BF_4] PVP $NaBH_4$ sugars	polymer- and ion-assisted growth	nano-rods/wires 15–40 nm × 100–700 nm $\sigma = 20$–30%	10 min >1 atm 80–180°C	[305, 307]
Te	Na_2TeO_3	additive-driven reduction	H_2O PVP (polyAA or CTAB) NH_4OH, N_2H_4	polymer-/surfactant-driven growth Ostwald ripening	nanorods, nanowires 20 nm × 2–10 μm	15 min >1 atm 150°C	[306]
$NaYF_4$:M (M=Yb^{3+}, Er^{3+}, Tm^{3+})	Na(TFA), $Y(TFA)_3$, $Yb(TFA)_3$, $Er(TFA)_3$, $Tm(TFA)_3$	Thermolysis	ODE OLAC	surfactant-assisted growth	cubes, cubo-octahedrons ca. 10 nm $\sigma = 5$–10%	5 min 1 atm 290°C	[308]

Table 6: (Continued)

Material	Precursors	Reaction type	Solvent additives	Formation mechanism	Relevant NC features (morphology size range, size variance)	Synthesis time temperature pressure	Ref.
$KMgF_3$ $KMgF_3$:Tb^{3+}	K_2CO_3, $MgCO_3$, CF_3COOH $Tb(TFA)_3$	Thermolysis	OLAC, OLAM	surfactant-assisted growth	spheres, platelets ca. 10 nm nanorods 5×100–200 nm σ = 5–10%	30 min 1 atm 290 °C	[309]
GdF_3:Eu^{3+}	$Gd(TFA)_3$ $Eu(TFA)_3$	Thermolysis	EG [bmim][BF_4]	polyol- and ion-assisted growth	aggregated irregular spheres ca. 6 nm polydisperse	15 min 1 atm 120 °C	[310]
LaF_3:Ce^{3+},Tb^{3+}	$La(NO_3)_3$ $Ce(NO_3)_3$ $Tb(NO_3)_3$ NH_4F	Thermolysis	EG	polyol-assisted growth	aggregate irregular spheres ca. 4.5 nm polydisperse	20 s 1 atm 80–120 °C	[84]
GaInP InP	$In(OAc)_3$ $Ga(PENT)_3$ $(TMS)_3P$	Thermolysis	ODE, decane HDDA	HDDA-assisted growth	spheres < 4 nm monodisperse	30 s–15 min 1 atm < P < 6 atm 280 °C	[287]
InP	In-palm $(TMS)_3P$	Thermolysis	Decane [hmim][BF_4] or [hmim][PF_6] or [hmim][Cl] or [hmim][Cl]	in-situ ion-assisted surface etching	spheres 2.7 nm monodisperse	1–25 min +15 min >1 atm 280 °C	[312]
$LaPO_4$: RE (RE=Ce^{3+}, Eu^{3+}, Tb^{3+})	$LaCl_3$, $CeCl_3$ $TbCl_3$, H_3PO_4	Thermolysis	EtOH, DMSO, DMF Py, ($MeBu_3N$)-($SO_2CF_3)_2N$)	solvent-/ion-assisted growth	agglomerated spheres 9–12 nm polydisperse	10 s 10^{-2} atm 300 °C	[313–316]
$LaPO_4$: RE (RE=Ce^{3+}, Eu^{3+},Tb^{3+})	La_2O_3, $Ce(NO_3)_3$ Eu_2O_3, Tb_4O_7	Thermolysis	H_2O HNO_3, $NH_4H_2PO_4$	ion-assisted growth	nanorods 6–30×400 nm	20 min 1 atm reflux	[318]
$LaPO_4$: RE (RE=Ce^{3+}, Eu^{3+},Tb^{3+})	$La(NO_3)_3$ $Ce(NO_3)_3$ $Tb(NO_3)_3$	Thermolysis	EG $NH_4H_2PO_4$	polyol-assisted growth	nanorods 10–15×60–70 nm monodisperse	20 s 1 atm 110 °C	[84]
$LaPO_4$:RE (RE=Eu^{3+}, Li^{3+})	$La(NO_3)_3$ $Eu(NO_3)_3$ $LiNO_3$	Thermolysis	H_2O EDTA, CTA, NH_4OH, $NH_4H_2PO_4$	ligand-assisted growth calcination required for crystallization	clustered spheres ca. 100 nm	30 min 1 atm 80 °C	[317]
$LiMePO_4$ (Me=Mn, Fe, Co, Ni)	LiOH, H_3PO_4, Mn-$(OAc)_2$ $Fe(OAc)_2$, Co-$(OAc)_2$, $Ni(OAc)_2$	Thermolysis and solvent reduction	TEG H_3PO_4, NH_4OH	polyol-assisted growth	nanothumb-like < 500 nm polydisperse	5–15 min >1 atm 300 °C	[319–321,323]

[a] AOT = sodium bis(2-ethylhexyl) sulphosuccinate; APDTC = 1-pyrrolidine dithio carboxylic acid ammonium salt; [bmim][(BF_4] = 1-butyl-3-methylimidazolium tetrafluoroborate; [BuPy][BF_4] = N-butylpyridinium tetrafluoroborate; CdSA = cadmium stearate; CTA = citric acid; CTAB = cetyltrimethylammonium bromide; CySCN = cyclohexylisothiocyanate; Diesel = commercial diesel; DMF = *N*,*N*′-dimethyl formamide; DOP = dioctyl phthalate; EG = ethylene glycol; EDA = ethylene diamine; Et = ethyl; EtOH = ethanol; FA = formaldehyde; Glyc = Glycerol; HDA = hexadecylamine; [hmim][Cl] = 1-hexyl-3-methylimidazolium chloride; [hmim][BF_4] = 1-hexyl-3-methylimidazolium tetrafluoroborate; HMTD = hexamethyldisilthiane; i-But = iso-Butyl; In-palm = indium palmitate; MAA = mercapto-acetic acid; [$MeBu_3N$][($SO_2CF_3)_2N$] = tributylmetylammonium triflyimide; MPA = 3-mercaptopropionic; NaCT = sodium citrate; NMP = 1-methyl-2-pyrrolidone; NTA = potassium nitrilotriacetate; ODE = 1-octadecene; OLAC = oleic acid; OLAM = oleylamine; OAc = acetate; polyAA = polyacrilic acid; PAA = porous anodic alumina membrane; PEG = polyethylene glycol; Ph = phenyl; PPA = polyphosphoric acid; PVP = poly(*N*-vinyl-2-pyrrolidone); SA = stearic acid; SDS = sodium dodecyl sulfate; THF = tetrahydrofuran; TEG = triethylene glycol; TDPA = tetradecylphosphonic acid; HDDA = 1-hexadecanoic acid; TFA = trifluoroacetate; TOP = tri-*n*-octylphosphine; TBP = tri-*n*-butylphosphine; TOPO = tri-*n*-octylphosphine oxide; TSC = trisodium citrate dihydrate; 1-thioglyc = 1-thioglycerol; TBP = tri-*n*-butylphosphine; TAA = thioacetamide; $(TMS)_3P$ = tris(trimethylsilyl)phopshine; $Zn(Un)_2$ = zinc undecylenate; $Ga(PENT)_3$ = gallium(III) 2,4-pentanedionate

ripening. It was shown that the presence of the strongly MW-absorbing [hmim][Cl] and TOPO could significantly alter the synthesis outcome relative to what was achievable under ordinary oil-bath convective heating. Indeed, depending on the temperature and MW power, the NC size could be easily tuned over the 2–5 nm range in short times (< 20 min) with elevate degree of monodispersity ($\sigma < 5$–7%), as judged from the sharp exciton absorption features and narrow band-edge photoluminescence peaks.[287–289] In line with these achievements, it was reported that high-quality size-tunable CdS, CdSe, CdTe (Figure 8a–d), PbS and PbSe NCs (Figure 8h) could be prepared in MW-transparent low-boiling alkanes under autogenic pressure conditions by exploiting the preferential MW energy coupling to polarizable phosphine-chalcogenide precursors, the activation of which entirely governed the critical nucleation and growth stages.[288–292] In all aforementioned cases remarkable practical advantages were evidenced. The ingredients were simply co-mixed at nearly room temperature and then uniformly MW-activated in sealed vessels without the need of performing a "hot-injection" of precursors to promote size focusing after nucleation, a technique that introduces a major source of irreproducibility in conventional lyothermal synthesis due to the difficulty to rapidly homogenize the reaction mixture and avoid thermal gradients.[63]

Monodisperse, ultrathin nanorods and nanowires of hexagonal-phase CdX and ZnX (X = S, Se) were synthesized within 1–3 min by a MW-assisted process carried out in a solvent environment composed of DMF and long-chain alkylamines[293] (Figure 8e,f). Metal ethyl xanthates were employed as single-source precursors for metal sulfides, while a mixture of metal acetate and selenourea were used to produce metal selenides. It was suggested that anisotropic growth of the rods/wires proceeded unidirectionally along the *c*-axis out of the chalcogen-terminated apex, promoted by the preferential adsorption of the sterically hindering alkylamines onto the longitudinal sidewalls as well as onto the opposed cation-terminated apex.

Various aqueous methods have been developed. Starting from $CdCl_2$ and NaHTe precursors and 3-mercaptopropionic acid (MPA) as stabilizer, 3.5 nm CdTe NCs were derived through time-programmed MW processing,[294] which operatively consisted of two stages: the NCs were initially formed through MW-induced nucleation at around 80 °C, and then constantly irradiated at higher temperatures of approximately 100–120 °C to promote NC growth and annealing by Ostwald ripening, with consequent elimination of smaller defective clusters. The as-synthesized NCs presented impressively narrow photoluminescence bands with appreciable quantum yield (QY = 30–68%) that could be further raised to 80–95% using thioglycolic acid (TGA) in place of MPA and applying a post-synthesis photochemical treatment.[294,295] $Zn_xCd_{1-x}S$ nanorods were synthesized upon MW dielectric heating of aqueous solutions of cadmium acetate, zinc acetate, Et_2NCS_2Na and ethylenediamine (EDA) ligand at 140–160 °C for 10 min.[296] The nanostructures were tailored with diameter and length tunable over the 5–10 nm and 30–150 nm intervals, respectively, depending on the Zn to Cd composition, and showed visible-light-activated photocatalytic activ-

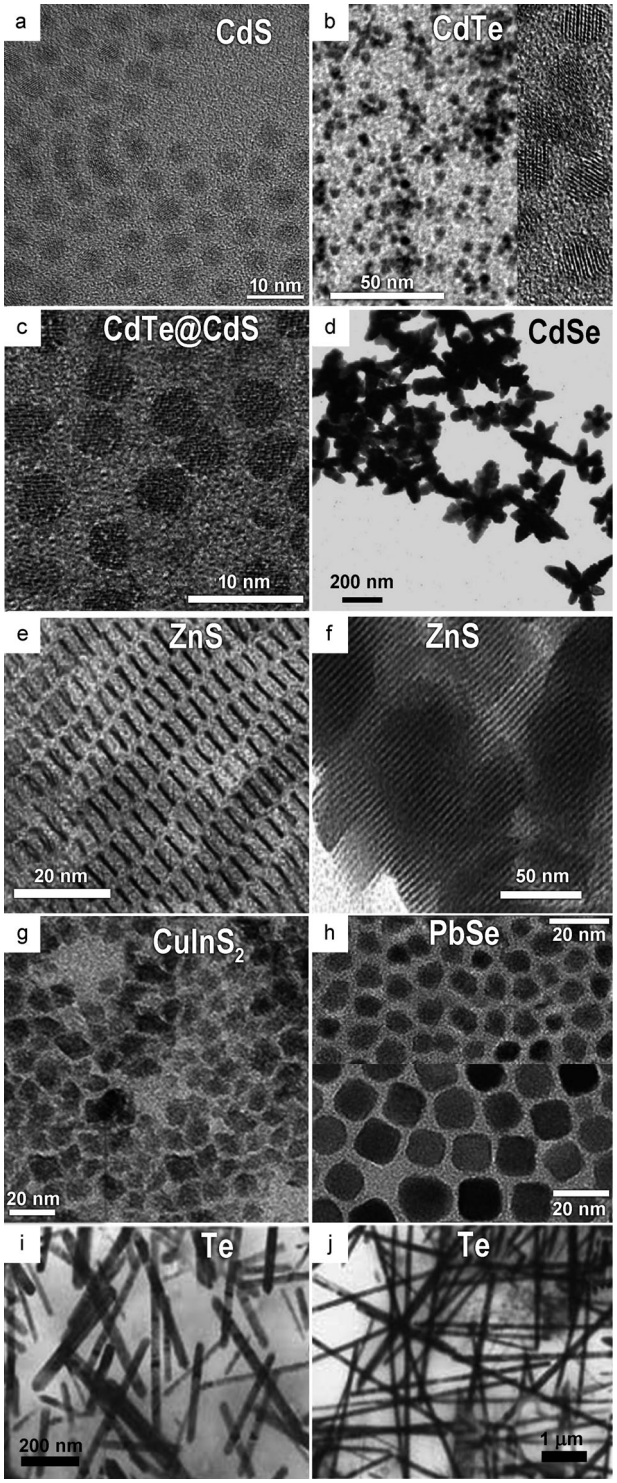

Figure 8. Examples of semiconductor NCs and HNCs prepared under MW irradiation. a) TEM image of spherical CdS NCs synthesized according to Ref. [289]; b) TEM image of monodisperse spherical CdTe NCs prepared according to Ref. [291] (the right part shows a high-resolution TEM overview of the same sample); c) TEM image of spherical CdTe@CdS core–shell HNCs synthesized according to Ref. [326]; d) TEM images of CdSe multipods prepared according to Ref. [340]; e),f) ZnS nanorods and nanowires, respectively, obtained according to Ref. [293]; g) TEM picture of irregularly spherical $CuInS_2$ NCs prepared according to Ref. [303]; h) PbS polyhedral (top) and cube-shaped (bottom) PbS NCs synthesized according to Ref. [292]; i),j) TEM images of Te nanorods and nanowires, respectively, prepared according to Ref. [305].

ity measured against methyl orange degradation. An ultrarapid synthesis (in 60 s) of electrically conductive CdS nanowires with diameters of 140–170 nm and lengths of 8–12 μm was reported, which involved intermittent MW treatment of aqueous $Cd(ClO_4)_2$ and thioacetamide in the presence of DNA molecules that acted as templating and stabilizing agents.[297]

The use of water-in-oil microemulsions as confining reactors for the preparation of CdS NCs was also investigated.[298,299] Specifically, calibrated volumes of water/heptane/sodium bis(2-ethylhexyl) sulphosuccinate (AOT) mixtures, each containing either $CdSO_4$ or Na_2S precursors, were mixed at (35 ± 2) °C and continuously MW irradiated for 4–50 min. Combined UV/Vis and FTIR spectroscopy monitoring of the reaction course revealed that the formation of CdS NCs was accelerated due to MW promotion of faster exchange of the reactants in the aqueous pools, and the growth process was inhibited after the NCs had reached the upper size limit of about 2.7 nm due to MW-driven shrinking of the micellar cores.[298] The enhancement of luminescence of the CdS NCs was tentatively ascribed to the anhydrous environment created under MW irradiation.

MW irradiation has been exploited as a means of facilitating the synthesis of NCs with a complex chemical composition. Early attempts demonstrating the utility of MWs in the preparation of semiconductor materials date back to the solid-state synthesis of $CuInS_xSe_{2-x}$ and $CuInSe_xTe_{2-x}$ materials starting from mixtures of elemental Cu, In, and chalcogen precursors.[300] In such circumstances, because of higher conductivity of Cu and low dielectric losses of In, the Cu was rapidly MW heated, leading to the melting of In. Consequently, X (Z = S, Se, Te) and Cu was allowed to react, forming CuX and/or Cu_2X, in which the Cu could be dissolved. The exothermic reaction provided sufficient heat to keep the system in a steadily molten state, ultimately producing solid solutions of metastable bulk phases that were precluded by conventional thermally assisted preparation.[300]

A few cases of ternary and quaternary chalcopyrite semiconductor NCs by means of MW-assisted liquid-phase synthesis are worth mentioning.[301–303] In one instance, agglomerated $CuIn_xGa_{1-x}S_2$ $(0 \le x \le 1)$ NCs were fabricated by co-reacting $[(Ph_3P)_2Cu(\mu\text{-}SEt)_2In(SEt)_2]$ and $[(Ph_3P)_2Cu(\mu\text{-}SEt)_2Ga(SEt)_2]$ compounds in benzyl acetate and 1,2-ethanedithiol, irradiating the mixture at selected reaction temperatures for approximately 1 h at 160–240 °C.[301] Under these experimental conditions, an accurate control of the stoichiometry and band gap was achieved for NCs in the 2.5–4.5 nm range. Nano- to micron-sized $CuInSe_2$ particles with variable shapes were obtained by MW-supported solvothermal synthesis in EDA.[304] The particle evolution was controlled by in-situ formation of nanocrystal seeds of different types. Plate-like morphologies originated from Cu embryos upon MW heating of a mixture of Se powder, $CuCl_2$ and $InCl_3$ co-dissolved in EDA, while rod-like objects were generated by combining a MW-pretreated EDA/Se solution, in which trigonal-phase elongated Se seeds had formed by dissolution–recrystallization of Se powders, with the other precursors. A reaction mechanism similar to that invoked in the solid-state synthesis[300] was proposed, according to which the initial formation of one selected metal selenide species was followed by dissolution of the remaining amino metal complexes into it. $CuInS_2$ NCs with variable 3–10 nm sizes were rapidly achieved by combining MW irradiation with an established non-aqueous route based on the co-reaction of copper and indium halides with elemental sulfur in OLAM at 120–220 °C[303] (Figure 8g).

Single-crystalline hexagonal-phase Te nanorods/nanowires (Figure 8i,j) with diameter and length tunable in the 15–40 nm × 100–700 nm intervals, respectively, were derived upon microwaving a mixture of TeO_2, $NaBH_4$ and PVP in *N*-butylpyridinium tetrafluoroborate ([BuPy][BF_4]) ionic liquid at 180 °C.[305] Control experiments pointed to the decisive role of MW heating and [BuPy][BF_4] in accelerating the growth process and guaranteeing anisotropic development of Te above a temperature threshold, likely owing to the propensity of $[BuPy]^+$ ions to coordinate to the facets parallel to the *c*-axis. Ultralong single-crystalline Te and Se nanowires (Figure 8i) with diameters of around 20 nm and lengths of up to tens of micrometers, which exhibited UV/Vis luminescence, were achieved by variously modified MW-assisted TeO_3^{2-}/SeO_3^{2-} reduction routes.[305–307] The growth process resulted in being strongly dependent on the reaction parameters, such as the amount of capping and reducing agents, pH value, reaction times, and the choice of extra added stabilizers (e.g., CTAB, PVP).

3.3.2. Metal Fluoride NCs

Monodisperse and highly luminescent up-converting NCs based on cubic-phase $NaYF_4$ co-doped with Yb^{3+} and Er^{3+} or Yb^{3+} and Tm^{3+}, and tetragonal-phase $Na_xLi_yYF_4$ co-doped with Yb^{3+} or Er^{3+}, were recently fabricated through a MW-assisted procedure carried out in ODE/OLAC mixtures at 290 °C.[308] The NCs originated from trifluoroacetate metal salt precursors that possessed a high MW absorption extinction coefficient and thus quickly decomposed thermally, resulting in release of fluoride species. By varying the dopant species, which simultaneously acted as surface-adsorbing agents, the NCs could switch in between a cubic- and tetragonal-phase structure, while also evolving in between cubo-octahedral and cubic shapes (Figure 9c).

Metal trifluoroacetate precursors were successfully exploited in solvent environments co-loaded with OLAC and OLAM surfactants to synthesize shape-controlled magnesium-fluoride-based NCs.[309] Upon variation of the OLAC/OLAM ratio, nearly monodisperse spherical and/or platelet-like NCs of cubic-phase $KMgF_3$, as well as nanorods of tetragonal-phased MgF_2 were accessed (Figure 9a,b). Investigation of the growth mechanism indicated that specific coordinating interactions held between K^+ ions and OLAM molecules and between Mg^{2+} ions and OLAC molecules, respectively, which explained the dramatic impact of the surfactant composition on the ultimate crystal phase and shape features of the product. The same synthetic strategy was applied to achieve up to 5% of Tb^{3+} ion inclusion into the $KMgF_3$ lattice without altering the morphology of the host NCs.[309] In yet another case, MW dielectric heating was employed for fast and efficient preparation of aggregated

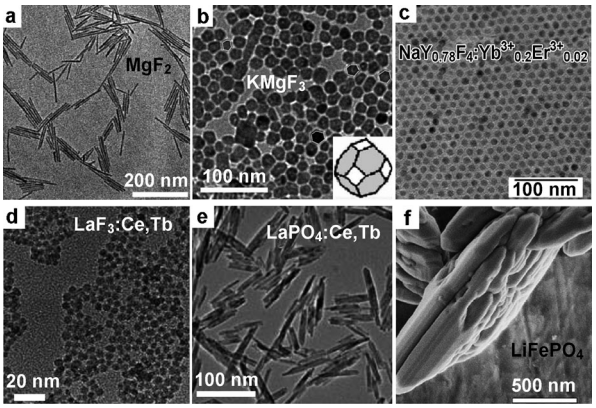

Figure 9. a),b) TEM images of MgF_2 nanorods and $KMgF_3$ truncated nanooctahedrons, respectively, synthesized according to Ref. [309]; c) TEM image of hexagonal-shaped $NaY_{0.78}F_4:Yb^{3+}_{0.2}Er^{3+}_{0.02}$ NCs adapted from Ref. [308]; d),e) TEM pictures of Ce^{3+}/Tb^{3+}-co-doped LaF_3 spherical NCs and Ce^{3+}/Tb^{3+}-co-doped $LaPO_4$ nanorods, prepared according to Ref. [84]; f) SEM image showing the side-view of plate-like $LiFePO_4$ mesocrystals synthesized according to Ref. [323].

6 nm Eu^{3+}-doped GdF_3 NCs with quantum efficiency as high as 145% using hydrated $Gd(OAc)_3$ and $Eu(OAc)_3$ salts as precursors in [bmim][BF_4].[310] It was found that the ionic liquid not only acted as synthesis medium but also played a role as fluoride source through decomposition of BF_4^- ions.

3.3.3. Metal Phosphide/Phosphate NCs

The colloidal synthesis of fluorescent III–V metal phosphides has notoriously been rather challenging and generally time-consuming owing to the highly covalent nature of their lattices, which makes high crystallinity and structural perfection at the surface difficult to achieve. Monodisperse spherical InGaP and InP NCs with sizes of up to about 4 nm were obtained by hexadecanoic-acid- assisted pyrolysis of indium acetate, gallium 2,4-pentanedionate and tris(trimethylsilyl)-phosphine in alkane solvents at 280 °C.[287] Direct coupling of the MW field to the precursors and efficient lattice annealing under pressurized and superheated conditions were considered to be responsible for the size-focusing regime that afforded extremely rapid (in less than 7 min) formation of high-quality NCs with sharp excitonic absorption features and photoluminescence QYs that were as high as 9–15% for InGaP without any post-synthesis chemical etching treatment to remove surface trap states (phosphorous vacancies).[311] Modification of the above approach with the addition of fluorinated ionic liquid, such as 1-hexyl-3-methyl imidazolium tetrafluoroborate ([hmim][BF_4]), led to 2.7 nm InP NCs showing photoluminescence QY that had increased from to around 4% (in the absence of the additive) to nearly 47%.[312] Besides acting as superheating agent, ([hmim][BF_4]) worked as in-situ etching agent for the growing NCs through releasing F^- ions upon MW-promoted decomposition. The nature and concentration of the selected ionic liquid drastically influenced the ultimate QY.

Variously modified MW-accelerated approaches to luminescent Ce^{3+}/Tb^{3+}-co-doped $LaPO_4$ NCs were developed using tributylmethylammonium triflylimide as solvent.[313–316] In the most successful circumstances, sample preparation proceeded by a two-step process involving the initial precipitation of inorganic embryos upon reactant mixing at 70 °C and precipitation, followed by a fast MW heating (10 s) of the suspension to 300 °C.[312] The resulting nanophosphors were thermally stable and resistant against air oxidation without the need for a protective shell coating. Highly luminescent and transparent layers were fabricated by ink-jet printing of Ce^{3+}/Tb^{3+}-co-doped $LaPO_4$ or Eu^{3+}-doped $LaPO_4$ NCs synthesized in ionic liquids under MW irradiation.[316]

Further examples pertain $LaPO_4$-based NCs, such as 100 nm Eu^{3+}/Li^+-co-doped $LaPO_4$ spheres in the monoclinic phase[317] and Ce^{3+}-, Eu^{3+}-, and/or Tb^{3+}-doped $LaPO_4$ nanorods in the hexagonal structure, with diameter of 6–30 nm and length of up to 400 nm, which were prepared combining sol–gel chemistry and MW irradiation.[318] Microcapillary reactors exposed to MWs were recently used to prepare monodisperse 10–15 nm × 60–70 nm Ce^{3+}/Tb^{3+}-co-doped $LaPO_4$ nanorods upon reacting the respective molecular precursors in EG at 110 °C.[84] In a similar manner, uniform 4.5 nm Ce^{3+}/Tb^{3+}-co-doped LaF_3 nanospheres were successfully delivered.

Lithium transition-metal phosphates, $LiMPO_4$ (M = Mn, Fe, Co, Ni), crystallizing in the olivine (orthorhombic) structure, are recognized as a low-cost non-toxic and safe potential cathodes for lithium-ion batteries.[319–322] Among the efforts documented, single-crystalline nano thumb-shaped $LiMPO_4$ NCs were prepared by MW heating a stoichiometric mixture of LiOH, H_3PO_4 and the corresponding metal acetate in tetraethylene glycol (TEG) at 300 °C for only 5–15 min.[319–321] TEG, an efficient MW-absorbing solvent, not only provided a reducing atmosphere that prevented metal oxidation, but also inhibited the nanoparticle agglomeration. Subsequently, the as prepared $LiMPO_4$ nano-thumbs were networked with multi-walled carbon nanotubes, giving rise to nanocomposites with markedly amplified electron mobility. In benzyl alcohol ambient, mesocrystals of $LiFePO_4$, $LiMnPO_4$, and $LiMn_{0.65}Fe_{0.35}O_4$ mesocrystals with excellent electrochemical performances were produced under ambient pressure using a microwave-directed liquid-phase synthesis within 3 min (Figure 9 f).[321]

3.3.4. Core–Shell HNCs

Reliable and simple procedures for the preparation of spherical CdSe@ZnS,[324,325] CdTe@CdS[326] core–shell, and CdTe@CdS@ZnS[327] core–shell1–shell2 semiconductor HNCs using MW dielectric heating, were reported, in which shell overgrowth allowed significantly enhanced luminescence and/or tunable emission wavelength.[6,36] It has emerged that MW irradiation was an effective tool to promote both non-hydrolytic[324] and hydrolytic[325–330] reaction pathways within the frame of seeded-growth schemes.[36] As an example, the preparation of water-soluble CdSe@ZnS core–shell NCs accomplished by a two-step procedure can be illustrated.[328] CdSe particles were first prepared upon MW irradiation of a mixture of $Cd(OAc)_2$ and Se, in a TOPO/TOP/HDA mixture under normal atmosphere. Then, the extracted CdSe NC cores were added to a butylamine/1-

methyl-2-pyrrolidone solution of MPA containing diethyl zinc and hexamethyldisilathiane for ZnS shell heterogeneous nucleation at 70 °C under MW exposure. The resulting MPA-capped CdSe@ZnS HNCs with sizes adjustable over the 2–6 nm range resulted in being water-soluble and produced tunable fluorescence in the visible range with QY = 11–25 %. In a similar way, 6 nm Mn:ZnSe@ZnS HNCs were obtained upon depositing a ZnS onto preformed Mn-doped ZnSe NCs, which were transferred by MPA replacement of the original hydrophobic capping ligands to water, where it reacted with the relevant zinc ion and sulfide precursors.[329] One-pot, single-step approaches, in which the core and shell growth processes were rapidly accomplished sequentially (in less than 2 min) in the same surfactant environment, were also devised to synthesize 2–5 nm CdSe@ZnS HNCs with variable shell thickness and appreciable size monodispersity, starting from moderately toxic precursors.[324]

4. Effects of MW Dielectric Heating in Nanocrystal Synthesis

There are currently more than 500 publications that describe the generation of inorganic NCs using MW dielectric heating, with the first reports dating back to the mid 1990s.[364,365] As highlighted in the preceding Sections, MW-synthesized NCs encompass virtually all known types of nanoscale materials, ranging from metals to oxides, chalcogenides and phosphates. In general most of these materials are of considerable industrial and technological importance, and therefore new and innovative routes for their production are highly desirable. The motivation for the use of MW energy has mainly been to design faster, cleaner, and economically more viable methods of synthesis. Since the early days of utilizing MW irradiation for NC generation,[237–239,364,365] the observed rate accelerations, and the higher quality of the derived NCs (e.g., narrower size distribution, increased phase purity and selectivity, lower surface defects, higher photoluminescence QY), have led to speculations on the involvement of so-called "specific" or "nonthermal" MW effects (see Section 2.1). In general, such effects are proposed when the outcome of a reaction performed under MW conditions is different from the conventionally heated counterpart at the same measured reaction temperature.[79] Unfortunately, while in organic or polymer chemistry the MW-dependent effects can be specifically discussed in terms of the reaction trajectory,[79] the lack of an in-depth mechanistic picture for NC formation makes the determination of the exact influence of MW irradiation on the intermediates and transition states for NC nucleation and growth more difficult. Having now reviewed the synthesis of different types of NCs under MW conditions (Section 3), the proposed MW effects relevant for NC formation will be discussed more in detail in the following Sections. It should be emphasized that many of the arguments in publications on this topic are highly speculative and therefore should be treated with reservation.

4.1. Thermal Effects

On the basis of the characteristics of the MW dielectric heating phenomena presented in Section 2, it can be argued that in the majority of published cases the reasons for the observed formation rate enhancements and altered NC size-morphological features comparing MW and conventional heating are probably due to purely thermal/kinetic effects, resulting from the higher bulk reaction temperatures and more rapid heating rates that can be attained in a MW irradiation experiment. This is particularly true for precursor solutions/solvents with a high $\tan\delta$ value, which can be rapidly "superheated" far above their boiling points when irradiated under MW conditions in a sealed vessel. The rapid increase in temperature can be very pronounced for media with extreme loss factors, such as ionic liquids, where achievement of temperature jumps of 200 °C within a few seconds is not uncommon.[72] Naturally, such temperature profiles are very difficult, if not impossible, to reproduce by standard thermal heating. In addition, practical difficulties in accurately monitoring the reaction temperature during a MW chemistry experiment often contribute to misinterpretations of the results, in particular when domestic MW ovens are employed or the measurement relies solely on external infrared temperature sensors.[72,77]

As mentioned in Section 2 to prepare highly uniform NCs it is necessary to induce a short burst of nucleation temporally separated from the subsequent growth stage. Depending on the inherent reactivity of the systems concerned, this condition has been practically realized either by exploiting the well-known "hot-injection" technique for swiftly delivering the precursors to the preheated growing mixture or by performing a "slow heating up" of the complete reaction mixture to a target temperature.[88–90] It has been suggested that efficient and uniform "in core" volumetric heating with minimized thermal gradients should result in rapid and more spatially uniform nucleation and growth of NCs.[332] These unique advantages inherent to MW dielectric heating have often been considered to be responsible for accelerating certain reactions, such as the reduction of metal precursors and the nucleation of the metal clusters, resulting in monodisperse NCs.[97]

Frequently, NCs prepared by MW irradiation are synthesized with comparatively smaller sizes and claimed to be characterized by narrower size distribution than those obtained by conventional heating. This fact can possibly be rationalized based on the timing of nucleation and growth periods (see Figure 2). In general, the higher the nucleation rate and the relative extent of monomer consumption in this stage are, the smaller the ultimate NCs will be, even though subsequent growth is relatively rapid.[366] This is because, for a fixed precursor amount introduced, the higher the concentration of nuclei generated is, the more the latter will have to compete for taking up the reactive monomers left in the solution in order to be able to grow (see Section 2.3).[20,21,88] Therefore, several authors have, in essence, rationalized the observed phenomena during NC formation under MW conditions by purely thermal/kinetic effects, stemming from the different ramp times and reaction temperatures compared

to the standard methods based on the "slow heating-up" techniques.[96,131,173,180,221,232,241,265,275,294,350,353,367] For example, it was reported that in the formation of highly crystalline metal oxide NCs (e.g., ZnO) by non-aqueous sol–gel reaction of benzyl alcohol and metal acetates or acetylacetonates at 120–200 °C, MW irradiation increased the overall NC development rate by a factor of about 5, leading to production of phase-pure NCs in 1–5 min.[187,188] Careful kinetic comparison between MW and conventional oil-bath heating showed that MW irradiation greatly propelled NC formation by accelerating both nucleation and growth. Indeed, the concurrence of two major effects was assessed: first, a more rapid dissolution of the precursor in the solvent and faster kinetics of the organic esterification reaction, both of which underlay fast monomer production and, consequently, led to an anticipated nucleation event; second, increased crystal lattice growth, although a detailed microscopic explanation for this phenomenon was not given.[188]

Very recently, the formation of $CuInS_2$ NCs from the co-reaction of CuI, $InCl_3$, and elemental S in OLAM at 220 °C has been investigated under both conventional heating and MW irradiation.[303] Preliminary comparative syntheses performed under apparently "similar" conditions (identical externally monitored reaction temperature) had provided $CuInS_2$ NCs with slightly different quality features, depending on the heating mode. To shed light into the role of MW irradiation, control syntheses were carefully executed in Pyrex and silicon carbide (SiC) reaction vials[81] in a dedicated MW reactor (Figure 1) under otherwise identical reaction conditions, as well as in a preheated oil bath. The use of the strongly MW-absorbing SiC vessel allowed separating purely thermal from specific and nonthermal MW effects.[81] The outcome of such experiments ensuring identical heating and cooling profiles, stirring rates, and reactor geometries are summarized in Figure 10. The results clearly demonstrated that the NC products obtained under conventional heating did not appreciably differ from those obtained under MW irradiation. Actually, the NCs exhibited the same crystal phase, primary crystallite size, shape, and size distribution and showed no significant differences in optical absorption behavior.

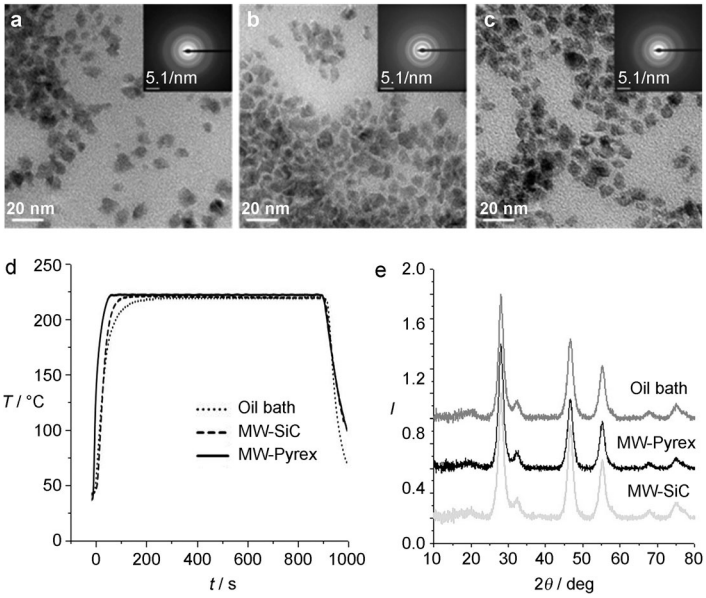

Figure 10. a)–c) TEM images and selected-area electron diffraction patterns (insets) of $CuInS_2$ NCs obtained after 15 min reaction at 220 °C on a 3 mL scale in a Pyrex (MW-Pyrex) and SiC (MW-SiC) vials in a MW reactor under otherwise completely identical conditions, as well as in a preheated oil bath at a bath temperature of 220 °C, respectively. d) Heating profiles for the $CuInS_2$-generating reaction mixtures corresponding to panels (a)–(c), e) X-ray diffraction patterns of the $CuInS_2$ NCs shown in panels (a)–(c,) respectively (reproduced from Ref. [303]).

4.2. Specific MW Effects

In addition to the above mentioned thermal/kinetic effects, MW effects that are caused by the uniqueness of the MW dielectric heating mechanisms should also be considered. These effects should be termed "specific MW effects" and should be defined as outcomes that cannot be achieved or duplicated by conventional heating, but essentially are still thermal effects (see Section 2.1).[68,80] For example, in a MW-heated system under open-vessel reflux conditions, the average bulk temperature of the solvent can be somewhat higher than the boiling temperature otherwise expected at atmospheric pressure. This is due to the fact that the MW power is dissipated at an exceedingly fast rate over the entire volume of the solvent, where nucleation points necessary for boiling incipit are absent.[368] The boiling can only initiate and proceed to a relevant extent in proximity of the reactor walls or at the solvent-air interface. This results in a reversed temperature profile with a steady average reflux temperature above the classical boiling point, a process known as "superheating".[239] For instance, by exploiting this effect rod-shaped Ti glycolates (which converted into TiO_2 nanorods upon annealing and organics removal),[239] hexagonal-type In_2O_3, and spherical type Tl_2O_3 were produced in few minutes using a modified domestic MW oven.[165]

In addition, using conventional conductive heating, crystals often tend to nucleate on container walls or dust particles and are more likely experience a slow growth rate due to randomly dispersed ions, a sluggish and non-uniform nucleation stage, availability of very few seeding nuclei, and heating inhomogeneity.[84] In contrast, MW dielectric heating produces efficient internal volumetric heating as described above (Section 2), reducing these "wall effects".[82] It was therefore proposed that in a MW-heated experiment numerous "hot spots" may form, which could trigger massive nucleation of seeds throughout the bulk solution, consequently leading to overall faster NC development and higher NC product yields. This effect is particularly evident when the synthesis is performed in microreactors where the relative wall area of the reaction space is dramatically increased relative to that associated to common vessels or flasks. For instance, Figure 11 highlights the case of Ce^{3+}/Tb^{3+}-co-doped LaF_3 NCs synthesized in EG media in a continuous-flow microcapillary.[84] MW irradiation led to monodisperse

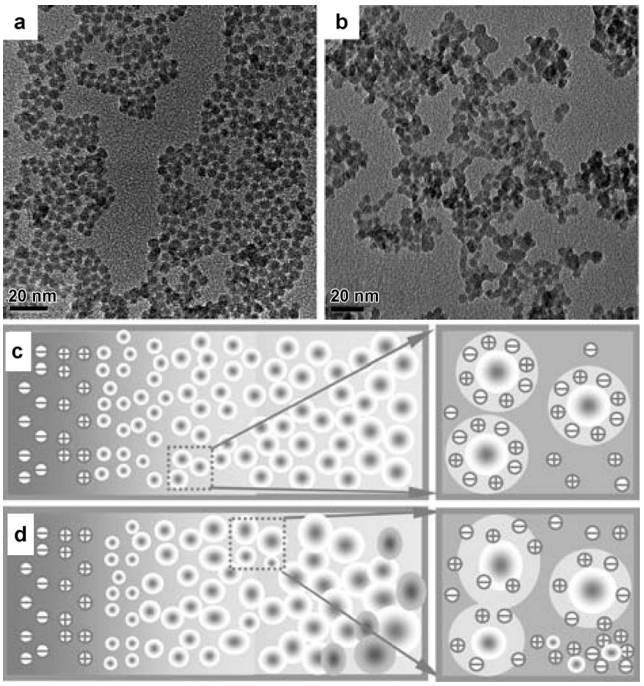

Figure 11. a),b) TEM images of Ce^{3+}/Tb^{3+}-co-doped LaF_3 NCs synthesized in flow microcapillary reactors under MW and oil-bath heating, respectively, according to the method described in Ref. [84]). c),d) Outline of the mechanisms proposed for the nucleation stage of the Ce^{3+}/Tb^{3+}-co-doped LaF_3 NCs under MW irradiation and oil-bath heating, respectively.

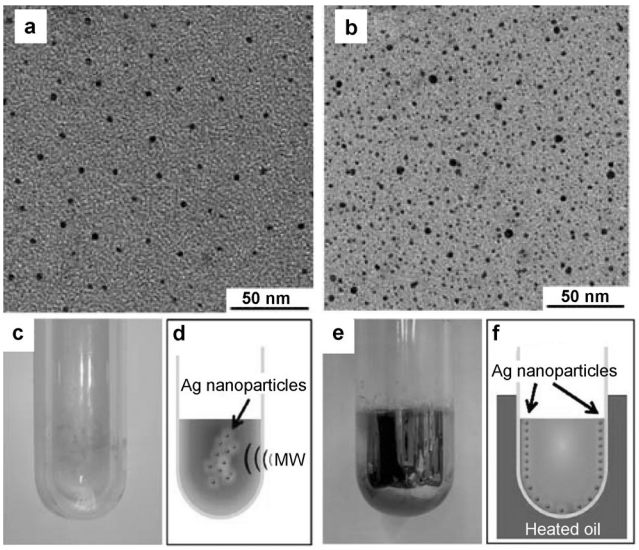

Figure 12. a),b) TEM images of Ag NCs synthesized in 150 mL Pyrex glass batch-type reactors under MW heating and conventional oil-bath heating, respectively, according to the method described in Ref. [139] c) and e) Photograph of the reactor after the sample removal after 4 min MW irradiation or oil-bath heating, respectively. d),f) outline of the temperature distribution in the reactor after the 4 min MW and oil-bath heating, respectively. Note that the experiments in panels (c)–(f) were carried out under non-stirring conditions.

(4.5 nm) and well-separated NCs, whereas oil-bath heating resulted in NCs with a broader distribution of sizes (3–8 nm) which tended to form aggregates (Figure 11 a,b). In the proposed reaction mechanism, MW irradition was assumed to not only induce a fast (hence, temporally limited) and spatially uniform nucleation burst in the polar liquid environment, but also to guarantee a uniform concentration of reactive monomers around the crystal embryos, which facilitated their subsequent growth under steady conditions (Figure 11 c,d).

Another intriguing example of the wall-effect phenomenon described above was observed in the preparation of Ag NCs from $Ag(NH_3)_2^+$ and CMC as reducing agent in a water-based environment.[139] Actually, as shown in Figure 12, the rate of formation of the Ag NCs and their size distributions were largely dependent on the heating methods applied, although the exact reaction temperature was identical. On the basis of dedicated experiments performed under non-stirring conditions, it was proposed that in the MW-heated experiment MW irradiation penetrated directly into the reaction mixture, causing the temperature to rise from inside mainly by dielectric loss, followed by subsequent transfer of heat to the surroundings through the reactor walls. Consequently, as the temperature near the inner walls of the reactor tended to be lower than at the center, NC formation progressed from inside the liquid outwards along the temperature (and concentration) gradient created (Figure 12 c). On the other hand, heat in an oil-bath heated vessel was most prominent at the reactor walls and was subsequently transmitted to the solution by thermal conduction and convection mechanisms. This ultimately led to the formation of a thin Ag film at the inner reactor walls as the NCs grew and accumulated preferentially at these locations (Figure 12 d).[139]

Another type of specific MW effect, known as "selective heating", which has been claimed several times in NC synthesis concerns the ability of MW energy to be preferentially absorbed by highly polar substrates. Briefly, when a mixture of compounds featured by different dielectric properties ($\tan\delta$ values) is exposed to a MW field, the material with the higher $\tan\delta$ value will absorb the energy preferentially and will get heated more rapidly compared to the others.[369,370] For example, it has been reported that under MW irradiation the surface temperature of oxides covered by MW-absorbing hydroxyl groups can dramatically change, leading to local overheating on the surface.[371] The concept of selective heating in the context of NC synthesis may be of particular interest when dealing with solid/liquid interfaces, the solid (i.e., a metal or metal oxide NC) being strongly MW-absorbing.[370]

A selective heating phenomenon was invoked in the MW-assisted hydrothermal treatment of $FeCl_3$ in aqueous $NH_4H_2PO_4$ solution, from which α-Fe_2O_3 nanorings, not otherwise reproducible under conventional heating, were derived.[219] In the proposed MW-induced nucleation–aggregation–dissolution mechanism, summarized in Figure 13, it was suggested that the α-Fe_2O_3 nanodisks initially formed by oriented aggregation could be selectively heated to substantially higher temperatures than that characterizing the remaining bulk mixture. The generation of "hot spots" at the surface of the nanodisks would promote their subsequent

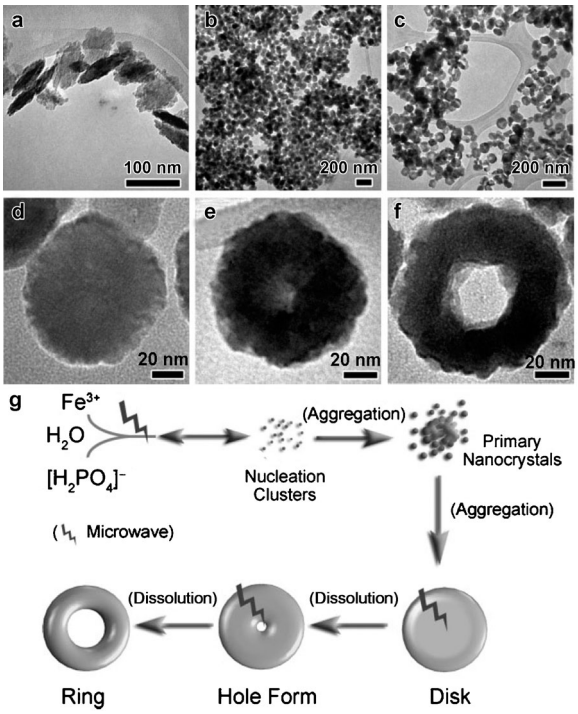

Figure 13. a)/d), b)/e), c)/f) Low- and high-magnification TEM pictures showing the morphology evolution of α-Fe_2O_3 nanostructures obtained by the MW-assisted hydrothermal protocol described in Ref. [220] at 220°C after 10 s (a,d), 50 s (b,e), and 5 min (c,f). g) Schematic illustration of α-Fe_2O_3 nanoring formation by MW irradiation.

localized etching by the highly polarizable phosphate ions, driving the conversion into α-Fe_2O_3 nanorings.[220]

In another study, prolonged MW irradiation was proven to induce fusion of preformed PVP-stabilized Ag nanowires in EG into wire-built networks.[98] Preliminary evidence was provided in support of the occurrence of dielectric "superheating" of the conducting Ag nanostructures via charge flow and resistive heating, likely originating from MW-field-induced electron polarization and charge localization. The creation of "hot spots" at the sharp apexes of the nanowires was also suggested, at which higher local temperatures could be experienced, thereby inducing metal welding in correspondence of those locations.[98] Analogous arguments were used to rationalize the observed MW impact in the synthesis of monodisperse ZnO NC clusters,[190] Ni and Ni_3P nanowires,[372] although the underlying growth mechanism were largely different. More recently, the selective MW heating concept has been applied to achieve the rapid growth of carbon nanotubes and nanofibers out of Fe nanoparticle catalysts patterned over silicon and other substrates, such as glass and Teflon.[373] In line with these results, it may be hypothesized that NCs of many dielectric or magnetic materials, pre-existing in a solution, can indeed act as strong MW absorbers, thereby showing enhanced or unexpected reactivity towards molecular monomer species or other clusters as a consequence of being selectively MW-heated. It could be reasonably assumed that such "activation" of NCs determines the outcome of all of those MW-assisted approaches, including seed-mediated protocols, in which anomalous growth rates or unexpected NC products were observed. Dedicated investigations aimed at assessment of these mechanistic aspects, which have been largely overlooked, are therefore greatly needed.

The potential involvement of selective heating principles was studied in detail in the preparation of shaped Au NCs by reducing $H[AuCl_4]$ in EG in the presence of PVP as stabilizer under three different heating regimes.[97,123] NC generation was realized using either constant MW power (fast heating) or in a controlled MW-pulsed mode, the controlled MW-pulsed mode simulating the slow heating rate obtained in an oil-bath (slow heating).[123] While capping PVP molecules should certainly influence the size-morphological evolution the NCs, the tendency towards a preferred shape distribution observed under fast MW heating was reiterated even when the same slow heating profile was realized by MW and oil-bath methods. There was some speculation on the interplay of some specific MW effects, such as the propulsion of nucleation under homogeneous heating conditions and/or creation "hot spots" at NC surface locations where the large dielectric-loss-constant PVP stabilizer was adsorbed (selective heating). However, the exact origin of the MW-directed synthesis outcome remains yet unclear at this stage.[97]

An extension of the selective-heating mechanistic concept was put forward to explain the effects observed in MW-assisted preparation of luminescent semiconductor CdSe, CdS, and CdTe NCs synthesized upon pyrolysis of phosphine-chalcogenide complex precursors in MW-transparent alkanes as solvents or in mixtures of surfactants with different MW-absorbing capabilities. It was suggested that selective coupling of MW energy to the precursors, eventually mediated by the presence of suitable MW-absorbing additives (e.g., TOPO, ionic liquids), could increase the local microscopic temperature with minimal thermal gradients, while transferring heat to the rest of liquid components convectively.[288] As a result of an instantaneous, massive precursor activation, a high and spatially uniform concentration of active monomers would be generated, leading to a short burst of homogeneous nucleation and subsequent steady-growth conditions, while participation of Ostwald ripening would be retarded over the time scale of the reaction.[287–292] In addition, MW irradiation was assumed to facilitate the formation of the thermodynamically expected NC products upon overcoming possible stability minima in the reaction trajectory, which could be expected to be associated with particular molecular intermediates (i.e., NC monomers) and/or extremely tiny NCs with discrete sizes[287] (so-called "magic-size" clusters"[374]). In line with these principles, other general approaches for the preparation of other nanomaterials, such as metal oxide NCs, were proposed, which essentially relied on the choice of precursors that possessed a dielectric constant significantly higher than that of the liquid medium component in order to absorb MW irradiation selectively.[163] However, control over the size, shape and dispersibility features of the resulting NCs remained rather difficult in the absence of stabilizing ligands and surfactants.[237–239,364,365]

In the case of micro-heterogeneous systems, such as microemulsions, MW irradiation can strongly interact with H_2O molecules[375] and therefore is able to reduce consider-

ably the time required for nucleation and growth of NCs. Stable, small, and crystalline CdS NCs were prepared in a water-in-oil microemulsion at only 35 °C under MW irradiation with the final NC diameter being smaller than that obtained under conventional conditions.[298] Additional experiments confirmed that upon MW irradiation, the H_2O cores was selectively heated and almost completely extracted from the aqueous pools of the reversed micelles.

4.3. Nonthermal MW Effects

In addition to "thermal" and "specific MW effects", the possibility of so-called "nonthermal MW effects", often referred to as "athermal effects", has also been suggested.[63,237–239,365] These should be classified as accelerations that cannot be rationalized by either purely thermal/kinetic or specific MW effects. Nonthermal effects are essentially related to a direct interaction of the MW electric field with specific molecules or materials in the reaction medium, which does not, however, result in any macroscopic temperature effect (in contrast to selective heating).[68,80] It has been argued, for example, that the presence of an electric field induces re-orientation of dipolar molecules and hence changes the pre-exponential factor A or the activation energy (entropy term) in the Arrhenius equation associated to the particular reaction kinetics.[187] A similar effect should be expected to be involved in polar reaction mechanisms, where the polarity increases on going from the ground state to the transition state, which would thus result in an enhancement of reactivity due to the activation energy barrier being decreased.[280] For instance, it was originally speculated that in the generation of ZnO NCs from nonhydrolytic reaction of acetates and benzyl alcohol the electromagnetic field could interact with a highly polar transition state, reducing the activation energy and thus accelerating the overall growth process.[187] In subsequent work by the same authors, these results have been re-interpreted as being the consequence of faster reaction kinetics and a more rapid dissolution of the precursor in the solvent (thermal or specific microwave effect).[188]

In another study, MW heating was proven to drastically decrease the time required to obtain Gd^{3+}-doped CeO_2 nanorods via anisotropic oriented-attachment pathways, compared to conventional heating. It was suggested that an instantaneous dipole moment induced in the polarizable NCs by the MW electromagnetic field generated insurgence of dispersive forces among the primary clusters that were formed at earlier reaction stages, thereby enhancing the effective collision frequency and, hence, the probability of irreversible coalescence events.[280,281] The effect of varying MW frequencies (2.45–18 GHz) was assessed in the case of CdS NCs precipitated in water-in-oil microemulsions.[299] It was observed that at constant temperature (30 °C), larger NCs were produced at 12 GHz, relative to those obtained in syntheses performed at other frequencies or by conventional heating. More detailed investigations on this issue revealed that the size features and surface morphology of the NCs were all influenced by the MW frequency and bandwidth sweep time. This was attributed to a dependence of the nucleation and crystal growth rates on the MW frequency, which could be correlated with the variation in transverse magnetic modes associated with MW irradiation.[172] Very recently, the frequency effect in the MW synthesis of Au NCs has been examined as a function of the reaction medium.[376] Whereas a change in MW frequency from 2.45 to 5.8 GHz at equal MW power levels affected the size and shape features of Au NCs synthesized in non-polar media, no frequency dependence of the product outcome was observed in the case of Au NCs grown in polar media.[376] Confirmation of an unambiguous impact of the MW frequency on the NC formation at constant temperature would be a genuine indication of the involvement of nonthermal MW effects.

In a more sophisticated study, the synthesis of SiGe alloy nanowires was carried out at high temperatures (900 °C) in the presence of the nominally pure magnetic component of a 2.45 GHz MW field.[377] It was proposed that variation of the H-field at 2.45 GHz induced an electric MW field, which acted as an additional driving force assisting the initiation of nanowire growth.

5. Conclusion and Outlook

The area of microwave-assisted synthesis of inorganic NCs has seen tremendous expansion over the past few years. As highlighted in this Review, an ever growing number of researchers, mainly in academic institutions, is currently exploiting this powerful technology to prepare NCs at significantly enhanced rate and yield. A further attractive advantage resides in the possibility of performing NC preparation using operatively simple, one-pot methods, based on "heating-up" techniques. It should be noted that, in many instances, the use of MW heating has been considered to lead to NCs with improved physical–chemical properties, compared to those fabricated by conventional methods. However, such claims have rarely been supported by convincing data. As a matter of fact, the degree of flexibility and the level of refinement in which the composition, size, shape and crystal structure of MW-synthesized nanostructures can currently be produced are still far from approaching those achievable by state-of-art colloidal routes under convective heating. While this inadequacy emerges in the case of single-material NCs (particularly in the case of oxide and doped materials), an even more sparsely and less successfully tackled area regards the development of multi-component HNCs, which are in fact limited to a few prototypes of binary heterostructures of selected material associations exclusively arranged in core–shell configuration. It is plausible that such delayed progress in MW synthesis is related to the inherent difficulties posed by commonly used MW equipment to apply dedicated techniques of time-programmed reactant or seed delivery, which are recognized as prerequisites to conveniently manipulate the delicate balance of thermodynamics and kinetic factors that govern NC/HNC formation.

At the time of writing, it is not entirely clear from a critical examination of the available literature as to whether the use of MW irradiation will mainly influence the outcome of

colloidal preparations by the exquisite control of the reaction temperature enabled by well-controlled heating and cooling rates in modern instrumentation, or whether other phenomena, such as wall effects or selective heating, or even nonthermal MW effects play a more decisive role. Given the large number of publications and proposed (often conflicting) theories in this area, a significant amount of detailed investigations will be required in order to arrive at a unified theory that explains in detail all the mechanisms by which MW irradiation may influence the formation of NCs/HNCs at different stages of their evolution in an electromagnetic MW field. Therefore, extreme care must be taken in the interpretation of published data. The reader must be aware that, perhaps similar to what has happened the field of microwave organic chemistry, it is quite probable that in the next few years the majority of claimed "specific" and "nonthermal" MW effects involved in NC synthesis will have to be reinterpreted as the result of erroneous temperature measurements.[77,81]

Finally, it is important to note that a comprehensive understanding of the underlying phenomena in MW-assisted NC synthesis is not only an academic exercise, but of utmost importance for the industrial preparation of NC materials. In order to make MW-assisted NC syntheses scalable, understanding the influence of the electromagnetic field (field density) on the individual reaction steps is vital in order to manufacture suitable equipment for scaled-up NC processing. One possibility is to use high-temperature continuous-flow processing for NC synthesis, applying high-temperature/high-pressure flow instrumentation where many of the features of a batch MW reactor can be mimicked, and flow reactions are readily scalable. Both microwave[56,83,84,86,178] and conventionally heated[87,378,379] continuous-flow technology for NC preparation are on the road towards widespread utilization.

In general, one of the major drawbacks of MW-assisted chemistry is equipment cost. While prices for dedicated MW reactors for chemistry applications have come down considerably since their first introduction in the late 1990s, the current price range for MW reactors is still many times higher than that of conventional heating equipment. This fact has severely limited the penetration of MW synthesis in academic laboratories around the world. This situation can be expected to change over the next several years when less-expensive equipment will likely become available.

This work was supported by a grant from the Christian Doppler Research Society (CDG) and partially by the Italian Ministry of Education, University and Research through the project AEROCOMP (contract MIUR no. DM48391).

Received: February 20, 2011
Published online: November 4, 2011

[1] G. A. Ozin, A. C. Arsenault, L. Cademartiri, *Nanochemistry: A Chemical Approach to Nanomaterials*, RSC, Cambridge, **2008**.
[2] C. Burda, X. B. Chen, R. Narayanan, M. A. El-Sayed, *Chem. Rev.* **2005**, *105*, 1025.
[3] A. P. Alivisatos, *J. Phys. Chem.* **1996**, *100*, 13226.
[4] V. Klimov, *Semiconductor and Metal Nanocrystals*, Marcel Dekker, New York, **2004**.
[5] *Semiconductor Nanocrystal Quantum Dots:Synthesis Assembly, Spectroscopy and Applications* (Ed.: A. L. Rogach), Springer, Vienna, **2008**.
[6] D. V. Talapin, J.-S. Lee, M. V. Kovalenko, E. V. Shevchenko, *Chem. Rev.* **2010**, *110*, 389.
[7] S. K. Ghosh, T. Pal, *Chem. Rev.* **2007**, *107*, 4797.
[8] R. Narayanan, R; M. A. El-Sayed, *J. Phys. Chem. B* **2005**, *109*, 12663; M. A. El-Sayed, *J. Phys. Chem. B* **2005**, *109*, 12663.
[9] C. N. R. Rao, G. U. Kulkarni, P. J. Thomas, P. P. Edwards, *Chem. Eur. J.* **2002**, *8*, 28.
[10] X. Chen, S. S. Mao, *Chem. Rev.* **2007**, *107*, 2891.
[11] M. Niederberger, N. Pinna, *Metal Oxide Nanoparticles in Organic Solvents—Synthesis Formation, Assembly and Application*, Springer, London, **2009**, p. 215.
[12] A.-H. Lu, E. L. Salabas, F. Schüth, *Angew. Chem.* **2007**, *119*, 1242; *Angew. Chem. Int. Ed.* **2007**, *46*, 1222.
[13] U. Jeong, X. Teng, Y. Wang, H. Yang, Y. Xia, *Adv. Mater.* **2007**, *19*, 33.
[14] N. A. Frey, S. Peng, K. Cheng, S. Sun, *Chem. Soc. Rev.* **2009**, *38*, 2532.
[15] M. Casavola, R. Buonsanti, G. Caputo, P. D. Cozzoli, *Eur. J. Inorg. Chem.* **2008**, 837.
[16] R. Buonsanti, M. Casavola, G. Caputo, P. D. Cozzoli, *Recent Pat. Nanotechnol.* **2007**, *1*, 224.
[17] N. Pinna, M. Niederberger, *Angew. Chem.* **2008**, *120*, 5372; *Angew. Chem. Int. Ed.* **2008**, *47*, 5292.
[18] M. Niederberger, *Acc. Chem. Res.* **2007**, *40*, 793.
[19] P. D. Cozzoli, T. Pellegrino, L. Manna, *Chem. Soc. Rev.* **2006**, *35*, 1195.
[20] *Advanced Wet-Chemical Synthetic Approaches to Inorganic Nanostructures* (Ed.: P. D. Cozzoli), Transworld Research Network, Kerala (India), **2008**, p. 453.
[21] Y. Xia, Y. Xiong, B. Lim, S. E. Skrabalak, *Angew. Chem.* **2009**, *121*, 62; *Angew. Chem. Int. Ed.* **2009**, *48*, 60.
[22] A. P. Alivisatos, *Ber. Bunsen-Ges.* **1997**, *101*, 1573.
[23] X. Batlle, A. Labarta, *J. Phys. D* **2002**, *35*, R15.
[24] *Surface Effects in Magnetic Nanoparticles* (Ed.: D. Fiorani), Springer, New York, **2005**.
[25] H. Zhang, E. W. Edwards, D. Wang, H. Möhwald, *Phys. Chem. Chem. Phys.* **2006**, *8*, 3288.
[26] M. J. S. Sharon, C. Glotzer, *Nat. Mater.* **2007**, *6*, 557.
[27] M. P. Pileni, *Acc. Chem. Res.* **2007**, *40*, 685.
[28] M. P. Pileni, *J. Appl. Phys. D* **2008**, *41*, 134002.
[29] Y. Cui, U. Banin, M. T. Bjork, A. P. Alivisatos, *Nano Lett.* **2005**, *5*, 1519.
[30] P.-E. Trudeau, M. Sheldon, V. Altoe, A. P. Alivisatos, *Nano Lett.* **2008**, *8*, 1936.
[31] M. T. Sheldon, P.-E. Trudeau, T. Mokari, L.-W. Wang, A. P. Alivisatos, *Nano Lett.* **2009**, *9*, 3676.
[32] D. V. Talapin, J.-S. Lee, M. V. Kovalenko, E. V. Shevchenko, *Chem. Rev.* **2009**, *109*, 389.
[33] D. J. Milliron, I. Gur, A. P. Alivisatos, *MRS Bull.* **2005**, *30*, 41.
[34] S. Kumar, G. D. Scholes, *Microchim. Acta* **2008**, *160*, 315.
[35] *Bio-Applications Of Nanoparticles, Vol. 620* (Ed.: W. C. W. Chan), Springer, New York, **2007**.
[36] L. Carbone, P. D. Cozzoli, *Nano Today* **2010**, *5*, 449.
[37] Y.-W. Jun, J.-S. Choi, J. Cheon, *Chem. Commun.* **2007**, 1203.
[38] J. Gao, H. Gu, B. Xu, *Acc. Chem. Res.* **2009**, *42*, 1097.
[39] D. August, R. W. Cliff, G. B. Moungi, *Adv. Mater.* **2009**, *21*, 3479.
[40] M. V. Kuznetsov, Y. G. Morozov in *Epdic 7: European Powder Diffraction, Pts 1 and 2, Vol. 378–373* (Eds.: R. Delhez, E. J. Mittemeijer), Trans. Tech Publications Ltd, Zürich-Uetikon, **2001**, p. 563.
[41] F. S. Li, Y. Wang, T. Wang, *J. Solid State Chem.* **2007**, *180*, 1272.

[42] J. Wang, Y. J. Wu, Y. J. Zhu, *Mater. Chem. Phys.* **2007**, *106*, 1.
[43] Y. B. Xu, Z. M. Ren, G. H. Cao, W. L. Ren, K. Deng, Y. B. Zhong, *Chem. Lett.* **2008**, *37*, 1200.
[44] K.-T. Kuo, S.-H. Hu, D.-M. Liu, S.-Y. Chen, *J. Mater. Chem.* **2010**, *20*, 1744.
[45] I. Bilecka, M. Niederberger, *Chimia* **2009**, *63*, 581.
[46] I. Bilecka, M. Niederberger, *Nanoscale* **2010**, *2*, 1358.
[47] G. R. Patzke, Y. Zhou, R. Kontic, F. Conrad, *Angew. Chem.* **2011**, *123*, 852; *Angew. Chem. Int. Ed.* **2011**, *50*, 826.
[48] E. Gavi, D. L. Marchisio, A. A. Barresi, *Chem. Eng. Sci.* **2007**, *62*, 2228.
[49] F. Aristizabal, R. J. Munz, D. Berk, *Aerosol Sci. Technol.* **2008**, *42*, 556.
[50] D. L. Marchisio, L. Rivautella, A. A. Barresi, *Aiche J.* **2006**, *52*, 1877.
[51] J. B. Edel, R. Fortt, J. C. deMello, A. J. deMello, *Chem. Commun.* **2002**, 1136.
[52] B. F. Cottam, S. Krishnadasan, A. J. deMello, J. C. deMello, M. S. P. Shaffer, *Lab Chip* **2007**, *7*, 167.
[53] S. Krishnadasan, R. J. C. Brown, A. J. deMello, J. C. deMello, *Lab Chip* **2007**, *7*, 1434.
[54] J. M. Köhler, M. Held, U. Hübner, J. Wagner, *Chem. Eng. Technol.* **2007**, *30*, 347.
[55] B. K. H. Yen, A. Günther, M. A. Schmidt, K. F. Jensen, M. G. Bavendi, *Angew. Chem.* **2005**, *117*, 5583; *Angew. Chem. Int. Ed.* **2005**, *44*, 5447.
[56] Y. Groisman, A. Gedanken, *J. Phys. Chem. C* **2008**, *112*, 8802.
[57] B. K. H. Yen, N. E. Stott, K. F. Jensen, M. G. Bawendi, *Adv. Mater.* **2003**, *15*, 1858.
[58] N. Jongen, M. Donnet, P. Bowen, J. Lemaitre, H. Hofmann, R. Schenk, C. Hofmann, M. Aoun-Habbache, S. Guillemet-Fritsch, J. Sarrias, A. Rousset, M. Viviani, M. T. Buscaglia, V. Buscaglia, P. Nanni, A. Testino, J. R. Herguijuela, *Chem. Eng. Technol.* **2003**, *26*, 303.
[59] S. N. Li, P. M. Gunther, J. M. Kohler, *J. Chem. Eng. Jpn.* **2009**, *42*, 338.
[60] D. L. Marchisio, F. Omegna, A. A. Barresi, P. Bowen, *Ind. Eng. Chem. Res.* **2008**, *47*, 7202.
[61] C. Lindenberg, J. Scholl, L. Vicum, M. Mazzotti, J. Brozio, *Chem. Eng. Sci.* **2008**, *63*, 4135.
[62] E. Gavi, D. L. Marchisio, A. A. Barresi, *J. Dispersion Sci. Technol.* **2008**, *29*, 548.
[63] C. de Mello Donegà, P. Liljeroth, D. Vanmaekelbergh, *Small* **2005**, *1*, 1152.
[64] M. Kawase, K. Miura, *Adv. Powder Technol.* **2007**, *18*, 725.
[65] For Reviews on microwave chemistry in the field of organic chemistry: a) C. O. Kappe, D. Dallinger, *Mol. Diversity* **2009**, *13*, 71; b) S. Caddick, R. Fitzmaurice, *Tetrahedron* **2009**, *65*, 3325; in peptide synthesis: c) J. M. Collins, N. E. Leadbeater, *Org. Biomol. Chem.* **2007**, *5*, 1141; in polymer synthesis: d) R. Hoogenboom, U. S. Schubert, *Macromol. Rapid Commun.* **2007**, *28*, 368; e) C. Ebner, T. Bodner, F. Stelzer, F. Wiesbrock, *Macromol. Rapid Commun.* **2011**, *32*, 254; in materials science: f) S. Barlow, S. R. Marder, *Adv. Funct. Mater.* **2003**, *13*, 517; in biochemical/analytical applications: g) J. R. Lill, E. S. Ingle, P. S. Liu, V. Pham, W. N. Sandoval, *Mass Spectrom. Rev.* **2007**, *26*, 657; h) S. L. Söderholm, M. Damm, C. O. Kappe, *Mol. Diversity* **2010**, *14*, 869; for an evaluation of the greenness of microwave chemistry: i) J. D. Moseley, C. O. Kappe, *Green Chem.* **2011**, *13*, 794.
[66] For recent books, see: a) *Microwaves in Organic Synthesis* 2nd ed. (Ed.: A. Loupy), Wiley-VCH, Weinheim, **2006**; b) *Microwave Methods in Organic Synthesis* (Eds.: M. Larhed, K. Olofsson), Springer, Berlin, **2006**; c) C. O. Kappe, A. Stadler, *Microwaves in Organic and Medicinal Chemistry*, Wiley-VCH, Weinheim, **2005**; d) D. Bogdal, A. Prociak, *Microwave-Enhanced Polymer Chemistry and Technology*, Blackwell Publishing, Oxford, **2007**; e) J. R. Lill, *Microwave Assisted Proteomics*, RSC Publishing, Cambridge, **2009**; f) *Microwave Heating as a Tool for Sustainable Chemistry* (Ed.: N. E. Leadbeater), CRC, Boca Raton, FL, **2011**; g) see also Ref. [68].
[67] For a more detailed description of these rather complex processes, see: a) C. Gabriel, S. Gabriel, E. H. Grant, B. S. Halstead, D. M. P. Mingos, *Chem. Soc. Rev.* **1998**, *27*, 213; b) D. M. P. Mingos, D. R. Baghurst, *Chem. Soc. Rev.* **1991**, *20*, 1.
[68] C. O. Kappe, D. Dallinger, S. S. Murphree, *Practical Microwave Synthesis for Organic Chemists—Strategies, Instruments, and Protocols*, Wiley-VCH, Weinheim, **2009**.
[69] a) C. O. Kappe, *Angew. Chem.* **2004**, *116*, 6408; *Angew. Chem. Int. Ed.* **2004**, *43*, 6250.
[70] For details, see: J. M. Kremsner, C. O. Kappe, *J. Org. Chem.* **2006**, *71*, 4651, and references therein.
[71] J. Robinson, S. Kingman, D. Irvine, P. Licence, A. Smith, G. Dimitrakis, D. Obermayer, C. O. Kappe, *Phys. Chem. Chem. Phys.* **2010**, *12*, 4750.
[72] D. Obermayer, C. O. Kappe, *Org. Biomol. Chem.* **2010**, *8*, 114.
[73] M. Gupta, E. W. W. Leong, *Microwaves and Metals*, Wiley, **2007**.
[74] a) A. G. Whittaker, D. M. P. Mingos, *J. Chem. Soc. Dalton Trans.* **2000**, 1521; b) B. H. P. van de Kruijs, M. H. C. L. Dressen, J. Meuldijk, J. A. J. M. Vekemans, L. A. Hulshof, *Org. Biomol. Chem.* **2010**, *8*, 1688; c) B. Gutmann, A. M. Schwan, B. Reichart, C. Gspan, F. Hofer, C. O. Kappe, *Angew. Chem.* **2011**, *123, 7778; Angew. Chem. Int. Ed.* **2011**, 50, 7636.
[75] Y.-L. Hsin, C.-F. Lin, Y.-C. Liang, K. C. Hwang, J.-C. Horng, J.-a. A. Ho, C.-C. Lin, J. R. Hwu, *Adv. Funct. Mater.* **2008**, *18*, 2048.
[76] Among recent studies, see, for example: a) J. Huo, L. Wang, H. Yu, *J. Mater. Sci.* **2009**, *44*, 3917; b) Y.-Q. Kang, M.-S. Cao, J. Yuan, L. Zhang, B. Wena, X.-Y. Fang, *J. Alloys Compd.* **2010**, *495*, 254; c) L. Yan, J. Wang, X. Han, Y. Ren, Q. Liu, F. Li, *Nanotechnology* **2010**, *21*, 095708; d) Z. Han, D. Li, M. Tong, X. Wei, R. Skomski, W. Liu, Z. D. Zhang, D. J. Sellmyer, *J. Appl. Phys.* **2010**, *107*, 09A929; e) M. Cao, H. Lianb, C. Hu, *Nanoscale* **2010**, *2*, 2619; f) K. Jia, R. Zhao, J. Zhong, X. Liu, *J. Magn. Magn. Mater.* **2010**, *322*, 2167; g) X.-L. Shi, M.-S. Cao, J. Yuan, X.-Y. Fang, *Appl. Phys. Lett.* **2009**, *95*, 163108; h) X.-L. Shi, M.-S. Cao, X.-Y. Fang, J. Yuan, Y.-Q. Kang, W.-L. Song, *Appl. Phys. Lett.* **2008**, *93*, 223112; i) H. Wen, M. Cao, G. Sun, W. Xu, D. Wang, X. Zhang, C. Hu, *J. Phys. Chem. C* **2008**, *112*, 15948; j) H. Li, Y. Huang, G. Sun, X. Yan, Y. Yang, J. Wang, Y. Zhang, *J. Phys. Chem. C* **2010**, *114*, 10088; k) Q. Su, J. Li, G. Zhong, G. Du, B. Xu, *J. Phys. Chem. C* **2011**, *115*, 1838; l) J. Cao, W. Fu, Haibin Yang, Q. Yu, Y. Zhang, S. Liu, P. Sun, X. Zhou, Y. Leng, S. Wang, B. Liu, G. Zou, *J. Phys. Chem. B* **2009**, *113*, 4642.
[77] M. A. Herrero, J. M. Kremsner, C. O. Kappe, *J. Org. Chem.* **2008**, *73*, 36.
[78] M. Damm, T. N. Glasnov, C. O. Kappe, *Org. Process Res. Dev.* **2010**, *14*, 215.
[79] For leading reviews, see: a) L. Perreux, A. Loupy, *Tetrahedron* **2001**, *57*, 9199; b) L. Perreux, A. Loupy in *Microwaves in Organic Synthesis*, 2nd ed. (Ed.: A. Loupy), Wiley-VCH, Weinheim, **2006**, chap. 4, pp. 134–218; c) A. De La Hoz, A. Diaz-Ortiz, A. Moreno, *Chem. Soc. Rev.* **2005**, *34*, 164; d) A. De La Hoz, A. Diaz-Ortiz, A. Moreno, in *Microwaves in Organic Synthesis*, 2nd ed. (Ed.: A. Loupy), Wiley-VCH, Weinheim, **2006**, chap. 5, pp. 219–277.
[80] C. O. Kappe, *Chem. Soc. Rev.* **2008**, *37*, 1127.
[81] a) D. Obermayer, B. Gutmann, C. O. Kappe, *Angew. Chem.* **2009**, *121*, 8471; *Angew. Chem. Int. Ed.* **2009**, *48*, 8321; b) B. Gutmann, D. Obermayer, B. Reichart, B. Prekodravac, M. Irfan, J. M. Kremsner, C. O. Kappe, *Chem. Eur. J.* **2010**, *16*, 12182.

[82] D. Dallinger, M. Irfan, A. Suljanovic, C. O. Kappe, *J. Org. Chem.* **2010**, *75*, 5278.
[83] E. K. Nyutu, W. C. Conner, S. M. Auerbach, C. H. Chen, S. L. Suib, *J. Phys. Chem. C* **2008**, *112*, 1407.
[84] X. Zhu, Q. Zhang, Y. Li, H. Wang, *J. Mater. Chem.* **2010**, *20*, 1766.
[85] For references on conventionally heated continuous-flow syntheses of NCs, see also: a) Ref. [56]; b) F. Bondioli, A. Bonamartini Corradi, A. M. Ferrari, C. Leonelli, *J. Am. Ceram. Soc.* **2008**, *91*, 3746; c) Ref. [84].
[86] W. X. Tu, H. Liu, *Chem. Mater.* **2000**, *12*, 564.
[87] A. Abou-Hassan, O. Sandre, V. Cabuil, *Angew. Chem.* **2010**, *122*, 6408; *Angew. Chem. Int. Ed.* **2010**, *49*, 6268.
[88] J. Park, J. Joo, S. G. Kwon, Y. Jang, T. Hyeon, *Angew. Chem.* **2007**, *119*, 4714; *Angew. Chem. Int. Ed.* **2007**, *46*, 4630.
[89] S. G. Kwon, T. Hyeon, *Acc. Chem. Res.* **2008**, *41*, 1696.
[90] S. G. Kwon, Y. Piao, J. Park, S. Angappane, Y. Jo, N.-M. Hwang, J.-G. Park, T. Hyeon, *J. Am. Chem. Soc.* **2007**, *129*, 12571.
[91] B. Viswanath, P. Kundu, A. Halder, N. Ravishankar, *J. Phys. Chem. C* **2009**, *113*, 16866.
[92] A. K. Ganguli, A. Ganguly, S. Vaidya, *Chem. Soc. Rev.* **2010**, *39*, 474.
[93] M. C. Daniel, D. Astruc, *Chem. Rev.* **2004**, *104*, 293.
[94] N. L. Rosi, C. A. Mirkin, *Chem. Rev.* **2004**, *104*, 1547.
[95] D. A. Giljohann, D. S. Seferos, W. L. Daniel, M. D. Massich, P. C. Patel, C. A. Mirkin, *Angew. Chem.* **2010**, *122*, 3352; *Angew. Chem. Int. Ed.* **2010**, *49*, 3280.
[96] S. Komarneni, *Curr. Sci. India* **2003**, *85*, 1730.
[97] M. Tsuji, M. Hashimoto, Y. Nishizawa, M. Kubokawa, T. Tsuji, *Chem. Eur. J.* **2005**, *11*, 440.
[98] L. Gou, M. Chipara, J. M. Zaleski, *Chem. Mater.* **2007**, *19*, 1755.
[99] T. Yamamoto, H. Yin, Y. Wada, T. Kitamura, T. Sakata, H. Mori, S. Yanagida, *Bull. Chem. Soc. Jpn.* **2004**, *77*, 757.
[100] F.-K. Liu, P.-W. Huang, Y.-C. Chang, C.-J. Ko, F.-H. Ko, T.-C. Chu, *J. Cryst. Growth* **2005**, *273*, 439.
[101] H. B. Yin, T. Yamamoto, Y. Wada, S. Yanagida, *Mater. Chem. Phys.* **2004**, *83*, 66.
[102] F.-K. Liu, P.-W. Huang, T.-C. Chu, F.-H. Ko, *Mater. Lett.* **2005**, *59*, 940.
[103] F. K. Liu, Y. C. Chang, F. H. Ko, T. C. Chu, *Mater. Lett.* **2004**, *58*, 373.
[104] A. Pal, S. Shah, S. Devi, *Colloids Surf. A* **2007**, *302*, 51.
[105] D. S. Li, S. Komarneni, *Z. Naturforsch. B* **2006**, *61*, 1566.
[106] Z. L. Jiang, Z. W. Feng, X. C. Shen, *Chin. Chem. Lett.* **2001**, *12*, 551.
[107] T. Yamamoto, Y. Wada, T. Sakata, H. Mori, M. Goto, S. Hibino, S. Yanagida, *Chem. Lett.* **2004**, *33*, 158.
[108] R. Abargues, R. Gradess, J. Canet-Ferrer, K. Abderrafi, J. L. Valdes, J. Martinez-Pastor, *New J. Chem.* **2009**, *33*, 913.
[109] M. Tsuji, Y. Nishizawa, M. Hashimoto, T. Tsuji, *Chem. Lett.* **2004**, *33*, 370.
[110] M. Tsuji, Y. Nishizawa, K. Matsumoto, N. Miyamae, T. Tsuji, X. Zhang, *Colloids Surf. A* **2007**, *293*, 185.
[111] H. Katsuki, S. Komarneni, *J. Mater. Res.* **2003**, *18*, 747.
[112] H. Katsuki, S. Komarneni, *J. Jpn. Soc. Powder Powder Metall.* **2003**, *50*, 745.
[113] A. Pal, S. Shah, S. Devi, *Mater. Chem. Phys.* **2009**, *114*, 530.
[114] A. Singh, V. Raykar, *Colloid Polym. Sci.* **2008**, *286*, 1667.
[115] S. Kundu, H. Liang, *Colloids Surf. A* **2008**, *330*, 143.
[116] I. Pastoriza-Santos, L. M. Liz-Marzan, *Langmuir* **2002**, *18*, 2888.
[117] S. Kundu, L. Peng, H. Liang, *Inorg. Chem.* **2008**, *47*, 6344.
[118] B. L. He, J. J. Tan, Y. L. Kong, H. F. Liu, *J. Mol. Catal. A* **2004**, *221*, 121.
[119] R. He, X. Qian, J. Yin, Z. Zhu, *J. Mater. Chem.* **2002**, *12*, 3783.
[120] F. Gao, Q. Lu, S. Komarneni, *Chem. Mater.* **2005**, *17*, 856.
[121] X. Sun, Y. Luo, *Mater. Lett.* **2005**, *59*, 4048.
[122] Y. J. Zhu, X. L. Hu, *Chem. Lett.* **2003**, *32*, 1140.
[123] M. Tsuji, M. Hashimoto, Y. Nishizawa, T. Tsuji, *Chem. Lett.* **2003**, *32*, 1114.
[124] M. Tsuji, N. Miyamae, M. Hashimoto, M. Nishio, S. Hikino, N. Ishigami, I. Tanaka, *Colloids Surf. A* **2007**, *302*, 587.
[125] M. Shen, Y. Sun, Y. Han, R. Yao, C. Yan, *Langmuir* **2008**, *24*, 13161.
[126] H. T. Zhu, C. Y. Zhang, Y. S. Yin, *J. Cryst. Growth* **2004**, *270*, 722.
[127] S. Komarneni, H. Katsuki, D. Li, A. S. Bhalla, *J. Phys. Condens. Matter* **2004**, *16*, S1305.
[128] W. X. Tu, H. F. Liu, *J. Mater. Chem.* **2000**, *10*, 2207.
[129] R. Harpeness, A. Gedanken, *J. Mater. Chem.* **2005**, *15*, 698.
[130] F. Bensebaa, N. Patrito, Y. Le Page, P. L'Ecuyer, D. S. Wang, *J. Mater. Chem.* **2004**, *14*, 3378.
[131] W. Yu, W. Tu, H. Liu, *Langmuir* **1999**, *15*, 6.
[132] S. Komarneni, D. Li, B. Newalkar, H. Katsuki, A. S. Bhalla, *Langmuir* **2002**, *18*, 5959.
[133] R. Minami, Y. Kitamoto, T. Chikata, S. Kato, *Electrochim. Acta* **2005**, *51*, 864.
[134] R. Harpeness, Z. Peng, X. Liu, V. G. Pol, Y. Koltypin, A. Gedanken, *J. Colloid Interface Sci.* **2005**, *287*, 678.
[135] M. Shen, Y. Du, N. Hua, P. Yang, *Powder Technol.* **2006**, *162*, 64.
[136] V. Abdelsayed, A. Aljarash, M. S. El-Shall, Z. A. Al Othman, A. H. Alghamdi, *Chem. Mater.* **2009**, *21*, 2825.
[137] M. B. Mohamed, K. M. AbouZeid, V. Abdelsayed, A. A. Aljarash, M. S. El-Shall, *ACS Nano* **2010**, *4*, 2766.
[138] B. Baruwati, V. Polshettiwar, R. S. Varma, *Green Chem.* **2009**, *11*, 926.
[139] S. Horikoshi, H. Abe, K. Torigoe, M. Abe, N. Serpone, *Nanoscale* **2010**, *2*, 1441.
[140] N. N. Mallikarjuna, R. S. Varma, *Cryst. Growth Des.* **2007**, *7*, 686.
[141] H. L. Nguyen, L. E. M. Howard, S. R. Giblin, B. K. Tanner, I. Terry, A. K. Hughes, I. M. Ross, A. Serres, H. Burckstummer, J. S. O. Evans, *J. Mater. Chem.* **2005**, *15*, 5136.
[142] R. Luque, A. M. Balu, J. M. Campelo, C. Gonzalez-Arellano, M. J. Gracia, D. Luna, J. M. Marinas, A. A. Romero, *Mater. Chem. Phys.* **2009**, *117*, 408.
[143] Z. J. Wu, S. H. Ge, M. H. Zhang, W. Li, K. Y. Tao, *J. Colloid Interface Sci.* **2009**, *330*, 359.
[144] S. Shironita, T. Takasaki, T. Kamegawa, K. Mori, H. Yamashita, *Catal. Lett.* **2009**, *129*, 404.
[145] T. C. Deivaraj, W. X. Chen, J. Y. Lee, *J. Mater. Chem.* **2003**, *13*, 2555.
[146] W. X. Chen, J. Zhao, J. Y. Lee, Z. L. Liu, *Chem. Lett.* **2004**, *33*, 474.
[147] D. L. Boxall, C. M. Lukehart, *Chem. Mater.* **2001**, *13*, 806.
[148] Y. J. Zhu, X. L. Hu, *Mater. Lett.* **2004**, *58*, 1517.
[149] S. Kundu, H. Liang, *Langmuir* **2008**, *24*, 9668.
[150] M. Tsuji, K. Matsumoto, N. Miyamae, T. Tsuji, X. Zhang, *Cryst. Growth Des.* **2007**, *7*, 311.
[151] L. Dongsheng, K. Sridhar, *J. Am. Ceram. Soc.* **2006**, *89*, 1510.
[152] M. Tsuji, N. Miyamae, S. Lim, K. Kimura, X. Zhang, S. Hikino, M. Nishio, *Cryst. Growth Des.* **2006**, *6*, 1801.
[153] M. Tsuji, R. Matsuo, P. Jiang, N. Miyamae, D. Ueyama, M. Nishio, S. Hikino, H. Kumagae, K. S. N. Kamarudin, X.-L. Tang, *Cryst. Growth Des.* **2008**, *8*, 2528.
[154] M. Tsuji, M. Nishio, P. Jiang, N. Miyamae, S. Lim, K. Matsumoto, D. Ueyama, X.-L. Tang, *Colloids Surf. A* **2008**, *317*, 247.
[155] R. Harpeness, A. Gedanken, *Langmuir* **2004**, *20*, 3431.
[156] H. Zhang, Y. Yin, Y. Hu, C. Li, P. Wu, S. Wei, C. Cai, *J. Phys. Chem. C* **2010**, *114*, 11861.
[157] T. Yamauchi, Y. Tsukahara, T. Sakata, H. Mori, T. Yanagida, T. Kawai, Y. Wada, *Nanoscale* **2010**, *2*, 515.

[158] N. M. Bahadur, T. Furusawa, M. Sato, F. Kurayama, I. A. Siddiquey, N. Suzuki, *J. Colloid Interface Sci.* **2011**, *355*, 312.
[159] M. Fernández-García, A. Martinez-Arias, J. C. Hanson, J. A. Rodriguez, *Chem. Rev.* **2004**, *104*, 4063.
[160] D. E. Clark, W. H. Sutton, *Annu. Rev. Mater. Sci.* **1996**, *26*, 299.
[161] G. Oskam, *J. Sol-Gel Sci. Technol.* **2006**, *37*, 161.
[162] J. P. Jolivet, S. Cassaignon, C. Chaneac, D. Chiche, E. Tronc, *J. Sol-Gel Sci. Technol.* **2008**, *46*, 299.
[163] K. J. Rao, K. Mahesh, S. Kumar, *Bull. Mater. Sci.* **2005**, *28*, 19.
[164] W.-H. Li, *Mater. Lett.* **2008**, *62*, 4149.
[165] C. R. Patra, A. Gedanken, *New J. Chem.* **2004**, *28*, 1060.
[166] J.-J. Zhu, J.-M. Zhu, X.-H. Liao, J.-L. Fang, M.-G. Zhou, H.-Y. Chen, *Mater. Lett.* **2002**, *53*, 12.
[167] S. Baldassari, S. Komarneni, E. Mariani, C. Villa, *Mater. Res. Bull.* **2005**, *40*, 2014.
[168] V. Polshettiwar, B. Baruwati, R. S. Varma, *Acs Nano* **2009**, *3*, 728.
[169] V. Polshettiwar, M. N. Nadagouda, R. S. Varma, *Chem. Commun.* **2008**, 6318.
[170] B. Baruwati, M. N. Nadagouda, R. S. Varma, *J. Phys. Chem. C* **2008**, *112*, 18399.
[171] M. L. Moreira, G. P. Mambrini, D. P. Volanti, E. R. Leite, M. O. Orlandi, P. S. Pizani, V. R. Mastelaro, C. O. Paiva-Santos, E. Longo, J. A. Varela, *Chem. Mater.* **2008**, *20*, 5381.
[172] E. K. Nyutu, C.-H. Chen, P. K. Dutta, S. L. Suib, *J. Phys. Chem. C* **2008**, *112*, 9659.
[173] W. Sun, Y. Pang, J. Li, W. Ao, *Chem. Mater.* **2007**, *19*, 1772.
[174] X. Zhu, J. Wang, Z. Zhang, J. Zhu, S. Zhou, Z. Liu, N. Ming, *J. Am. Ceram. Soc.* **2008**, *91*, 2683.
[175] Y. Li, H. Li, R. Cao, *J. Am. Ceram. Soc.* **2009**, *92*, 2188.
[176] A. Phuruangrat, D. J. Ham, S. J. Hong, S. Thongtem, J. S. Lee, *J. Mater. Chem.* **2010**, *20*, 1683.
[177] B. Hu, L.-H. Wu, S.-J. Liu, H.-B. Yao, H.-Y. Shi, G.-P. Li, S.-H. Yu, *Chem. Commun.* **2010**, *46*, 2277.
[178] L. Espinal, K. A. Malinger, A. E. Espinal, A. M. Gaffney, S. L. Suib, *Adv. Funct. Mater.* **2007**, *17*, 2572.
[179] X. Jia, W. He, X. Zhang, H. Zhao, Z. Li, Y. Feng, *Nanotechnology* **2007**, *18*, 075602.
[180] Z. Luo, H. Li, J. Xia, W. Zhu, J. Guo, B. Zhang, *Mater. Lett.* **2007**, *61*, 1845.
[181] T. Muraliganth, A. V. Murugan, A. Manthiram, *Chem. Commun.* **2009**, 7360.
[182] X. Hu, J. Yu, *Chem. Asian J.* **2006**, *1*, 605.
[183] L. Li, J. Ren, *Mater. Res. Bull.* **2006**, *41*, 2286.
[184] See Ref. [85b].
[185] Y.-W. Jun, J.-S. Choi, J. Cheon, *Angew. Chem.* **2006**, *118*, 3492; *Angew. Chem. Int. Ed.* **2006**, *45*, 3414.
[186] E. Hammarberg, A. Prodi-Schwab, C. Feldmann, *Thin Solid Films* **2008**, *516*, 7437.
[187] I. Bilecka, I. Djerdj, M. Niederberger, *Chem. Commun.* **2008**, 886.
[188] I. Bilecka, P. Elser, M. Niederberger, *ACS Nano* **2009**, *3*, 467.
[189] L. Combemale, G. Caboche, D. Stuerga, *J. Solid State Chem.* **2009**, *182*, 2829.
[190] X. Hu, J. Gong, L. Zhang, J. C. Yu, *Adv. Mater.* **2008**, *20*, 4845.
[191] J. J. Schneider, R. C. Hoffmann, J. Engstler, A. Klyszcz, E. Erdem, P. Jakes, R.-A. Eichel, L. Pitta-Bauermann, J. Bill, *Chem. Mater.* **2010**, *22*, 2203.
[192] Z. Ai, K. Deng, Q. Wan, L. Zhang, S. Lee, *J. Phys. Chem. C* **2010**, *114*, 6237.
[193] H. Zhang, X. Zhong, J.-J. Xu, H.-Y. Chen, *Langmuir* **2008**, *24*, 13748.
[194] A. Taubert, Z. Li, *Dalton Trans.* **2007**, 723.
[195] G. Bühler, D. Thölmann, C. Feldmann, *Adv. Mater.* **2007**, *19*, 2224.
[196] K. Ding, Z. Miao, Z. Liu, Z. Zhang, B. Han, G. An, S. Miao, Y. Xie, *J. Am. Chem. Soc.* **2007**, *129*, 6362.
[197] D. Zhang, G. Li, X. Yang, J. C. Yu, *Chem. Commun.* **2009**, 4381.
[198] H. Hu, H. Yang, P. Huang, D. Cui, Y. Peng, J. Zhang, F. Lu, J. Lian, D. Shi, *Chem. Commun.* **2010**, *46*, 3866.
[199] X. Xu, M. Zhang, J. Feng, M. Zhang, *Mater. Lett.* **2008**, *62*, 2787.
[200] W.-W. Wang, Y.-J. Zhu, G.-F. Cheng, Y.-H. Huang, *Mater. Lett.* **2006**, *60*, 609.
[201] J. Xia, H. Li, Z. Luo, H. Shi, K. Wang, H. Shu, Y. Yan, *J. Phys. Chem. Solids* **2009**, *70*, 1461.
[202] R. Jalal, E. K. Goharshadi, M. Abareshi, M. Moosavi, A. Yousefi, P. Nancarrow, *Mater. Chem. Phys.* **2010**, *121*, 198.
[203] L. Wu, J. Lian, G. Sun, X. Kong, W. Zheng, *Eur. J. Inorg. Chem.* **2009**, 2897.
[204] S.-W. Cao, Y.-J. Zhu, G.-F. Cheng, Y.-H. Huang, *J. Hazard. Mater.* **2009**, *171*, 431.
[205] S.-W. Cao, Y.-J. Zhu, *Acta Mater.* **2009**, *57*, 2154.
[206] S. Anandan, J. J. Wu, *Mater. Lett.* **2009**, *63*, 2387.
[207] C.-Y. Cao, Z.-M. Cui, C.-Q. Chen, W.-G. Song, W. Cai, *J. Phys. Chem. C* **2010**, *114*, 9865.
[208] F. Gao, Q. Lu, S. Komarneni, *J. Nanosci. Nanotechnol.* **2006**, *6*, 3812.
[209] X.-H. Liao, J.-J. Zhu, J.-Z. Xu, H.-Y. Chen, J.-M. Zhu, *Chem. Commun.* **2001**, 937.
[210] H. Wang, J.-J. Zhu, J.-M. Zhu, X.-H. Liao, S. Xu, T. Ding, H.-Y. Chen, *Phys. Chem. Chem. Phys.* **2002**, *4*, 3794.
[211] A. Bonamartini Corradi, F. Bondioli, A. M. Ferrari, T. Manfredini, *Mater. Res. Bull.* **2006**, *41*, 38.
[212] D. S. Raj, T. Krishnakumar, R. Jayaprakash, N. Donato, M. Latino, G. Neri, *Sci. Adv. Mater.* **2010**, *2*, 432.
[213] L.-H. Ai, J. Jiang, *Powder Technol.* **2009**, *195*, 11.
[214] Y. Ding, L. Xu, C. Chen, X. Shen, S. L. Suib, *J. Phys. Chem. C* **2008**, *112*, 8177.
[215] H. Wang, J.-Z. Xu, J.-J. Zhu, H.-Y. Chen, *J. Cryst. Growth* **2002**, *244*, 88.
[216] D. P. Volanti, M. O. Orlandi, J. Andres, E. Longo, *CrystEngComm* **2010**, *12*, 1696.
[217] Y. Zhao, J.-J. Zhu, J.-M. Hong, N. Bian, H.-Y. Chen, *Eur. J. Inorg. Chem.* **2004**, 4072.
[218] J. Liu, S. Wang, Q. Wang, B. Geng, *Sens. Actuators B* **2009**, *143*, 253.
[219] X. Hu, J. C. Yu, J. Gong, Q. Li, G. Li, *Adv. Mater.* **2007**, *19*, 2324.
[220] X. Hu, J. C. Yu, *Adv. Funct. Mater.* **2008**, *18*, 880.
[221] H. Katsuki, S. Komarneni, *J. Am. Ceram. Soc.* **2001**, *84*, 2313.
[222] B. Xue, R. Liu, Z.-D. Xu, Y.-F. Zheng, *Chem. Lett.* **2008**, *37*, 1058.
[223] W. W. Wang, Y. J. Zhu, M. L. Ruan, *J. Nanopart. Res.* **2007**, *9*, 419.
[224] X. Liao, J. Zhu, W. Zhong, H.-Y. Chen, *Mater. Lett.* **2001**, *50*, 341.
[225] X. Guo, Y. Deng, D. Gu, R. Che, D. Zhao, *J. Mater. Chem.* **2009**, *19*, 6706.
[226] H. Katsuki, A. Shiraishi, S. Komarneni, W. J. Moon, S. Toh, K. Kaneko, *J. Ceram. Soc. Jpn.* **2004**, *112*, 384.
[227] X. Hu, J. C. Yu, J. Gong, *J. Phys. Chem. C* **2007**, *111*, 11180.
[228] X. Du, C. Wang, M. Chen, Y. Jiao, J. Wang, *J. Phys. Chem. C* **2009**, *113*, 2643.
[229] L.-X. Yang, Y.-J. Zhu, H. Tong, W.-W. Wang, G.-F. Cheng, *J. Solid State Chem.* **2006**, *179*, 1225.
[230] P. Yu, X. Zhang, Y. Chen, Y. Ma, Z. Qi, *Mater. Chem. Phys.* **2009**, *118*, 303.
[231] K. Wang, T. Huang, H. Liu, Y. Zhao, H. Liu, C. Sun, *Colloids Surf. A* **2008**, *325*, 21.
[232] R. Pan, Y. Wu, Q. Wang, Y. Hong, *Chem. Eng. J.* **2009**, *153*, 206.
[233] D.-S. Wu, C.-Y. Han, S.-Y. Wang, N.-L. Wu, I. A. Rusakova, *Mater. Lett.* **2002**, *53*, 155.
[234] J. Jouhannaud, J. Rossignol, D. Stuerga, *J. Solid State Chem.* **2008**, *181*, 1439.
[235] M. Krishna, S. Komarneni, *Ceram. Int.* **2009**, *35*, 3375.

[236] J. Spatz, S. Mößmer, M. Möller, M. Kocher, D. Neher, G. Wegner, *Adv. Mater.* **1998**, *10*, 473.
[237] P. Periyat, N. Leyland, D. E. McCormack, J. Colreavy, D. Corr, S. C. Pillai, *J. Mater. Chem.* **2010**, *20*, 3650.
[238] T. Yamamoto, Y. Wada, H. Yin, T. Sakata, H. Mori, S. Yanagida, *Chem. Lett.* **2002**, 964.
[239] V. G. Pol, Y. Langzam, A. Zaban, *Langmuir* **2007**, *23*, 11211.
[240] G. J. Wilson, G. D. Will, R. L. Frost, S. A. Montgomery, *J. Mater. Chem.* **2002**, *12*, 1787.
[241] M. Inada, K. Kamada, N. Enomoto, J. Hojo, *J. Ceram. Soc. Jpn.* **2006**, *114*, 814.
[242] E. Gressel-Michel, D. Chaumont, D. Stuerga, *J. Colloid Interface Sci.* **2005**, *285*, 674.
[243] S. Baldassari, S. Komarneni, E. Mariani, C. Villa, *J. Am. Ceram. Soc.* **2005**, *88*, 3238.
[244] T. Suprabha, H. Roy, J. Thomas, K. Praveen Kumar, S. Mathew, *Nanoscale Res. Lett.* **2009**, *4*, 144.
[245] A. B. Corradi, F. Bondioli, B. Focher, A. M. Ferrari, C. Grippo, E. Mariani, C. Villa, *J. Am. Ceram. Soc.* **2005**, *88*, 2639.
[246] L. X. Zhang, P. Liu, Z. X. Su, *Chin. J. Chem.* **2006**, *24*, 19.
[247] N. Le Houx, G. Pourroy, F. Camerel, M. Comet, D. Spitzer, *J. Phys. Chem. C* **2010**, *114*, 155.
[248] X.-L. Hu, Y.-J. Zhu, S.-W. Wang, *Mater. Chem. Phys.* **2004**, *88*, 421.
[249] S. Cho, S.-H. Jung, K.-H. Lee, *J. Phys. Chem. C* **2008**, *112*, 12769.
[250] S. Komarneni, M. Bruno, E. Mariani, *Mater. Res. Bull.* **2000**, *35*, 1843.
[251] D. Ledwith, S. C. Pillai, G. W. Watson, J. M. Kelly, *Chem. Commun.* **2004**, 2294.
[252] S. C. Padmanabhan, D. Ledwith, S. C. Pillai, D. E. McCormack, J. M. Kelly, *J. Mater. Chem.* **2009**, *19*, 9250.
[253] D. K. Bhat, *Nanoscale Res. Lett.* **2008**, *3*, 31.
[254] L.-Y. Yang, S.-Y. Dong, J.-H. Sun, J.-L. Feng, Q.-H. Wu, S.-P. Sun, *J. Hazard. Mater.* **2010**, *179*, 438.
[255] P. Zhu, J. Zhang, Z. Wu, Z. Zhang, *Cryst. Growth Des.* **2008**, *8*, 3148.
[256] S. Erten-Ela, S. Cogal, S. Icli, *Inorg. Chim. Acta* **2009**, *362*, 1855.
[257] J. Liang, Z. Deng, X. Jiang, F. Li, Y. Li, *Inorg. Chem.* **2002**, *41*, 3602.
[258] F. Bondioli, A. M. Ferrari, C. Leonelli, C. Siligardi, G. C. Pellacani, *J. Am. Ceram. Soc.* **2001**, *84*, 2728.
[259] C. Bousquet-Berthelin, D. Chaumont, D. Stuerga, *J. Solid State Chem.* **2008**, *181*, 616.
[260] F. Bensebaa, F. Zavaliche, P. L'Ecuyer, R. W. Cochrane, T. Veres, *J. Colloid Interface Sci.* **2004**, *277*, 104.
[261] L. Zhang, X.-F. Cao, Y.-L. Ma, X.-T. Chen, Z.-L. Xue, *CrystEngComm* **2010**, *12*, 207.
[262] L. Zhenyu, X. Guangliang, Z. Yalin, *Nanoscale Res. Lett.* **2007**, *2*, 40.
[263] T. Krishnaveni, S. Komarneni, S. R. Murthy, *Synth. React. Inorg. Met.-Org. Chem.* **2006**, *36*, 143.
[264] K. Sadhana, K. Praveena, S. Bharadwaj, S. R. Murthy, *J. Alloys Compd.* **2009**, *472*, 484.
[265] L. Xu, Y.-S. Ding, C.-H. Chen, L. Zhao, C. Rimkus, R. Joesten, S. L. Suib, *Chem. Mater.* **2008**, *20*, 308.
[266] M.-Y. Cheng, B.-J. Hwang, *J. Colloid Interface Sci.* **2009**, *337*, 265.
[267] H. Wu, M. Shao, J. Gu, X. Wei, *Mater. Lett.* **2004**, *58*, 2166.
[268] J. Liu, K. Li, H. Wang, M. Zhu, H. Yan, *Chem. Phys. Lett.* **2004**, *396*, 429.
[269] C. S. Xavier, J. C. Sczancoski, L. S. Cavalcante, C. O. Paiva-Santos, J. A. Varela, E. Longo, M. S. Li, *Solid State Sci.* **2009**, *11*, 2173.
[270] O. Palchik, J. Zhu, A. Gedanken, *J. Mater. Chem.* **2000**, *10*, 1251.
[271] W. Sun, J. Li, *Mater. Lett.* **2006**, *60*, 1599.
[272] S. H. Jhung, J.-H. Lee, J. W. Yoon, Y. K. Hwang, J.-S. Hwang, S.-E. Park, J.-S. Chang, *Mater. Lett.* **2004**, *58*, 3161.
[273] L. Junliang, Z. Yanwei, G. Cuijing, Z. Wei, Y. Xiaowei, *J. Eur. Ceram. Soc.* **2010**, *30*, 993.
[274] H. Zhang, J. Liu, H. Wang, W. Zhang, H. Yan, *J. Nanopart. Res.* **2008**, *10*, 767.
[275] A. J. Paula, M. A. Zaghete, E. Longo, J. A. Varela, *Eur. J. Inorg. Chem.* **2008**, 1300.
[276] S. Mahapatra, S. K. Nayak, G. Madras, T. N. G. Row, *Ind. Eng. Chem. Res.* **2008**, *47*, 6509.
[277] H. Wang, Y. Meng, H. Yan, *Inorg. Chem. Commun.* **2004**, *7*, 553.
[278] J. H. Ryu, C. S. Lima, W.-C. Oh, K. B. Shim, *J. Ceram. Process. Res.* **2004**, *5*, 316.
[279] F. Bondioli, A. M. Ferrari, L. Lusvarghi, T. Manfredini, S. Nannarone, L. Pasquali, G. Selvaggi, *J. Mater. Chem.* **2005**, *15*, 1061.
[280] M. Godinho, C. Ribeiro, E. Longo, E. R. Leite, *Cryst. Growth Des.* **2008**, *8*, 384.
[281] M. Godinho, R. D. Goncalves, E. R. Leite, C. W. Raubach, N. L. V. Carreno, L. F. D. Probst, E. Longo, H. V. Fajardo, *J. Mater. Sci.* **2010**, *45*, 593.
[282] F. Conrad, Y. Zhou, M. Yulikov, K. Hametner, S. Weyeneth, G. Jeschke, D. Günther, J.-D. Grunwaldt, G. R. Patzke, *Eur. J. Inorg. Chem.* **2010**, 2036.
[283] A. F. Shojaie, M. H. Loghmani, *Chem. Eng. J.* **2010**, *157*, 263.
[284] E. Hammarberg, A. Prodi-Schwab, C. Feldmann, *J. Colloid Interface Sci.* **2009**, *334*, 29.
[285] G. Glaspell, L. Fuoco, M. S. El-Shall, *J. Phys. Chem. B* **2005**, *109*, 17350.
[286] F. Bondioli, C. Leonelli, T. Manfredini, A. M. Ferrari, M. C. Caracoche, P. C. Rivas, A. M. Rodríguez, *J. Am. Ceram. Soc.* **2005**, *88*, 633.
[287] J. A. Gerbec, D. Magana, A. Washington, G. F. Strouse, *J. Am. Chem. Soc.* **2005**, *127*, 15791.
[288] A. L. Washington Ii, G. F. Strouse, *J. Am. Chem. Soc.* **2008**, *130*, 8916.
[289] A. L. Washington, G. F. Strouse, *Chem. Mater.* **2009**, *21*, 3586.
[290] A. L. Washington, G. F. Strouse, *Chem. Mater.* **2009**, *21*, 2770.
[291] Q. Song, X. Ai, T. Topuria, P. M. Rice, F. H. Alharbi, A. Bagabas, M. Bahattab, J. D. Bass, H.-C. Kim, J. C. Scott, R. D. Miller, *Chem. Commun.* **2010**, *46*, 4971.
[292] M. A. Sliem, A. Chemseddine, U. Bloeck, R. A. Fischer, *CrystEngComm* **2011**, *13*, 483.
[293] A. B. Panda, G. Glaspell, M. S. El-Shall, *J. Am. Chem. Soc.* **2006**, *128*, 2790.
[294] Y. He, H.-T. Lu, L.-M. Sai, W.-Y. Lai, Q.-L. Fan, L.-H. Wang, W. Huang, *J. Phys. Chem. B* **2006**, *110*, 13352.
[295] Y. He, L.-M. Sai, H.-T. Lu, M. Hu, W.-Y. Lai, Q.-L. Fan, L.-H. Wang, W. Huang, *Chem. Mater.* **2007**, *19*, 359.
[296] W. Li, D. Li, W. Zhang, Y. Hu, Y. He, X. Fu, *J. Phys. Chem. C* **2010**, *114*, 2154.
[297] S. Kundu, H. Lee, H. Liang, *Inorg. Chem.* **2009**, *48*, 121.
[298] E. Caponetti, D. C. Martino, M. Leone, L. Pedone, M. L. Saladino, V. Vetri, *J. Colloid Interface Sci.* **2006**, *304*, 413.
[299] E. Caponetti, L. Pedone, R. Massa, *Mater. Res. Innovations* **2004**, *8*, 44.
[300] C. C. Landry, J. Lockwood, A. R. Barron, *Chem. Mater.* **1995**, *7*, 699.
[301] C. Sun, J. S. Gardner, G. Long, C. Bajracharya, A. Thurber, A. Punnoose, R. G. Rodriguez, J. J. Pak, *Chem. Mater.* **2010**, *22*, 2699.
[302] J. Gardner, E. Shurdha, C. Wang, L. Lau, R. Rodriguez, J. Pak, *J. Nanopart. Res.* **2008**, *10*, 633.
[303] A. Pein, M. Baghbanzadeh, T. Rath, W. Haas, E. Maier, H. Amenitsch, F. Hofer, C. O. Kappe, G. Trimmel, *Inorg. Chem.* **2011**, *50*, 193.

[304] C.-C. Wu, C.-Y. Shiau, D. W. Ayele, W.-N. Su, M.-Y. Cheng, C.-Y. Chiu, B.-J. Hwang, *Chem. Mater.* **2010**, *22*, 4185.
[305] Y.-J. Zhu, W.-W. Wang, R.-J. Qi, X.-L. Hu, *Angew. Chem.* **2004**, *116*, 1434; *Angew. Chem. Int. Ed.* **2004**, *43*, 1410.
[306] J. W. Liu, F. Chen, M. Zhang, H. Qi, C. L. Zhang, S. H. Yu, *Langmuir* **2010**, *26*, 11372.
[307] X.-H. Liao, H. Wang, J.-J. Zhu, H.-Y. Chen, *Mater. Res. Bull.* **2001**, *36*, 2339.
[308] H.-Q. Wang, T. Nann, *Acs Nano* **2009**, *3*, 3804.
[309] Z. Quan, P. Yang, C. Li, J. Yang, D. Yang, Y. Jin, H. Lian, H. Li, J. Lin, *J. Phys. Chem. C* **2009**, *113*, 4018.
[310] C. Lorbeer, J. Cybinska, A.-V. Mudring, *Chem. Commun.* **2010**, *46*, 571.
[311] D. V. Talapin, N. Gaponik, H. Borchert, A. L. Rogach, M. Haase, H. Weller, *J. Phys. Chem. B* **2002**, *106*, 12659.
[312] D. D. Lovingood, G. F. Strouse, *Nano Lett.* **2008**, *8*, 3394.
[313] G. Bühler, C. Feldmann, *Angew. Chem.* **2006**, *118*, 4982; *Angew. Chem. Int. Ed.* **2006**, *45*, 4864.
[314] A. Zharkouskaya, C. Feldmann, K. Trampert, W. Heering, U. Lemmer, *Eur. J. Inorg. Chem.* **2008**, 873.
[315] G. Bühler, A. Zharkouskaya, C. Feldmann, *Solid State Sci.* **2008**, *10*, 461.
[316] G. Bühler, C. Feldmann, *Appl. Phys. A* **2007**, *87*, 631.
[317] W. Li, J. Lee, *J. Phys. Chem. C* **2008**, *112*, 11679.
[318] L. Ma, L.-M. Xu, W.-X. Chen, Z.-D. Xu, *Mater. Lett.* **2009**, *63*, 1635.
[319] A. V. Murugan, T. Muraliganth, P. J. Ferreira, A. Manthiram, *Inorg. Chem.* **2009**, *48*, 946.
[320] T. Muraliganth, A. V. Murugan, A. Manthiram, *J. Mater. Chem.* **2008**, *18*, 5661.
[321] A. V. Murugan, T. Muraliganth, A. Manthiram, *J. Phys. Chem. C* **2008**, *112*, 14665.
[322] A. K. Padhi, K. S. Nanjundaswamy, J. B. Goodenough, *J. Electrochem. Soc.* **1997**, *144*, 1188.
[323] I. Bilecka, A. Hintennach, I. Djerdj, P. Novak, M. Niederberger, *J. Mater. Chem.* **2009**, *19*, 5125.
[324] J. Ziegler, A. Merkulov, M. Grabolle, U. Resch-Genger, T. Nann, *Langmuir* **2007**, *23*, 7751.
[325] W. Schumacher, A. Nagy, W. J. Waldman, P. K. Dutta, *J. Phys. Chem. C* **2009**, *113*, 12132.
[326] Y. He, H. T. Lu, L. M. Sai, W. Y. Lai, Q. L. Fan, L. H. Wang, W. Huang, *J. Phys. Chem. B* **2006**, *110*, 13370.
[327] Y. He, H. T. Lu, L. M. Sai, Y. Y. Su, M. Hu, C. H. Fan, W. Huang, L. H. Wang, *Adv. Mater.* **2008**, *20*, 3416.
[328] M. D. Roy, A. A. Herzing, S. H. De Paoli Lacerda, M. L. Becker, *Chem. Commun.* **2008**, 2106.
[329] D. Zhu, X. Jiang, C. Zhao, X. Sun, J. Zhang, J.-J. Zhu, *Chem. Commun.* **2010**, *46*, 5226.
[330] W. Jian, J. Zhuang, W. Yang, Y. Bai, *J. Lumin.* **2007**, *126*, 735.
[331] J. Zhu, M. Zhou, J. Xu, X. Liao, *Mater. Lett.* **2001**, *47*, 25.
[332] Y. Wada, H. Kuramoto, J. Anand, T. Kitamura, T. Sakata, H. Mori, S. Yanagida, *J. Mater. Chem.* **2001**, *11*, 1936.
[333] S. Karan, B. Mallik, *J. Phys. Chem. C* **2007**, *111*, 16734.
[334] T. Serrano, I. Gómez, R. Colás, J. Cavazos, *Colloids Surf. A* **2009**, *338*, 20.
[335] J. He, X.-N. Zhao, J.-J. Zhu, J. Wang, *J. Cryst. Growth* **2002**, *240*, 389.
[336] M.-Q. Zhu, Z. Gu, J.-B. Fan, X.-B. Xu, J. Cui, J.-H. Liu, F. Long, *Langmuir* **2009**, *25*, 10189.
[337] J. Zhu, O. Palchik, S. Chen, A. Gedanken, *J. Phys. Chem. B* **2000**, *104*, 7344.
[338] O. Palchik, R. Kerner, A. Gedanken, A. M. Weiss, M. A. Slifkin, V. Palchik, *J. Mater. Chem.* **2001**, *11*, 874.
[339] A. V. Firth, Y. Tao, D. Wang, J. Ding, F. Bensebaa, *J. Mater. Chem.* **2005**, *15*, 4367.
[340] X. Cao, C. Zhao, X. Lan, D. Yao, W. Shen, *J. Alloys Compd.* **2009**, *474*, 61.
[341] J. L. Duan, L. X. Song, J. H. Zhan, *Nano Res.* **2009**, *2*, 61.
[342] L. Li, H. Qian, J. Ren, *Chem. Commun.* **2005**, 528.
[343] H. Grisaru, O. Palchik, A. Gedanken, V. Palchik, M. A. Slifkin, A. M. Weiss, Y. R. Hacohen, *Inorg. Chem.* **2001**, *40*, 4814.
[344] X.-H. Liao, N.-Y. Chen, S. Xu, S.-B. Yang, J.-J. Zhu, *J. Cryst. Growth* **2003**, *252*, 593.
[345] X.-H. Liao, J.-J. Zhu, H.-Y. Chen, *Mater. Sci. Eng. B* **2001**, *85*, 85.
[346] F. Bensebaa, C. Durand, A. Aouadou, L. Scoles, X. Du, D. Wang, Y. Le Page, *J. Nanopart. Res.* **2010**, *12*, 1897.
[347] H. Grisaru, O. Palchik, A. Gedanken, V. Palchik, M. A. Slifkin, A. M. Weiss, *Inorg. Chem.* **2003**, *42*, 7148.
[348] H. Grisaru, V. Pol, A. Gedanken, I. Nowik, *Eur. J. Inorg. Chem.* **2004**, 1859.
[349] T. Ding, J.-R. Zhang, S. Long, J.-J. Zhu, *Microelectron. Eng.* **2003**, *66*, 46.
[350] Y. Zhao, X.-H. Liao, J.-M. Hong, J.-J. Zhu, *Mater. Chem. Phys.* **2004**, *87*, 149.
[351] A. Phuruangrat, T. Thongtem, S. Thongtem, *Appl. Surf. Sci.* **2008**, *254*, 7553.
[352] A. Phuruangrat, T. Thongtem, S. Thongtem, *Mater. Lett.* **2009**, *63*, 667.
[353] T. Ding, J.-J. Zhu, *Mater. Sci. Eng. B* **2003**, *100*, 307.
[354] Y. Zhao, J. M. Hong, J. J. Zhu, *J. Cryst. Growth* **2004**, *270*, 438.
[355] R. He, X.-F. Qian, J. Yin, H.-A. Xi, L.-J. Bian, Z.-K. Zhu, *Colloids Surf. A* **2003**, *220*, 151.
[356] D. Han, C. Song, X. Li, *Mater. Chem. Phys.* **2009**, *116*, 41.
[357] H. Qian, X. Qiu, L. Li, J. Ren, *J. Phys. Chem. B* **2006**, *110*, 9034.
[358] H. Wang, J.-R. Zhang, J.-J. Zhu, *J. Cryst. Growth* **2001**, *233*, 829.
[359] O. Palchik, R. Kerner, Z. Zhu, A. Gedanken, *J. Solid State Chem.* **2000**, *154*, 530.
[360] F. Gao, Q. Lu, X. Meng, S. Komarneni, *J. Mater. Sci.* **2008**, *43*, 2377.
[361] R. Harpeness, A. Gedanken, *New J. Chem.* **2003**, *27*, 1191.
[362] R. Harpeness, A. Gedanken, A. M. Weiss, M. A. Slifkin, *J. Mater. Chem.* **2003**, *13*, 2603.
[363] Q. Lu, F. Gao, S. Komarneni, *J. Mater. Res.* **2004**, *19*, 1649.
[364] a) S. Komarneni, M. C. D'Arrigo, C. Leonelli, G. C. Pellacani, H. Katsuki, *J. Am. Ceram. Soc.* **1998**, *81*, 3041; b) S. Komarneni, R. Roy, Q. H. Li, *Mater. Res. Bull.* **1992**, *27*, 1393.
[365] M. Z. C. Hu, M. T. Harris, C. H. Byers, *J. Colloid Interface Sci.* **1998**, *198*, 87.
[366] S. H. Jhung, T. Jin, Y. K. Hwang, J.-S. Chang, *Chem. Eur. J.* **2007**, *13*, 4410.
[367] S. Komarneni, H. Katsuki, *Pure Appl. Chem.* **2002**, *74*, 1537.
[368] D. M. Oman, K. M. Dugan, J. L. Killian, V. Ceekala, C. S. Ferekides, D. L. Morel, *Sol. Energy Mater. Sol. Cells* **1999**, *58*, 361.
[369] K. J. Rao, B. Vaidhyanathan, M. Ganguli, P. A. Ramakrishnan, *Chem. Mater.* **1999**, *11*, 882.
[370] W. C. Conner, G. A. Tompsett, *J. Phys. Chem. B* **2008**, *112*, 2110.
[371] S. J. Vallee, W. C. Conner, *J. Phys. Chem. B* **2006**, *110*, 15459.
[372] X. Hu, J. C. Yu, *Chem. Mater.* **2008**, *20*, 6743.
[373] D. Tamara, W. Wim, H. Stephanie, S. S. Ulrich, *Adv. Funct. Mater.* **2009**, *19*, 1287.
[374] Z. A. Peng, X. Peng, *J. Am. Chem. Soc.* **2002**, *124*, 3343.
[375] D. Issadore, K. J. Humphry, K. A. Brown, L. Sandberg, D. A. Weitz, R. M. Westervelt, *Lab Chip* **2009**, *9*, 1701.
[376] S. Horikoshi, H. Abe, T. Sumi, K. Torigoe, H. Sakai, N. Serpone, M. Abe, *Nanoscale* **2011**, *3*, 1697.
[377] C. L. Dube, S. C. Kashyap, D. C. Dube, D. K. Agarwal, *Appl. Phys. Lett.* **2009**, *94*, 213107.
[378] S. Marre, K. F. Jensen, *Chem. Soc. Rev.* **2010**, *39*, 1183.
[379] A. M. Nightingale, J. C. de Mello, *J. Mater. Chem.* **2010**, *20*, 8454.

